A Primer

on

Numerical and Physical Modelling in Geotechnical Engineering

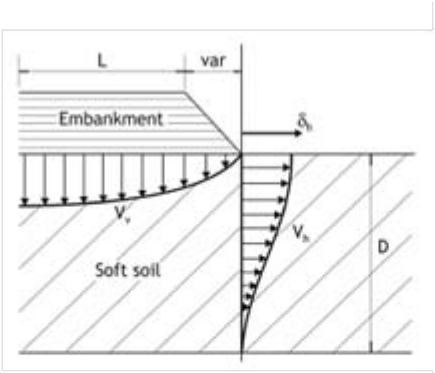

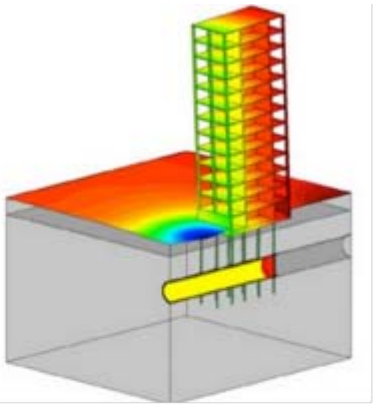

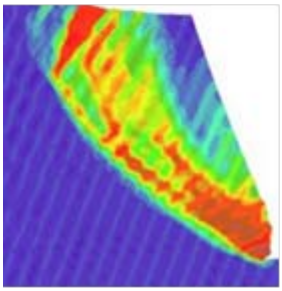

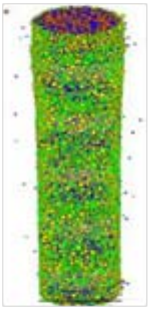

$$c(x=0,t)=c_0+\frac{nD_e}{H_s}\int_0^t\left(\frac{\partial c}{\partial x}\right)\Big|_{x=0}\mathrm{d}\tau$$

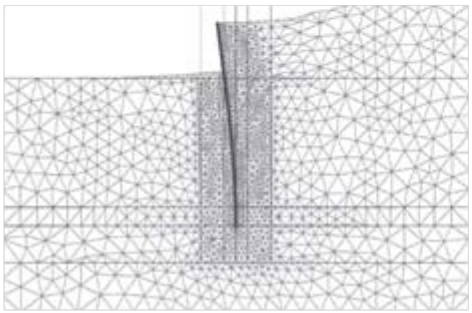

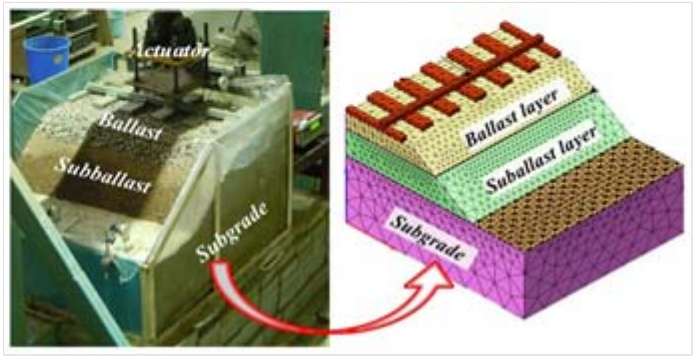

Technical Committee No. 8

Indian Geotechnical Society, New Delhi

September 2016

Foreword

The Indian Geotechnical Society has formed several Technical Committees in the early 2015 in order to generate relevant technical information and also to generate technical activities of the members. The Technical Committee No. 8 is formed especially to deliberate on the Numerical and Physical Modelling of geotechnical engineering and come out with a report that will be useful to geotechnical community. Both these aspects are important from the stand point of both researchers and practicing engineers.

With the active support from the IGS Ludhiana chapter, the TC has organized a one day workshop at Gurunanak Dev Engineering college campus on 3rd October 2015. The workshop was attended by more than 120+ delegates representing different parts of India from Academia and Industry. All lectures by taskforce members were planned in four sessions, two in the forenoon session and afternoon session. Prof. JN Jha, Professor and Head of the Department of Civil Engineering and the team of his faculty members at the college took an active role and provided all the logistical support for the organization of the workshop.

The workshop was attended by more than 120 delegates representing different parts of India from academia and industry. All the Technical Committee members gave lectures on different topics of the workshop and interacted with the delegates. Immediately after the workshop concluded, the members of the TC had deliberated on developing a small booklet that will guide the geotechnical engineering students, researchers and practicing engineers on various topics of numerical and physical modelling. This primer is a result of those deliberations.

The committee is immensely happy with this innovative initiative of the Indian Geotechnical Society and compliment the President and the EC members of the society. The committee members acknowledge the immense support received from the Indian Geotechnical Society and the IGS Ludhiana chapter, especially the authorities of Gurunanak Dev Engineering College, Ludhiana. We hope that this booklet will be useful in guiding the geotechnical community on appropriate numerical modelling and laboratory testing aspects. Please contact any of the members for obtaining more information on any relevant topic.

Prof. B.V.S. Viswanadham, IIT Bombay
Prof. BK Maheshwari, IIT Roorkee
Prof. J.T. Shahu, IIT Delhi
Dr. Priti Maheshwari, IIT Roorkee
Dr. T.V. Bharat, IIT Guwahati
Dr. B. Munwar Bhasha, IIT Hyderabad
Prof. K. Rajagopal, IIT Madras (Chair Person of the TC)

Table of Contents

Sl No.	Topic	Author(s)	Page No.
1	Centrifuge-based Physical Modeling of Geotechnical Structures	*Dr.-Ing.* B.V.S. Viswanadham	1
2	Physical Modeling of Typical Geotechnical Structures	Prof. J.T. Shahu	14
3	Guidelines for use of Numerical Procedures in Geotechnical Engineering	Prof. K. Rajagopal and Dr. B. Munwar Basha	20
4	Physical and Numerical Modeling for Dynamic Soil-Structure Interaction Problems	Prof. B.K. Maheshwari	33
5	Finite Difference Method in Numerical Modelling	Dr. Priti Maheshwari	53
6	Inverse Analysis in Geotechnical Engineering	Dr. Tadikonda Venkata Bharat	57
7	Reliability Based Load Resistance Factor Design (LRFD) for External Seismic Stability of Reinforced Soil Walls	Dr. B Munwar Basha	61

Centrifuge-based Physical Modeling of Geotechnical Structures

B.V.S. Viswanadham
Professor, Department of Civil Engineering,
Indian Institute of Technology Bombay, Mumbai
viswam@civil.iitb.ac.in

ABSTRACT: In the recent past, Centrifuge modeling has become one of the powerful tools for physical modeling in geotechnical engineering. Centrifuge modeling concerns the study of geotechnical processes using small scale models subjected to acceleration fields of magnitude many times Earth's gravity. These small scale model tests have proved to be particularly valuable in revealing mechanisms of deformation and collapse and in providing data for validation of numerical analyses. In this paper, the state-of-the-art of centrifuge modelling technique along with the attributes of a large beam centrifuge at the Indian Institute of Technology Bombay is presented. The paper also discusses the results of recent centrifuge model tests carried-out on this equipment for predicting the model behaviour of: (i) Cantilever sheet pile wall, (ii) steep reinforced slopes for urban areas and (iii) compacted soil liners of landfills.

1 INTRODUCTION

Physical modeling is concerned with replicating a process or a phenomenon in a reduced scale version of the prototype. A wide range of geotechnical problems can be investigated using physical modeling techniques. In the recent past, Centrifuge modeling has become one of the powerful tools for physical modeling in geotechnical engineering. Centrifuge modeling concerns the study of geotechnical processes using small scale models subjected to acceleration fields of magnitude many times Earth's gravity. These tests have proved to be particularly valuable in revealing mechanisms of deformation and collapse and in providing data for validation of numerical analyses. Validation of any numerical procedure depends heavily on reliable experimental data. In geotechnical engineering, centrifuge testing has been recognized as a useful tool to produce data for the validation of numerical procedures and insight into failure mechanisms. The paper presents the results of recent centrifuge model tests carried-out on this equipment for predicting the model behaviour of: (i) Cantilever sheet pile wall, (ii) geotextile reinforced slopes in urban areas and (iii) compacted soil liners of landfills along with scaling considerations for modeling sheet pile walls in a centrifuge.

2 CENTRIFUGE MODELING

Body force due to gravity plays an important role in geotechnical engineering problems. When studies are undertaken to understand the behaviour of real structures through scaled models, it is found impossible to simulate the body forces in the normal 1*g* field. The stress levels in a reduced scale model tested at normal gravity will be much smaller than in the prototype leading to different soil properties and loading conditions. Consequently, many phenomena of interest to the geotechnical engineer cannot be reproduced in laboratory models. Some of the problems cannot be modeled at all because of size considerations and unknown likeliness of occurrence (like landslides or natural hazards) or because of time effects (consolidation process) are involved. It has been realized that this deficiency can be overcome with the use of centrifuge modeling technique in which models are subjected to predetermined, high acceleration levels to produce similarity conditions satisfactorily in most conditions.

Centrifuge modeling is a technique for simulating the mechanical response of full-scale geotechnical structures in reduced-scale physical models. Analogues to this technique include flume testing in hydraulic engineering and wind tunnel testing in structural engineering. To achieve mechanical similitude in geotechnical models, it is necessary to replicate the materials' effective stress state. For example, if a model is made at 1/100 scale, it should be tested under an acceleration of 100 times earth's gravity.

In the international scene, considerable progress has been made in the last two decades in the utilization of this technique for a variety of complex problems and the interest of the geotechnical community in this area is reflected by the number of conferences and symposia held on this topic and also by the number of centrifuge facilities built in various parts of the world. Centrifuge modeling is now firmly established as a dependable research tool that can provide solutions to many of the hitherto intractable problems in geotechnical engineering. A wide range of geotechnical problems can be investigated. The aim of centrifuge modeling is to reproduce prototype stress conditions at homologous points in the model. This is achieved by subjecting a model scaled by a factor N to a centrifugal acceleration N times normal gravity.

In the field situation, the vertical stress due to self-weight at a depth d_p is given by $\sigma_p = \gamma d_p$, where γ is the unit weight of the soil. In a $1g$ model, whose linear dimension is reduced by a factor N the vertical stress due to self-weight also gets reduced by a factor N. Thus the resulting vertical stress σ_m will be given by $\sigma_{m(1g)} = \gamma d_p/N$. However, if the same model is tested in a centrifuge where the unit weight is increased by a factor N the resulting vertical stress σ_m is the same as in the prototype as follows: $\sigma_{m(Ng)} = (\gamma N)d_p/N = \gamma d_p = \sigma_p$. This can be achieved by rotating the model in a horizontal plane at a desired angular velocity ω. Centrifuge scaling relationships and errors due to variation in acceleration along the radius have been discussed extensively in the literature (Schofield, 1980).

2.1 Reason for Model Testing on the Centrifuge and Typical applications

Geotechnical materials such as soil and rock have nonlinear mechanical properties that depend on the effective confining stress and stress history. The centrifuge applies an increased "gravitational" acceleration to physical models in order to produce identical self-weight stresses in the model and prototype. The one to one scaling of stress enhances the similarity of geotechnical models and makes it possible to obtain accurate data to help solve complex problems such as earthquake-induced liquefaction, soil-structure interaction and underground transport of pollutants such as dense non-aqueous phase liquids. Centrifuge model testing provides data to improve our understanding of basic mechanisms of deformation and failure and provides benchmarks useful for verification of numerical models. A geotechnical centrifuge is used to conduct model tests to study geotechnical problems such as the strength, stiffness and capacity of foundations for bridges and buildings, settlement of embankments, stability of slopes, earth retaining structures, tunnel stability and seawalls. Other applications include explosive cratering, contaminant migration in ground water, frost heave and sea ice. The centrifuge may be useful for scale modeling of any large-scale nonlinear problem for which gravity is a primary driving force.

2.2 Scaling Laws

If a 0.5 m deep model container is filled with soil, placed on the end of a centrifuge and subject to a centrifugal acceleration of 100 g, the pressures and stresses are increased by a factor of 100. So, the vertical stress at the base of the model container is equivalent to the vertical stress at a depth of 0.5 m x 100 = 50 m in the earth and the 0.5 m deep model

represents 50 m of prototype soil. The reason for the centrifuge is to enable small scale models to feel the same stresses as a full scale prototype. This can be stated mathematically as:

$$N_\sigma = \sigma_{\text{model}} / \sigma_{\text{prototype}} = 1 \quad (1)$$

Here σ represents any quantity with units of pressure (modulus, shear strength, stress, pressure). The asterisk denotes a scale factor for that quantity. The stress scales in proportion to the product of density (ρ), gravity (g), and depth (L). If we force $N_\sigma = 1$, it follows that

$$N_\sigma = \rho^* g^* L^* = 1 \quad (2)$$

If the same materials are used in model and prototype so that the scale factor for density is: $N_\rho = 1$, then the gravity scale factor $N_g = 1/L$. In other words, if the model is 100 times smaller than the prototype, then the model gravity must be 100 times greater than the prototype gravity. Similar logic to that presented above can be used to derive a consistent set of scale factors for other quantities.

2.3 Geotechnical Centrifuges

Geotechnical centrifuges benefit from the additional centripetal forces acting on a model while the centrifuge is rotating and increases self-weight of the soil and maintains identical stress-strain behaviour of soil for both in model and prototype. Fig.1 illustrates two different types of centrifuges, namely (i) Beam centrifuge with a swinging basket (ii) Drum centrifuge. Most of the centrifuge centers worldwide use beam centrifuges. In the beam centrifuge, a model is usually placed on a swinging basket on one side of the arm and balanced by a counterweight on the other side. The model swings up while the centrifuge rotates: gravitational forces act vertically, and centripetal forces horizontally, on the swinging basket. This causes an artificial acceleration field to act on the sample, while the basket rotates into the direction of the sum of the acceleration components. This acceleration field provides the increase of gravity on the sample. They are very few drum centrifuges in operation worldwide. In a drum centrifuge, the soil sample is constructed in the channel (on the periphery of a drum) over the whole circumference of the machine. The advantage of a drum centrifuge over a beam centrifuge is the possible of accessing the soil model by the central tool table, which also rotates in synchronization with drum. The tools (like actuators), can be activated and their positions can be changed without disturbing the soil sample in the drum. This improves the flexibility of modeling and limits the number of stress cycles or short durations during which the model must be exposed to 1g and Ng conditions. Fig. 2 illustrates a soil layer in prototype and its corresponding centrifuge model.

As can be seen from Fig. 2, due to rotation acceleration field the variation of vertical stress in a centrifuge model is non-linear with depth against a linear variation of geostatic stress with depth in the prototype. This non-linear variation cause under stressing with in the top two-thirds portion and overstressing at the bottom of the container. The error due to under stressing and overstressing can overcome by inducing a desired enhanced gravity at point (herein it is referred as an effective radius R_e) where the prototype and model stresses are identical. The error due to vertical stress can be maintained well below 3 % if the ratio of model height to the effective radius ($h_m/R_e<0.2$).

Fig. 3 presents the variation of centrifugal acceleration in models of a 10 m soil layer [N =50]. The prototype soil layer of 10 m thick was assumed to model in two different centrifuges, one is having a small radius equal to 1.0 m and in the second case, the radius of

the centrifuge equals to 4.0 m. Due to radial acceleration field, the g-level varies horizontally (except in a drum centrifuge) as well as vertically. The variation of g-level with depth as well as horizontal distance is on the higher side for the model tested in a small centrifuge than the model tested in a large centrifuge. This necessitates the requirement of large centrifuge.

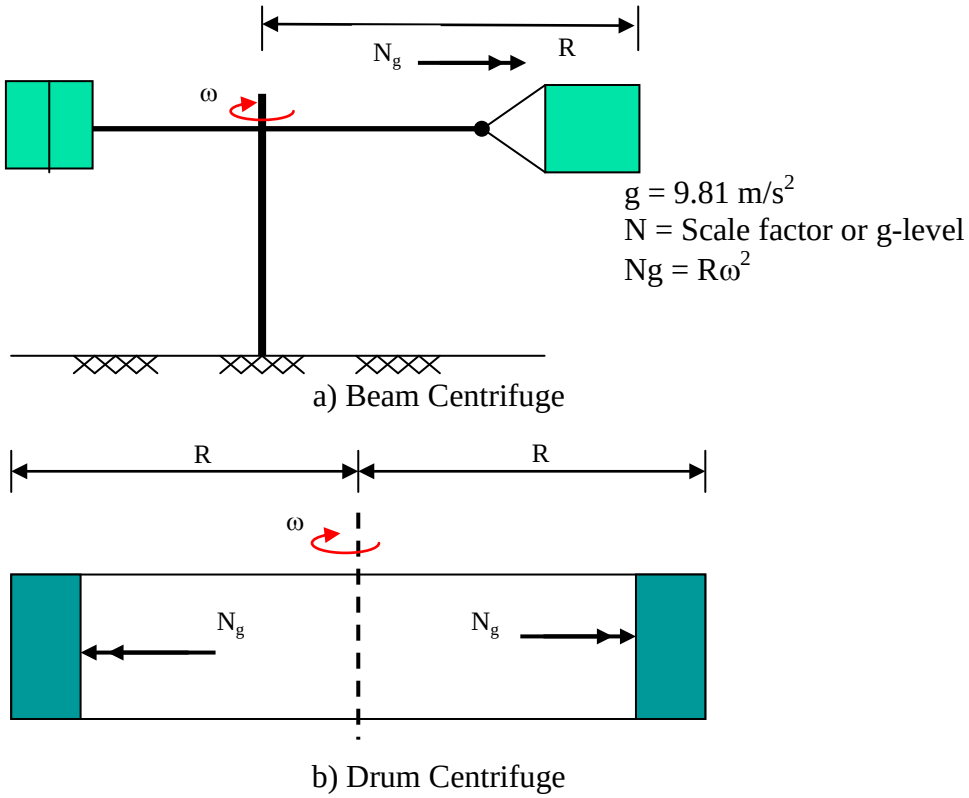

Figure 1: Schematic sketch illustrating mechanics relating to two types of centrifuges

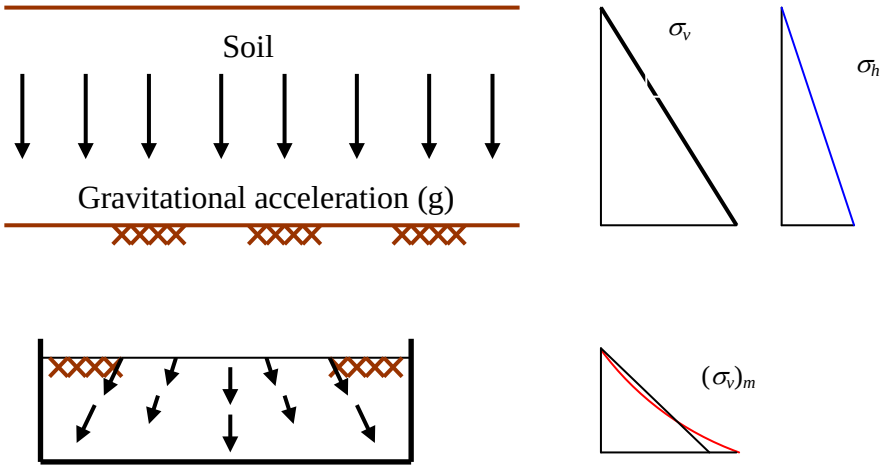

Figure 2: A soil layer in prototype and its corresponding centrifuge model

2.4 Centrifuge Equipment

The large beam centrifuge at Indian Institute of Technology Bombay (IIT Bombay) is being used for studying number of problems of importance in geotechnical and geoenvironmental engineering. The 4.5 m beam centrifuge is housed in 11 m concrete chamber at the ground level with a height of 3.3 m. A 450 kW DC motor housed in the motor room located below ground level powers the centrifuge. The instrumentation and console rooms are located on either side of the entrance door of the centrifuge chamber. The centrifuge capacity is 250 g-ton with a maximum payload of 2.5 t at 100*g* and at higher acceleration of 200*g* the allowable payload is 0.625 t. The centrifuge has a swing basket at one end and an adjustable counterweight at the other end. Summary of major parameters of the beam centrifuge at IIT Bombay are given in Table 1. The other specifications are given elsewhere by Chandrasekaran (2001). Centrifuge can be operated at the desired *g*-level through a console or a computer interface with a programmable logic controller with the power supply. Fig. 4 presents details of payloads and capacities of beam centrifuges in the world along with large beam centrifuge beam facility at Indian Institute of Technology Bombay.

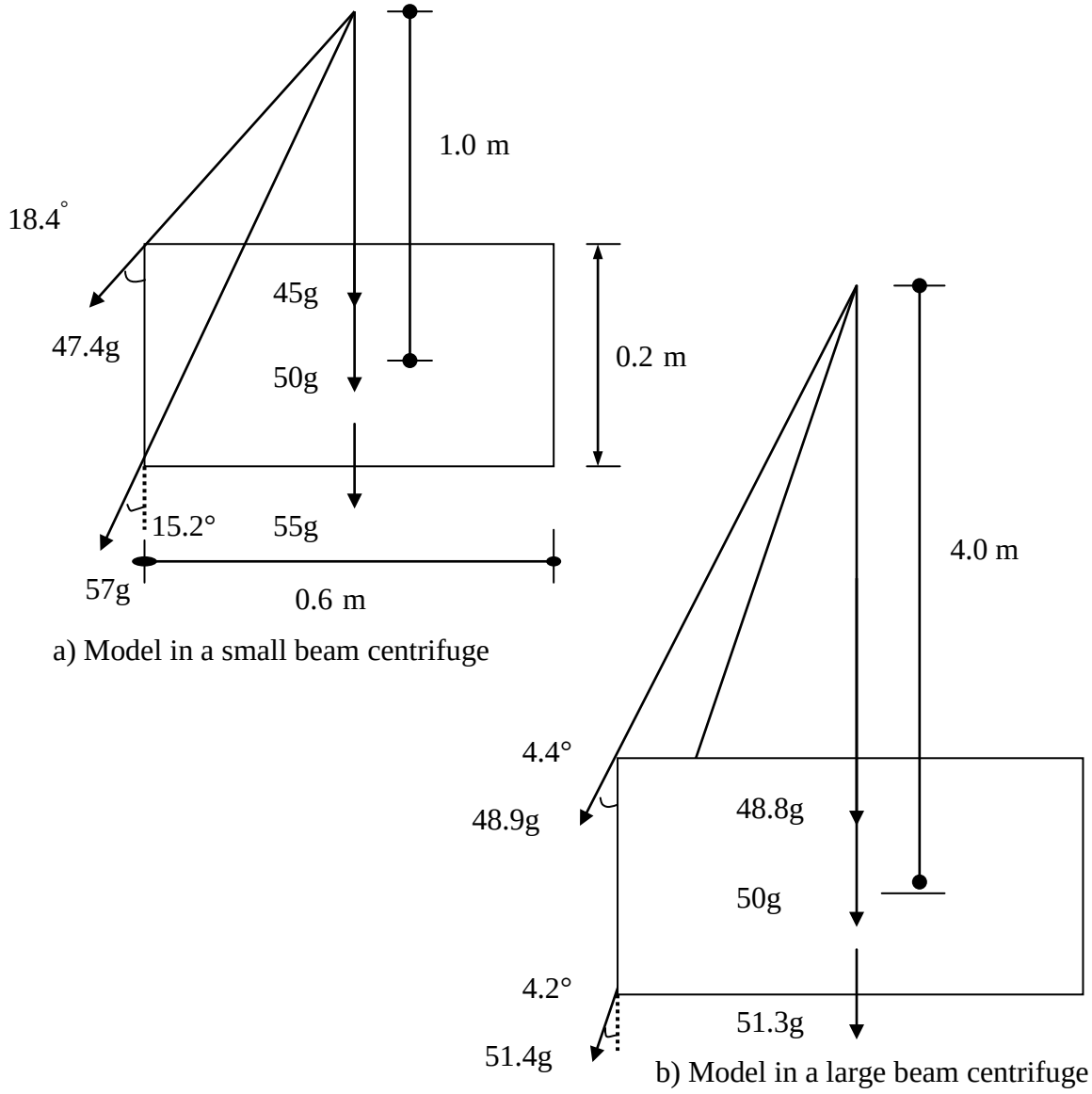

Figure 3: Variation of centrifugal acceleration in models of a 10 m soil layer [N =50].

Table 1: Details of the centrifuge equipment.

Parameter	Details
Maximum radial acceleration	200g
Maximum pay load	2.5 t
Capacity	250 g-t
Radius	*4.5 m
Model area	-1.0 m x 1.2 m (0.66 m height)
	- 0.76 m x 1.2 m (1.2 m height)

* Measured from central axis of shaft to the top surface of the swinging basket

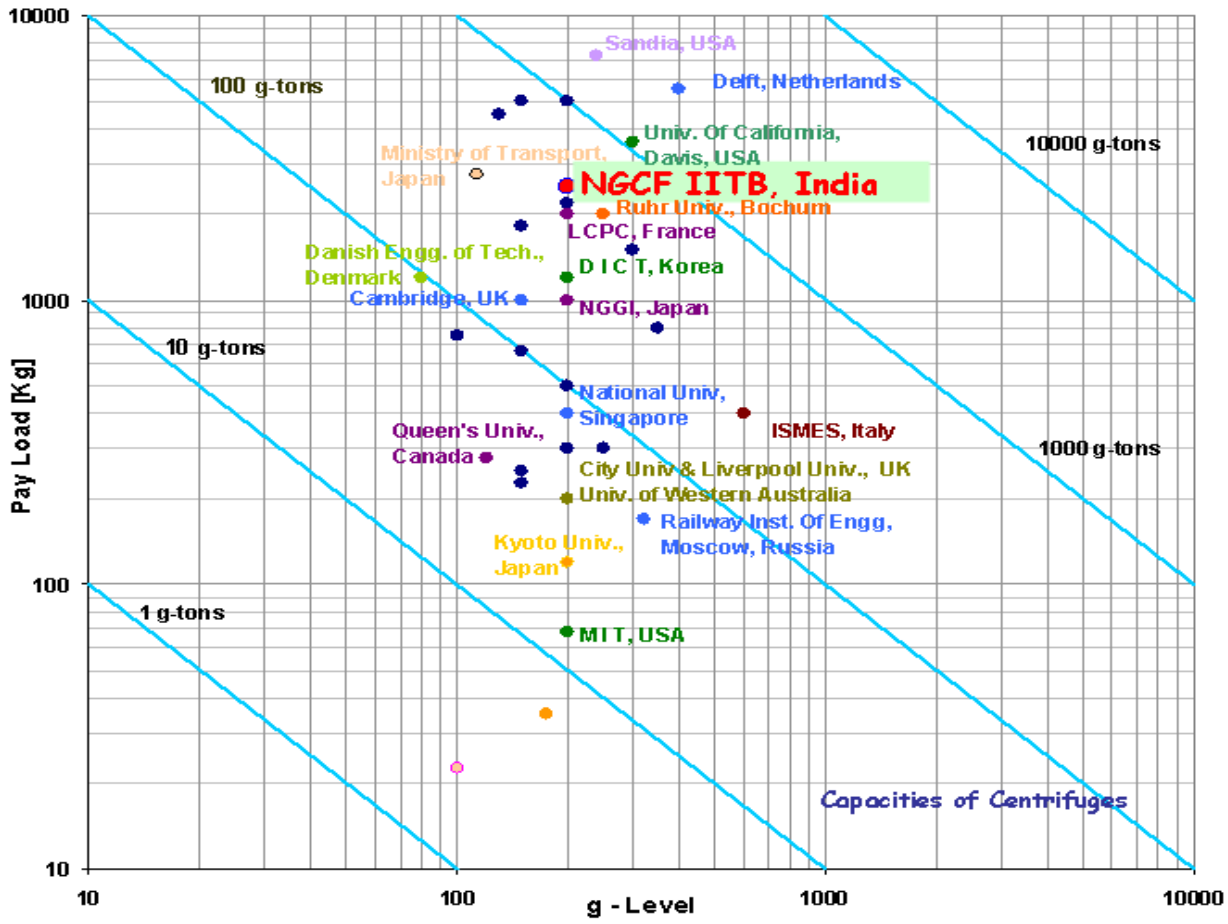

Figure 4: Variation of payload with g-level for selected beam centrifuges

2.5 Scaling Considerations for Modeling Sheet Pile Walls in a Centrifuge

For a cantilever sheet pile wall in the field, the earth pressure due to granular fill at a depth h is given by $(\sigma_h)_p = k_a\gamma h$, where γ is the unit weight of the soil and k_a is the coefficient of the active earth pressure. In a 1g model, whose linear dimension is reduced by a factor N the earth pressure due to granular fill also gets reduced by a factor N. Thus the resulting earth pressure $(\sigma_h)_m$ will be given by $(\sigma_h)_{m\ (1g)} = k_a\gamma h/N$. However, if the same model is tested in a centrifuge where the unit weight is increased by a factor N the resulting vertical stress $(\sigma_h)_m$ is the same as in the prototype as follows: $(\sigma_h)_{m\ (Ng)} = k_a(\gamma N)h/N = (\sigma_h)_p$. This can be achieved by rotating the model in a horizontal plane at a desired angular velocity ω. The above situation is illustrated schematically in Fig. 5. A set of scaling laws related the behaviour of the centrifuge model to the prototype. For the case of modeling of sheet-pile walls in a geotechnical centrifuge, a set of scaling relations are given in Table 2. Thus for a model that is $1/N^{th}$ scale of the prototype and tested at Ng the stresses and strains will be same at homologous points in the prototype. Therefore the non-linear constitutive behaviour of the soil is fully captured in the centrifuge modeling technique and the soil model will mobilize the correct stiffness corresponding to the stresses and strains in the prototype. All of which can be derived by simple dimensional analysis.

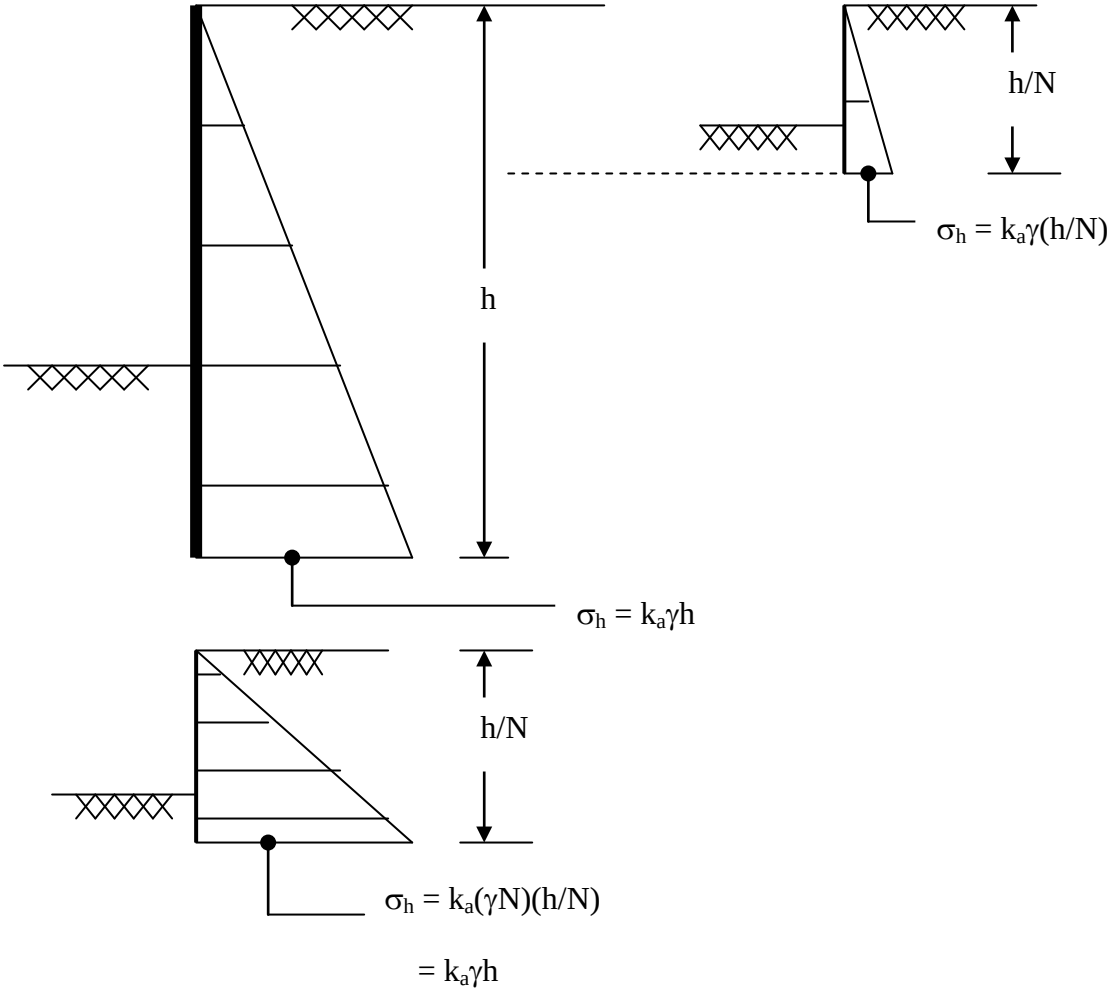

Figure 5: Principle of centrifuge modeling technique

Table 2: Summary of scaling relations

Parameter	Prototype	Model
Length [m]	1	#1/N
Area [m^2]	1	$1/N^2$
Volume [m^3]	1	$1/N^3$
Velocity [m/sec]	1	1
Acceleration [m/sec^2]	1	N
Mass [kg]	1	$1/N^3$
Mass density [kg/m^3]	1	1
Force [kN]	1	$1/N^2$
Stress [kN/m^2]	1	1
Strain [%]	1	1
Time [Consolidation] sec	1	$1/N^2$
Time [dynamic] sec	1	1/N
Bending Moment per unit width (N-m/m)	1	$1/N^2$
*Flexural rigidity/unit width (kN- m^2/m)	1	$1/N^3$
Geotextile tensile strength (kN/m)	1	1/N
Geotextile stiffness (kN/m)	1	1/N

N = Scale factor or gravity level; #L_m/L_p=1/N; Where L_m is the length dimensions in the model and L_p is the Length dimensions in the prototype;*Valid for $E_m = E_p$; E = Young's modules of elasticity [kN/m^2]; Suffix m = model; p = prototype.

3 PREDICTION OF THE BEHAVIOUR OF DIFFERENT GEOTECHNICAL STRUCTURES

The following sections deal with summary of results of the following: (i) Deformation behaviour of Cantilever Sheet Pile wall, (ii) Stability and deformation behaviour of geotextile reinforced steep slope, and (iii) deformation behaviour of compacted clay liners of landfills. Centrifuge tests were executed in a large beam centrifuge. The models were constructed using selected model materials by satisfying the scaling considerations given in Table 2. Details of model test package and instrumentation are discussed elsewhere.

3.1 Deformation Behaviour of Cantilever Sheet-Pile Wall

Cantilever sheet pile walls are routinely used in geotechnical practice. While their design is common place, the interaction between the soil and the sheet pile wall required to generate the active and passive pressures is quite interesting. Many researchers have addressed this

problem. One of the mechanisms of failure of these walls especially with granular backfill is by formation of a plastic hinge.

Centrifuge tests were carried out on model sheet pile walls supporting granular fill at the large Beam Centrifuge Facility at Indian Institute of Technology Bombay. The centrifugal acceleration was increased gradually until the sheet pile wall suffered failure due to formation of a plastic hinge. The deflections of the sheet pile wall and the settlement of the backfill were monitored using LVDT's. Video image capturing software was also used to monitor the state of the model in-flight. One of the main features of the National Geotechnical Centrifuge Facility at IIT Bombay is its large platform. This made it possible to use a large container (760 mm in length, 410 mm in depth and 200 mm in width). The friction between front and rear walls and soil is reduced by applying a thin layer of white petroleum grease and by placing thin flexible polythene sheet strips of width 100 mm. With this arrangement, it was found that the friction effects can be reduced and plane strain conditions are achieved. The soil used in the centrifuge test was uniformly graded locally available Goa sand. The void ratio of the model was 0.751 and the relative density was about 55 %. The maximum void ratio for this sand is 0.96 and minimum void ratio is 0.58. In this model the sand was dry.

Fig. 6 presents situation of the model at different acceleration levels. As can be seen, rupture surfaces were getting initiated at 20g and thereafter they were completely developed at 30 g. The test was carried-out upto 50g and stopped after observing the considerable lateral movement of the wall at the top. The highlighted portion of wall situation during centrifuge test at 35g is shown in Fig. 6d, wherein formation of multiple rupture surfaces can be noted. Fig. 6d illustrates the state of wall at 35 g during the centrifuge test. For the model wall section used in the centrifuge test, plastic moment calculations were performed to estimate the plastic moment capacity. The plastic moment capacity of the model wall section per meter width may be calculated by using equation (3)

$$M_p = f_y Z_p \quad (3)$$

Where Zp = plastic modulus, which is equal to $\frac{bt^2}{4}$, t = thickness of the model sheet pile wall, b is the width of the sheet pile wall and fy is the yield stress of Aluminum alloy. Choosing b = 1m and t = 0.003 m, the plastic modulus of the section is calculated to be 2.7225 x 10-6 m2. Substituting for Zp and fy from above in equation 1, the plastic moment capacity is obtained as 326.7 Nm/m (with fy is 120 MPa).

As discussed earlier, the computed maximum bending moment at 30g is already 258 Nm/m and which is still found to be less than the estimated plastic moment capacity. It was observed that the wall attained plastic moment capacity at 35 – 40 g during centrifuge test. In the centrifuge test, the plastic hinge was determined using the deflected shape of the sheet pile wall during post test investigation.

3.2 Prediction of Deformation Behaviour of Geotextile Reinforced Slopes

The application of polymeric reinforcement in the construction of steep reinforced slopes is becoming more common. The reinforcement permits construction of stable slopes at angles steeper than that would be possible without reinforcement, allows the use of weaker soils, and provides a reduction in the land - take. The interaction between the soil and the reinforcement layers provides tensile resistance to the driving forces caused by self weight and any applied surcharge. The internal mechanisms of failure of these geotextile reinforced slopes are particularly due to: (i) rupture of reinforcement layers and (ii) pull-out failure along the soil-geotextile interface. Centrifuge tests were carried out on model geotextile reinforced slopes with 63° slope inclination, reinforcement layers spaced at 30 mm vertically and with a ratio of length of reinforcement to height of slope equal to 0.85) constructed of sand at the large

Beam Centrifuge Facility as a part of on-going MHRD project. To maintain a flexible facing for a geotextile-reinforced slope, the wrap-around technique was adopted. The centrifugal acceleration was increased gradually until the geotextile-reinforced slope suffered failure either due to rupture of reinforcement layers or through pullout. The lateral displacements of the geotextile reinforced slope and the surface settlement of slope were monitored using LVDTs. Video image capturing software was also used to monitor displacements of the model in-flight. The centrifuge test results were found to give useful information about the behaviour of geotextile reinforced slopes under pre-failure conditions and at failure.

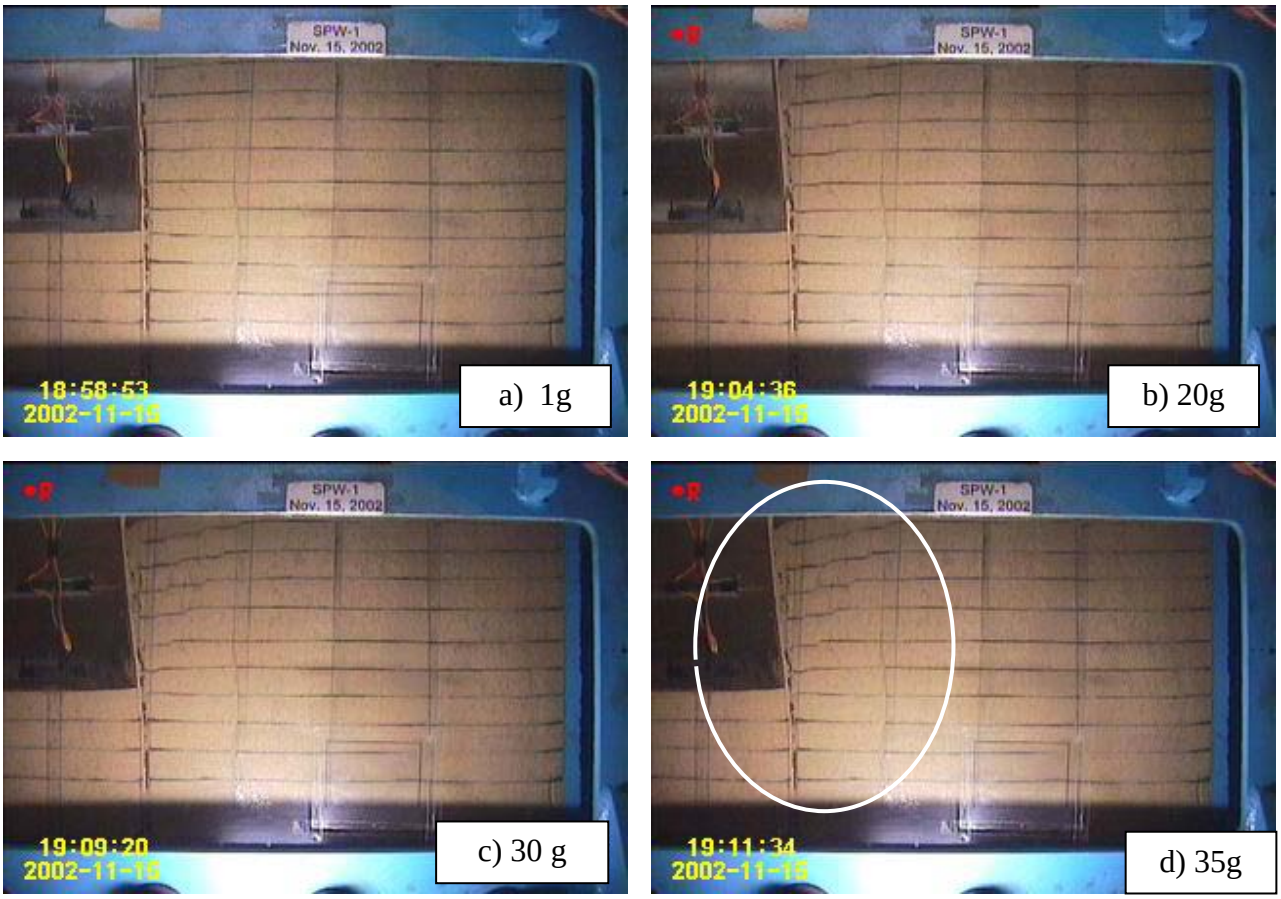

Figure 6: Deformation of cantilever sheet pile wall during the centrifuge test

Fig. 7 shows the model before and during the centrifuge test at 25 g for a test RS4. Initiation of the failure surface was observed to take place at 15 g before it developed completely at 25 g. The test was carried-out up to 30g and stopped after observing the collapse of the reinforced slope model. The failure surface can be seen in Fig. 7b.

Fig. 8 presents variation of surface settlements measured on the top of the slope during centrifuge model testing for model MRS7 with time. L4 in the figure indicates LVDT placed at the crest and L3, L2, L1 are LVDTs placed away from the crest with 100 mm center-to-center distance. As can be seen, at the onset of failure the measured drastic increase in surface settlement reading for L4 enables to predict the g-level at which the collapse of the reinforced slope during the centrifuge test.

.

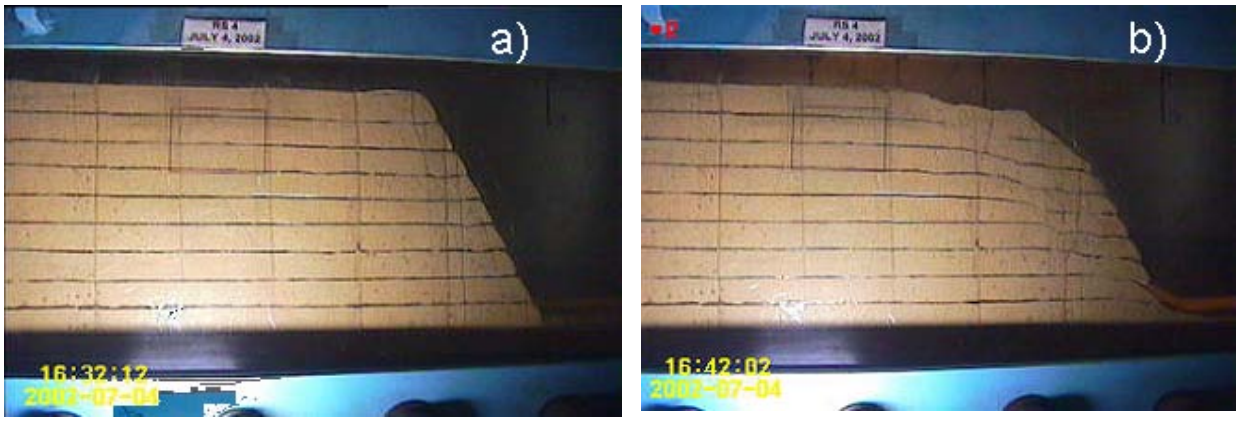

Figure 7: Deformation of geotextile reinforced slope before and during the centrifuge test

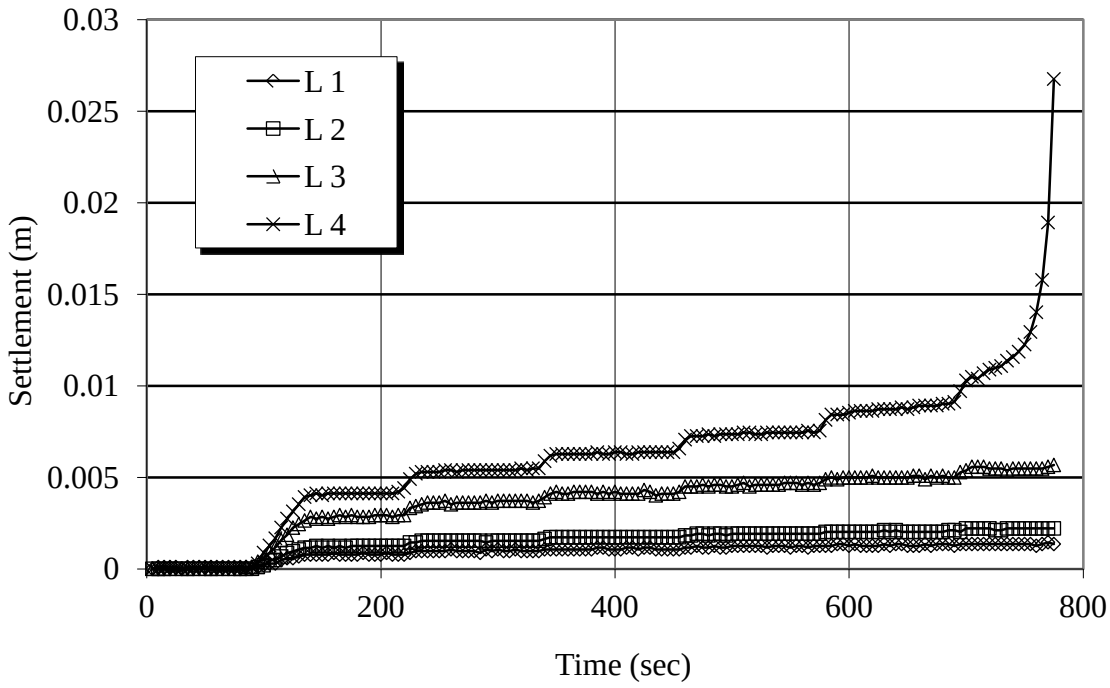

Figure 8: Variation of surface settlement of the slope with time (model dimensions)

3.3 Prediction of Deformation Behaviour of Compacted Clay Liners of Landfills

Among different impermeable layers, compacted clay liners are regarded as one of the most significant components of liner system and are being widely used worldwide as a waste containment system in landfills. One of the failures associated with clay liners of landfills is the occurrence of non-uniform settlements, resulting due to sudden collapse of waste, or decomposition of waste materials, and/or the subgrade over which the lining system is laid. These problems lead to poor performance and often result in cracking of compacted clay liners of liner systems. This problem is more pronounced in case of a top lining system than the bottom lining system because the former is subjected to low overburden pressure as well as settlement due to readjustment and ongoing biodegradation of the wastes that lies underneath.

The following paragraphs present the use of a geo-centrifuge to predict the deformation behaviour of compacted clay liners. A special device for inducing non-uniform settlements during centrifuge test has been custom designed, developed and calibrated. The model clay liner material has been selected in such a way that it envelopes the material characteristics of the clay liners that are used as an impermeable barrier in a liner system. A large container having internal dimensions of 760 mm in length, 410 mm in depth and 450 mm in width was used in the present study. Results of three models, namely SSL3, SSL4 and SSL7 are presented. All the models were subjected to 40g by rotating the model at 93 rpm about a vertical axis in the horizontal plane. By this arrangement it was possible to model a landfill area as large as 520 m^2 in the prototype scale and simulates the ongoing non-uniform settlements undergoing over large areas of landfills. Two thicknesses of liners were considered. For the model SSL3 and SSL4, the thickness of liners is 50 mm (2 m) and 30 mm (1.2 m) compacted at maximum dry unit weight and optimum moisture content as per standard Proctor compaction respectively. For the model SSL7, the model clay liner of 30 mm thick (1.2 m) was compacted at its maximum dry unit weight and optimum moisture content as per modified compaction. Equivalent thickness of liners is given within the parentheses. All the models were subjected to non-uniform settlements upto a maximum central settlement equal to 25 mm (1.0 m) with a constant settlement rate of 0.85 mm/min.

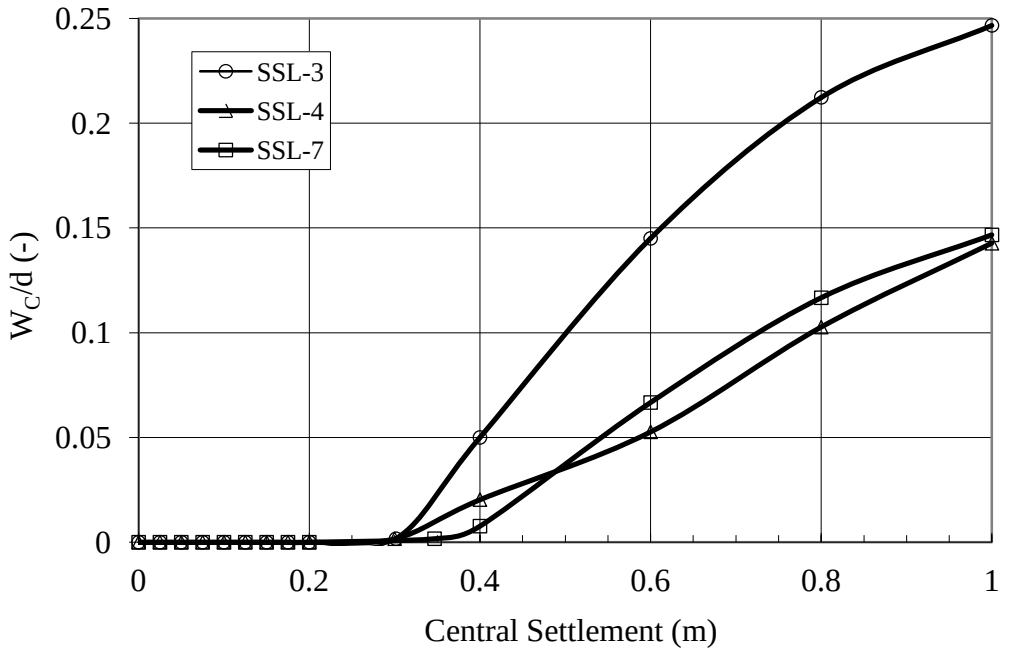

Figure 9: Variation of W_c/d with central settlement

Digital image analysis techniques were used to ascertain the initiation of cracking and to compute strains both on the surface and the cross section of the clay liner. Fig. 9 presents the variation of ratio of crack width to the liner thickness (W_c/d) with maximum central settlement for models SSL3, SSL4 and SSL7 respectively. Digital image analysis of the portion of the liner viewed through a camera fixed on the top of the model enabled to monitor the prognosis of the crack development on the surface. Fig. 10 presents variation of maximum outer fiber strain (measured from the markers embedded along the cross-section of the model clay liner) with a curvature radius at the maximum curvature zone along the top surface of the model liner. With a decrease in the curvature radius, an increase in the outer fiber strain can be observed. The results indicate that thick liners attract higher outer fiber strains than thin liners and also experience wide width cracking. The clay liner compacted at

its maximum dry unit weight and optimum moisture content as per modified compaction was observed to experience delay in the initiation of cracking and the liner was observed to crack at a curvature radius R = 90 m against R = 170 m. These centrifuge tests predict the significant influence of thickness and compactive effort on the deformation behaviour of compacted clay liners of landfills at the onset of non-uniform settlements.

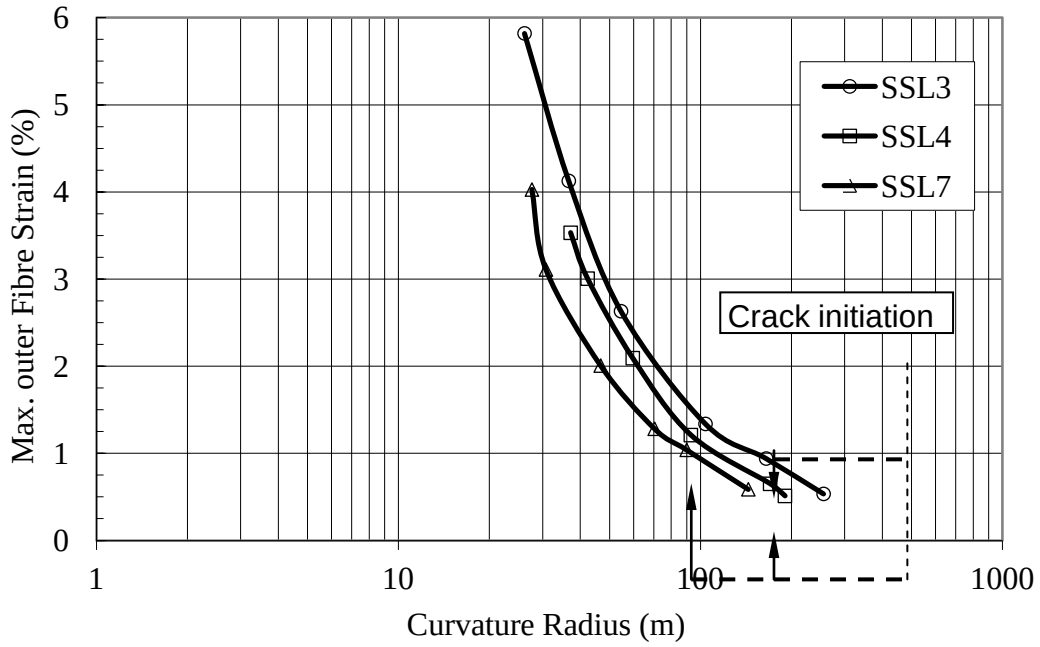

Figure 10: Variation of maximum outer fiber strain with curvature settlement

4 CONCLUSIONS

Centrifuge modeling is a technique for simulating the mechanical response of full-scale geotechnical structures in reduced-scale physical models. The paper discusses the results of recent centrifuge model tests carried-out on a large beam centrifuge facility available at Indian Institute of Technology Bombay for predicting the model behaviour of: (i) Cantilever sheet pile wall, (ii) steep reinforced slopes in urban areas and (iii) compacted soil liners of landfills. Further the potential of centrifuge modeling technique in predicting the behaviour of geotechnical structures have been demonstrated adequately.

ACKNOWLEDGEMENTS

The author would like to thank the Sudarshan team at National Geotechnical Centrifuge Facility, IIT Bombay for their untiring support in execution of centrifuge model tests and upkeep of the laboratory. Special thanks are also due to (both current and former) students for their efforts in planning and execution of centrifuge model tests.

REFERNCES

1. Chandrasekaran, V.S. (2001) Numerical and Centrifuge modelling in soil-structure interaction. *Indian Geotechnical Journal*, 31(1), 1-59.
2. Schofield, A.N. (1980) Cambridge University Geotechnical Centrifuge Operation. *Geotechnique*, 30(3), 227-268.

Physical Modeling of Typical Geotechnical Structures

J.T. Shahu
Professor, Department of Civil Engineering,
Indian Institute of Technology Delhi
shahu@civil.iitd.ac.in

1 INTRODUCTION

Physical modeling plays a fundamental role in development of geotechnical understanding. To investigate the engineering behavior of civil engineering structures, it is often practical and economical to replicate the prototype structure into small scale model and carry out the necessary testing. Model tests provide an alternative way to directly reflect the behavior of the prototype under simulated conditions and are used to validate theoretical or empirical hypotheses. However, the success of such an approach depends upon the accuracy of the modeling process. The modeling process is explained below through physical modeling of two different prototype geotechnical structures, namely, stone column group foundation and geosynthetic reinforced railway track structure.

2 STONE COLUMN GROUP FOUNDATION

Similitude ratio refers to the ratio of any linear dimension of the model to the corresponding dimension of the prototype. Whereas usually it is the short-term bearing capacity of the foundation that is critical consideration under small stone column foundation groups, it is the long-term drained settlement response of the large groups that is important. In this article, modeling details of fully drained model tests on groups of stone column-mat foundation placed in a slurry deposited clayey soil bed of known effective stress state are presented (refer Shahu and Reddy 2011; Wood et al. 2000).

The model tests have not been performed with any particular prototype in mind but are shown as a generic study. All tests were conducted in the laboratory at constant temperature and humidity conditions, and each test took approximately 45–60 days for completion. Because the mechanism of deformation and pore pressure dissipation in a floating stone column group foundation is rather complex, the fully drained behavior can only be ensured in load-controlled tests. Important details related to boundaries, dimensions, materials, and loading conditions in the model vis-a-vis the actual prototype were given due consideration as presented below.

For fully drained loading conditions, the longer the drainage path, the longer the duration of the test. To reduce the total test duration, a minimum possible similitude ratio is desirable owing to extremely low permeability of the clayey soil. Also, the bigger the size of the footing, the heavier the footing load required. A typical prototype stone column diameter varies from 0.6 to 1.0 m and length from 5–20 m. It was observed that the model columns can be reliably installed ensuring proper continuity and integrity if the column diameter is at least 13 mm. Because of this, 13 mm diameter columns were used in model tests, giving rise to a similitude ratio between 0.013 and 0.022. Usually, l/d ratio in the prototype stone columns varies between 5 and 20, in which l and d are the column length and diameter, respectively. Based on this, the l/d ratio in the model tests was adopted as 8 and 12 (corresponding to the model column lengths of 100 and 150 mm).

The model tank boundaries were determined on the basis of criterion that induced stresses should be insignificant at the tank boundaries. Assuming an equivalent footing located at two-third depth of the columns and 2:1 spread, Fig. 1 shows the stress distribution for 100 mm diameter footing and 150 mm long columns (representing the worst case). At a depth

equal to twice the width of the foundation, induced stresses may be assumed to be approximately equal to 11% of the applied stresses. Thus, Fig. 1 shows that the induced stresses become insignificant at tank boundaries if the tank diameter and tank depth are 300 mm or more. On the basis of this, all tests were conducted in tanks of 300 mm diameter and 300 mm depth.

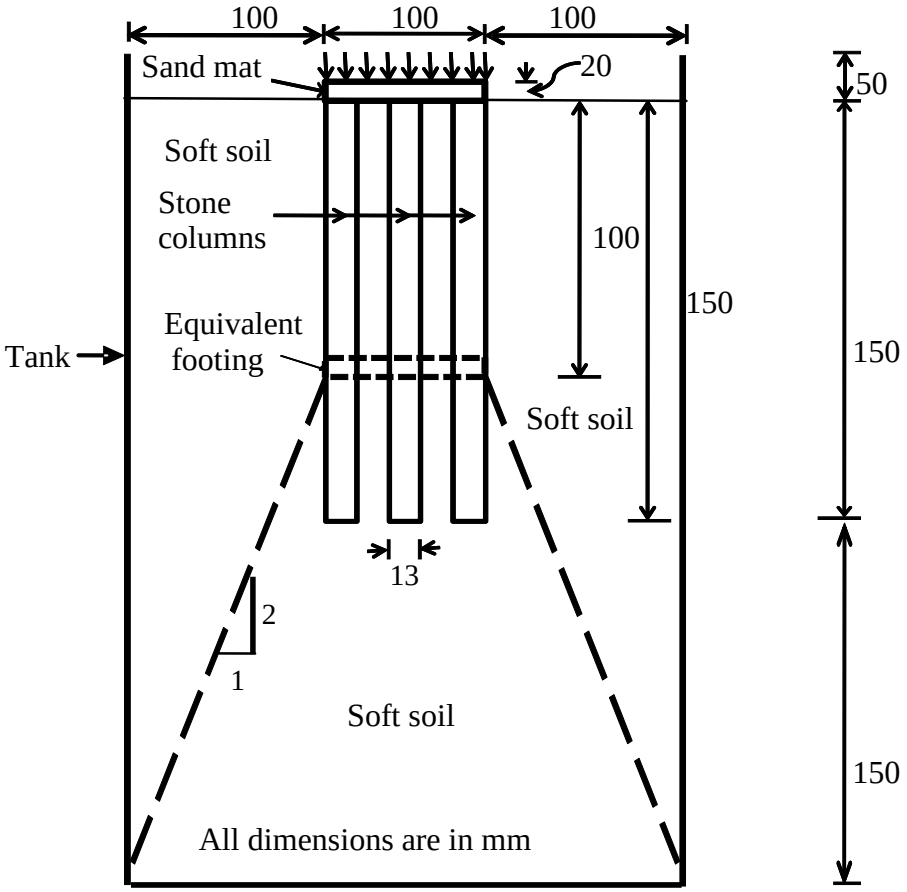

Figure 1: Schematic view of stone column foundation

Prototype stone columns (diameter d = 0.6–1.0 m) are usually made of stones of particle sizes D = 25–50 mm. Thus, $d = D$ ratio approximately varies between 12 and 40. The column diameters used in the model tests were 13 and 25 mm. The particle sizes of the made-up Badarpur sand used in the model tests as the granular material for the column and mat were kept between 1 mm and 425 μm. Thus the ratio $d = D$ in the model tests has values ranging from 13–59, which compare well with the corresponding values for the prototype foundation.

3 GEOSYNTHETIC REINFORCED RAILWAY TRACKS

The model presented below is representative of typical prototype track structures found in northern and central parts of India. Based on practical considerations, a full panel model track with a similitude ratio of one-third is used in this study. A schematic view of the model track panel is presented in Fig. 2(a). A comparison of the prototype track and the model track is provided in Table 1.

Model dimensions were scaled down as per the similitude ratio in such a way that induced stresses in the model remain the same as those in the prototype. It was assumed that the rail transfers stresses on to the sleepers by beam action and that the sleepers then transfer the

stresses to the ballast layer mainly by direct bearing. Rectangular steel sleepers were used in the model with all of the dimensions reduced as per the similitude ratio except thickness to simulate the load transfer by bearing. The thickness of the model steel sleepers t_s was reduced by comparing the flexural rigidity (EI) of the model steel sleepers with that of the prototype pre-stressed cement concrete sleepers (refer Sowmiya and Shahu 2016). Based on symmetry, only one-half of the model track was constructed and a smooth boundary was provided along the center line (Fig. 2b). A load was applied on the top of the rail that, based on the equivalence of induced stresses in the model and the prototype, was equal to one-ninth of that applied on the prototype track.

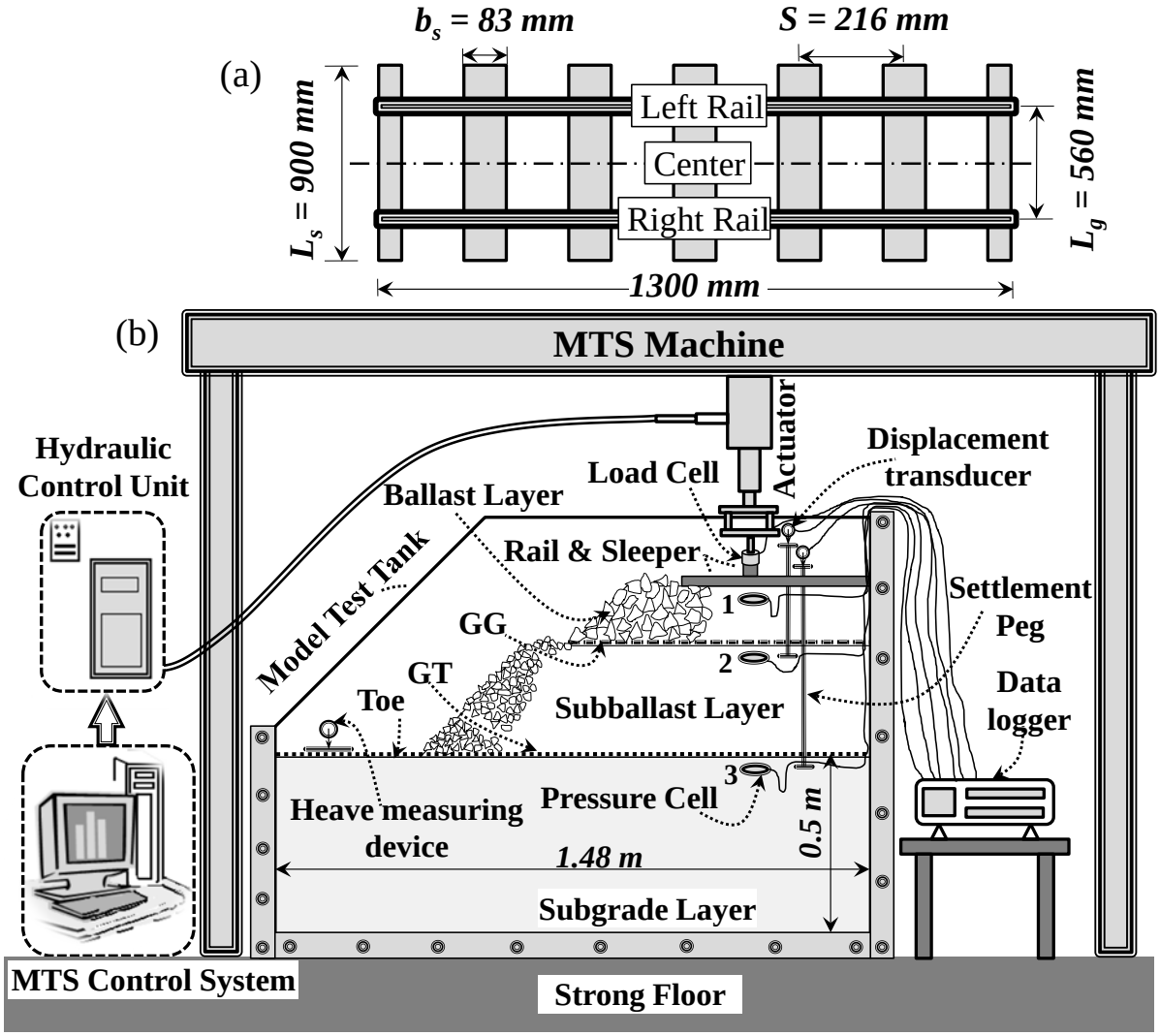

Figure 2: A schematic view of track panel and model test setup (a) Model track panel (b) Model test setup with MTS controlling unit (after Sowmiya and Shahu 2016)

A geogrid is employed at the ballast-subballast interface and/or a geotextile is used at the subballast-subgrade interface. The scaling down of the stiffness and strength of the geogrid is required because in spite of the equivalence of vertical stresses at the interface, tensile stresses induced in geogrid in the model will not be similar to the geogrid stresses in the prototype due to differences in linear dimensions of model and prototype (refer Sowmiya and Shahu 2016). Also, the scaling down of the aperture size of the geogrid is required in order to simulate ballast-geogrid interaction (for example, strike through of ballast particles from the plane of geogrid) similar to that in the field.

Table 1: Comparison of Model and Prototype

Material/Parameters	Model	Prototype	Scale
Geogrid			
Aperture, (mm)	30	90	3
Rib thickness, (mm)	2.0	6.0	3
Secant modulus (at 5%), kN/m	513	4617	9
Geotextile			
AOS, (mm)	0.14	0.14	Same
Thickness, (mm)	2.2	6.6	3
Secant modulus (at 5%), kN/m	90	810	Sowmiya & Shahu (2016)
Sleeper			
L_s (m)	0.9	2.7	3
b_s (cm)	8.3	25.0	3
S (cm)	21.6	65.0	3
t_s (cm)	3.45 (steel)	21.0 (PCC)	Sowmiya & Shahu (2016)
Rail			
I_r (cm^4)	26.64	2158	$3^4 = 81$
L_g (m)	0.56	1.68	3
Ballast			
Particle size (D_{max}), mm	30	90	3
Layer thickness (mm)	116.6	350	3
Subballast			
Particle size (D_{max}), mm	20	60	3
Layer thickness (mm)	200	600	3
Subgrade			
Particle size (Dhanaury clay), (D_{max}) mm	0.075	0.075	Same
Thickness, (m)	0.5	1.5	3
Mud-pumping	Same	Same	Same
Stresses and Displacements	Same	Same	Same

Note: AOS = Apparent opening size, L_g = Gauge length; I_r = rail moment of inertia; L_s = Sleeper length; b_s = Sleeper width; S = Sleeper spacing; D_{max} = Maximum particle size; t_s = thickness of sleeper; Also refer Fig. 2(a).

A geotextile serves multiple functions in a track, namely, drainage, separation, filtration and, to some extent, reinforcement. All types of nonwoven geotextiles, namely, needle punched, heat-bonded and chemical bonded, have been used in railway tracks as separators between track bed ballast and subgrade soils. Geotextiles should be sufficiently thin and flexible so that they can easily adapt to minor irregularities in the subgrade soil, and they should also be able to filter and effectively drain out the water from the subgrade. The chosen geotextile with an apparent opening size of 0.14 mm was found to be adequate for filtration and drainage functions.

The stiffnesses of ballast and subballast layers were similar to prototype in spite of particle size reduction of these materials. With the scaling down of geotextile and geogrid stiffnesses

as stated above, displacements of different layers in reinforced and unreinforced track models are expected to be similar to those in the field in magnitude.

Since mud-pumping is in part a filtration problem, the aperture opening size (AOS) of the geotextile in relation to subballast and subgrade soils is important. Ideally speaking, the diameter of the particles of both subgrade soils and subballast should be multiplied by 3 under prototype conditions. The same would be the case for the geotextile AOS. In such a case, for filter condition, geotextile retention criteria will not be affected because both the subgrade particles and the geotextile filtration opening size are multiplied by the same scale factor under prototype conditions.

However, in the present case, the particles of subgrade soils, namely, Dhanaury clay and Delhi silt, being fine grained, were not scaled because this would have been very difficult and if possible, would have changed their mechanical behavior (for example, clay and silt content would have changed). AOS of the geotextile used in the model was similar to AOS of thermal bonded geotextiles used in the field. The subballast gradation was reduced to one-third. However, the reduced subballast gradation still fell within the range of the RDSO specification for full size subballast. Therefore, because the geotextile, overlying subballast, and retained subgrade soils as well as induced vertical stresses in the model were all similar to those in the prototype, the mud-pumping behavior observed in the model tracks with and without geotextile is expected to be siilar to that of the prototype.

4 GUIDELINES FOR DESIGNING OF EXPERIMENTS

(1) Detailed explanation given above along with Table 1 can be used for designing model tests. Additional guidelines are given in Table 2, where 1/n is similitude ratio and small strain stiffness is assumed to be dependent upon effective stress level,σ, according to relationship of the form: $G \propto \sigma^{\alpha}$. For details of designing of experiments on shake table, refer Iai (1989). For more information on scaling laws, refer Wood (2004).

(2) Note that modeling of geotechnical structures involves not only the reduction of prototype dimensions by an appropriate similitude ratio but also the reduction of particle sizes, stiffness and strength properties of the constituent materials by the same simulation ratio, an important aspect that is often neglected by many researchers. If dimensions are reduced but not the particle sizes and properties of constituent materials, then this will create distortion in the model and the model behavior may no longer represent the prototype behavior.

(3) Modeling details become complex in case of composite structures, such as geosynthetic reinforced structures or seismic testing of structures, such as shake table tests. It is also complicated to model prototype structures where coupled diverse multiple processes needs to be simulated, such as mud-pumping and deformation in railway tracks. The guidelines given above along with Tables 1 and 2 can be used for designing model tests in such cases.

(4) For reduction of parameters to be monitored during model tests, dimensional analysis may be used as a guideline (refer Wood 2004, and Shahu and Reddy 2011).

Table 2: Scaling Laws (Wood 2004)

Quantity	Laboratory Models
Length	1/n
Mass density	1
Acceleration	1
Stiffness	$1/n^{\alpha}$
Stress	1/n
Force	$1/n^{3}$
Force/unit length	$1/n^{2}$
Strain	$1/n^{(1-\alpha)}$
Displacement	$1/n^{(2-\alpha)}$
Permeability	1
Hydraulic gradient	1
Frequency	$n^{(1-\alpha/2)}$

REFERENCES

1. Iai, S. (1989) Similitude for shaking table tests on soil-structure-fluid models in 1g gravitational field. *Soils and Foundations*. 29,105-118.
2. Sowmiya, L.S. and Shahu, J.T. (2016) Reinforcement and mud-pumping benefits of geosynthetics in railway tracks: Model tests. *Geotextiles and Geomembranes*. Doi: 10.1016/j.geotexmem.2016.01.005.
3. Shahu, J.T. and Reddy, Y.R. (2011) Clayey soil reinforced with stone column group: model tests and analysis. *Journal of Geotechnical and Geoenvironmental Engineering*. 137, 1265-74.
4. Wood, D.M. (2004) Geotechnical Modelling. Spon Press, London. p.488.
5. Wood, D.M., Hu, W. and Nash, D.F.T. (2000) Group effects in stone column foundations: model tests. *Geotechnique*. 50, 689-698.

Guidelines for use of Numerical Procedures in Geotechnical Engineering

K. Rajagopal
Professor, Department of Civil Engineering,
Indian Institute of Technology Madras, Chennai
gopalkr@iitm.ac.in

B. Munwar Basha
Assistant Professor, Department of Civil Engineering,
Indian Institute of Technology Hyderabad
basha@iith.ac.in

1 INTRODUCTION

There are a number of methods to analyze the geotechnical problems starting from closed-form analytical methods to finite element/finite difference based numerical methods. Each method has its own advantages and disadvantages. The solution will be accurate only if all the following conditions are satisfied by it.

- Equilibrium of forces – external forces should be exactly equal to the internal forces (reactions)
- Compatibility (relation between displacements at different locations within a continuum) – these can also be called as continuity equations
- Constitutive behaviour (stress-strain equations of the material)
- Boundary conditions – force or displacement conditions.

The following table gives an indication of the different conditions satisfied by various solution methods.

Table 1: Different conditions satisfied by various solution approaches

Analysis method	Solution requirements				
	Equilibrium	Compatibility	Constitutive behaviour	Boundary conditions	
				force	displacement
Closed form (linear elastic)	Yes	Yes	Only linear elastic	Yes	Yes
Limit equilibrium	Yes	No	Rigid-plastic	Yes	No
Stress field	Yes	No	Rigid-plastic	Yes	No
Lower Bound	Yes	No	Ideal plasticity	Yes	No
Upper Bound	No	Yes	Ideal plasticity	No	Yes
Beam-spring approaches (Winkler models)	Yes	Marginally	Soil is modelled by elastic springs	Yes	Yes
Numerical analyses (finite element, finite difference, discrete element method)	Yes	Yes	Any constitutive model is possible	Yes	Yes

One good example for limit equilibrium analysis is the stability analysis of slopes. An example for lower bound solution is the derivation of bearing capacity of a strip footing as $4C_u$ by equating the lateral stresses just at the edge of the footing. An example for upper bound solution is the bearing capacity of strip footing resting on clay soil as $2\pi C_u$ ($6.28\ C_u$) obtained by assuming a circular slip surface drawn with one edge as the centre of the circle.

Based on the field variables, the problems can be categorized as uncoupled and coupled problems as illustrated in Table 2. The approach to the solution depends on the nature of problem being analyzed.

Table 2: Categories of geotechnical problems and the field variables

Uncoupled problems involve only one set of primary variables	Coupled problems involve two or more sets of variables and their coupling effects
1. Mechanical: variables: displacements 2. Seepage: variable: pore water pressure 3. Heat transfer: variable: temperature	1. Hydro-mechanical: variables: displacements & pore water pressure 2. Thermo-mechanical: Variables: displacements & temperature 3. Thermo-hydro-mechanical: Variables: displacements, pore pressure & temperature

This report gives a brief explanation on some aspects of applying the finite element procedures for analysis of geotechnical problems. It gives only a brief outline in a nut shell and the interested readers may refer to relevant text books for more detailed description.

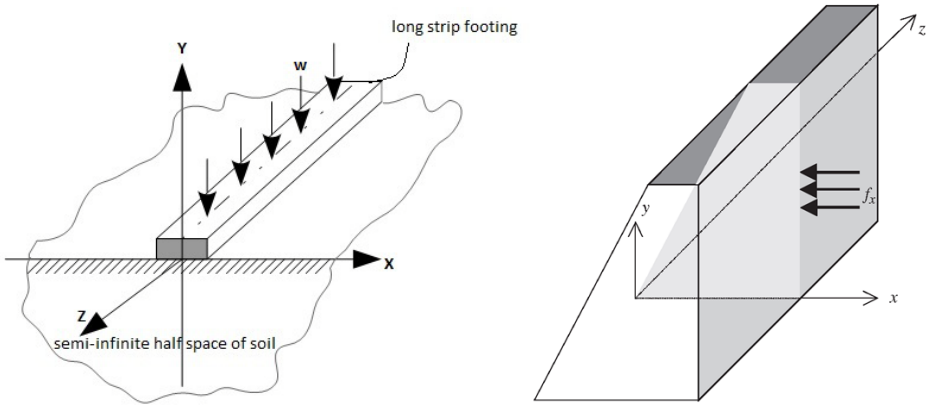

Figure 1: Typical examples for plane strain simulations

2 IS IT BETTER TO USE TWO-DIMENSIONAL OR THREE-DIMENSIONAL ANALYSIS?

Any geotechnical problem can be described as a three-dimensional model. However, the cost of 3-dimensional analysis is an order of magnitude more than that required for 2-dimensional analysis in terms of the time required for model generation, running the program, interpretation of results and memory space required.

Most geotechnical problems with geometries having long lengths compared to other dimensions can be simulated using 2-dimensional models. For example, problems of

retaining walls, embankments, tunnels, etc. can be analyzed as plane strain (2-dimensional) problems. All problems in which out of plane strains are negligible can be simulated using plane strain idealization.

The problems which have radial symmetry in both geometry and loading (e.g. circular footing subjected to uniform pressure, triaxial compression tests, one-dimensional consolidation test, etc.) can be simulated using axisymmetric models.

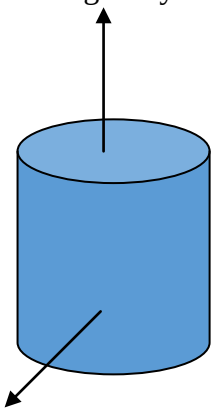

Figure 2: Axisymmetric idealization

A single circular pile subjected to vertical concentric loading may be approximated using axisymmetric model due to radial symmetry. On the other hand, the same pile subjected to lateral loads needs to be analyzed using full 3-dimensional models due to lack of radial symmetry in the applied load and the resulting stresses in soil.

A finite element mesh for a full 3-dimensional analysis of an embankment supported on geosynthetic reinforcement layer at the ground level and piles in the foundation soil is shown in Fig. 3. The same problem can be idealized using axisymmetric model by considering one single interior pile and the surrounding soil as shown in Fig. 4. The finite element model by considering 3-d column model by considering one single interior pile and the surrounding soil is shown in Fig. 5. The horizontal layer of reinforcement and other details of the soil and embankment are shown in Fig. 5.

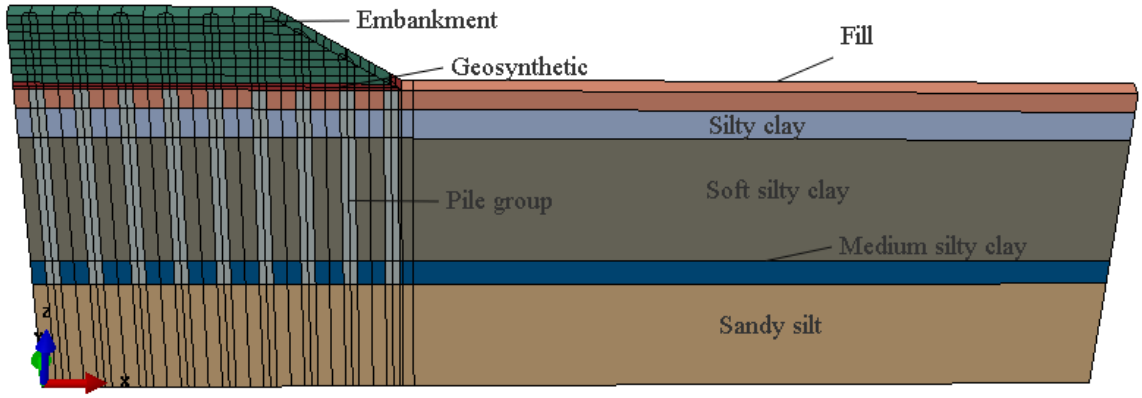

Figure 3: 3-dimensional finite element mesh for embankment supported on piles and geosynthetic layer

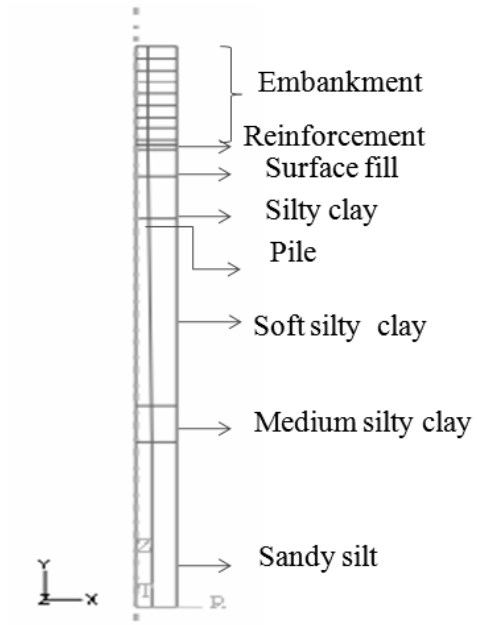

Figure 4: Axisymmetric model for piled embankment

A comparison of the computational efforts in terms of the CPU time, the size of the finite element model for different models is made in Table 3. It could be seen that the use of full 3-dimensional finite element model results in significant increase in the computational effort. The initial analyses may be performed using 2-dimensional approximations for understanding the fundamental mechanism. Later, the analyses could be extended to 3-dimensional analysis for clearer understanding.

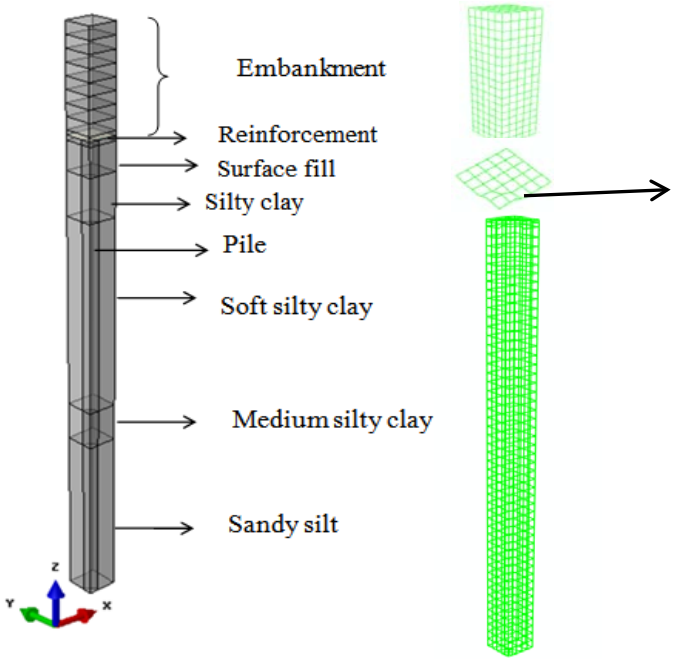

Figure 5: 3-d column model for piled embankment problem

Table 3: Computational times for different model approximations

Model	No. of elements in Embankment	No of Geosynthetic Elements	No. of Pile Elements	No. of elements in Foundation	CPU Time
Axi-symmetric	234	9	184	891	15 Min.
3D Column	1860	25	452	9439	45 min.
Full 3D	22,814	274	6074	47,906	96 hours

3 YOUNG'S MODULUS

Young's modulus could be initial modulus, tangent modulus or secant modulus. Depending on the nature of strains to model, the relevant Young's modulus can be used, Fig. 6. If behaviour at small strains is required to be modelled, initial modulus may be appropriate while the behaviour at large strains is better simulated using secant modulus at higher strain levels.

The laboratory determined Young's modulus is always on the lower side due to sample disturbance effects or due to the loss of pre-consolidation/cementation effects. No amount of care taken in remoulding of soil samples in the laboratory can re-create the in situ soil state and the in situ cementation. Hence, it is best to obtain the Young's modulus through back calculation of field observed deformations or settlements. The Young's modulus value can be obtained through several empirical equations as shown in Table 4.

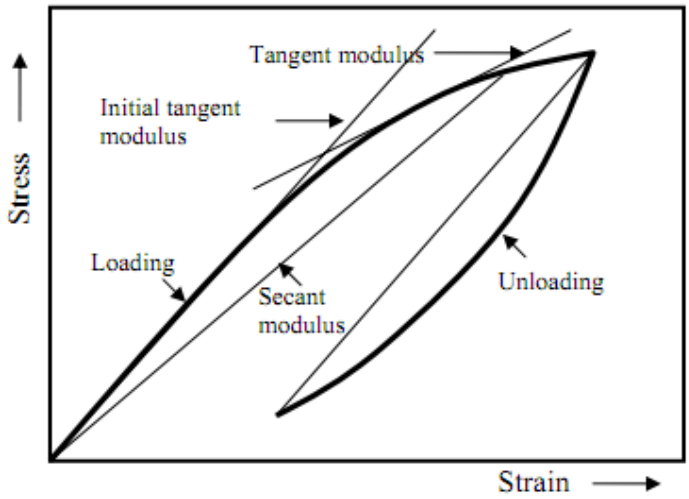

Figure 6: Definition of different types of soil modulus

For simulating the deformations during excavation (unloading), very high Young's modulus values are to be used as the response under unloading is much stiffer compared to

that under loading. Typically, the Young's modulus during unloading should be set at least 3 times higher than that during loading.

Table 4: Empirical relations for the Young's modulus

Type of soil	SPT	CPT
Sand (dry)	500(N+15)	2 to 4 q_c
	(15000 to 22000) lnN	$(1+D_r^2)$ q_c
	(35000 to 50000) logN	
Sand (saturated)	18000 + 750 N	6 to 30 q_c
Gravelly sand and gravel	1200 (N+6)	
	600 (N+6) N≤ 15	
	600(N+6)+2000, N>15	
clayey sand	320 (N+15)	3 to 6 q_c
silty sand	300 (N+6)	1 to 2 q_c
soft clay		3 to 8 q_c

The Young's modulus of granular soils or normally consolidated clay soils increased with increasing confining pressure. This behaviour is best simulated using Janbu's equation relating the Young's modulus and the confining pressure as follows:

$$E_i = K_e P_a \left(\frac{\sigma_3}{P_a} \right)^n \tag{1}$$

in which, E_i is the initial Young's modulus, K_e is a non-dimensional constant, P_a (≈102 kPa) is the atmospheric pressure in the same units as E_i, σ_3 is the confining pressure and n is an exponent.

4 WHAT IS A SUITABLE VALUE FOR POISSON'S RATIO OF SOILS?

The Poisson's ratio controls the volume change behaviour of soils. A fully undrained problem can be analyzed by using a Poisson's ratio value very close of 0.5 (say 0.499). It cannot be set equal to 0.50 because of singularity problems in the constitutive equation (ref. (1–2ν) term in the denominator)

The Poisson's ratio values for dry sands may range from 0.3 to 0.35 while the same for soft clay soils could be more than 0.40. The Poisson's ratio value for brittle materials (like dry clay) will be very low of the order of 0.1 to 0.15.

The rate of volumetric strains under loading is not uniform in the soils. Initially, there is volumetric compression and then dilation during plastic deformations followed by constant volume state in limiting conditions. All elastic volume changes are compressive in nature while the dilation (or volume expansion) is due to plastic strains. After the limit state, the volume of soils remains constant. At this state, the Poisson's ratio value should be very close to 0.50 to numerically simulate the constant volume state during the plastic deformations.

The variability in the Poisson's ratio (ν_t) is best represented in the numerical analyses by writing the stress-strain relations in terms of tangent bulk modulus (K_t) and shear modulus (G_t). The Poisson's ratio is related to both these as follows,

$$\nu_t = \frac{3K_t - 2G_t}{6K_t + 2G_t} \tag{2}$$

While the bulk modulus is kept constant during the analysis, the tangent shear modulus is reduced to a very low value after the limit state. As the tangent shear modulus approaches zero (small value), the tangent Poisson's ratio automatically approaches 0.50 as is evident from Equation 2.

5 TYPE OF FINITE ELEMENTS

The soil (continuum) is best represented using triangular elements in 2-d problems and tetrahydral elements in 3-d problems as their shape functions are derived using complete polynomials and satisfy all the monotonic convergence requirements. The 3-node triangles arranged with four per rectangle is found to be an excellent method to obtain accurate predictions of all plasticity problems of plane strain and axisymmetric problems. A typical finite element mesh made up of 3-node triangles is shown in Fig. 7.

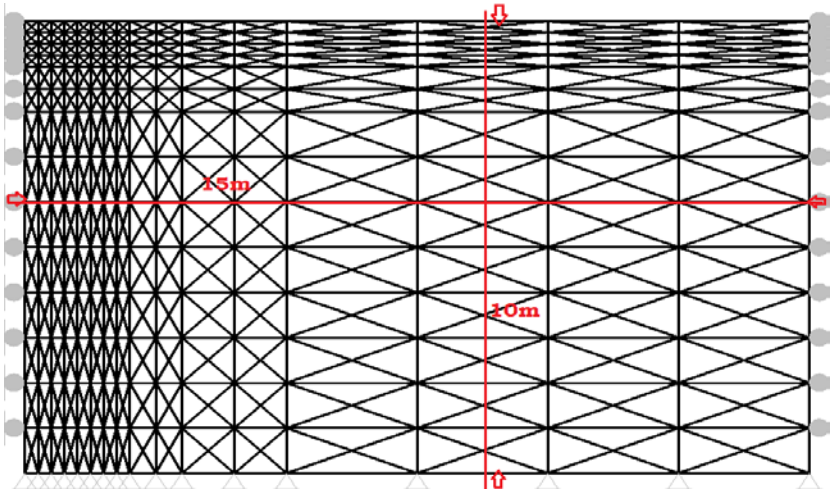

Figure 7: Finite element mesh made up of 3-node triangular elements

6 SIZE OF MESH

The distance to the boundaries of the finite element mesh depends on the exact problem being analyzed and the constitutive model employed to describe the soil behaviour. Usually, the required size of the mesh is much larger in the linear elastic problems compared to the elastic-plastic problems. In the case of elastic-plastic type problems, the boundaries should be should be located far away such the entire failure mechanism is contained within the boundaries of the mesh.

Schematic meshes for the analysis of a linear-elastic soil subjected to foundation pressure using pure finite elements and finite elements coupled with mapped infinite elements are shown in Fig. 8. The percentage error in the settlement at the centre of a flexible circular footing with different boundary distances is illustrated in Fig. 9. It is seen that even when the mesh boundaries are located at 40 times the radius of the footing, the percentage error in surface settlement is more than 5% with pure finite elements. However, when mapped infinite elements are joined with finite elements, the percentage error drops to less than 2% even with a very small mesh as illustrated in Fig. 8.

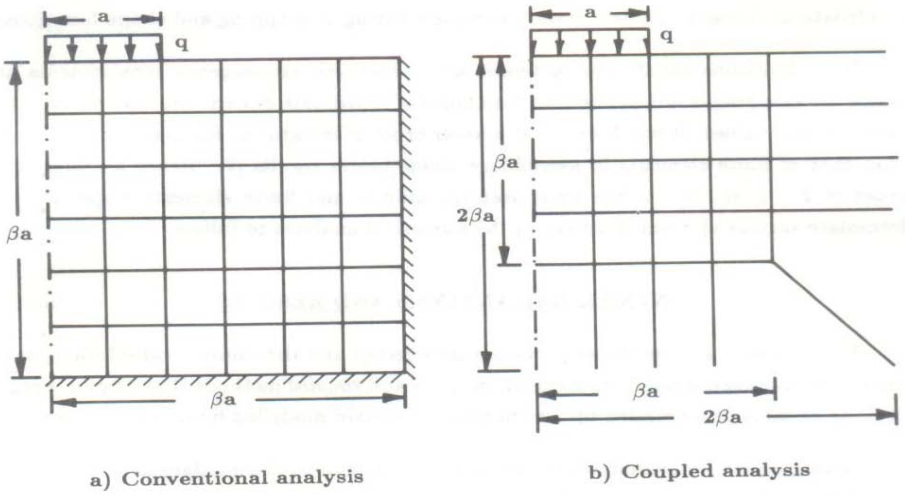

Figure 8: Schematic for choosing the distance to boundaries in finite element analysis

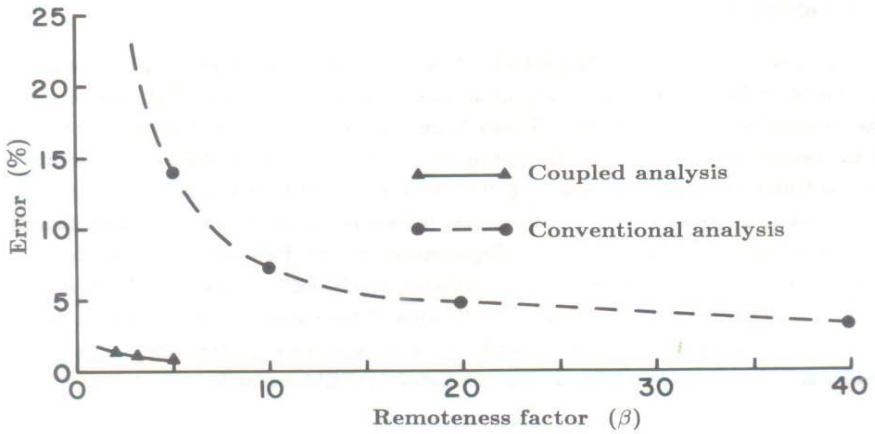

Figure 9: Variation of percentage error with distance to the mesh boundaries

The slip circle failure mechanism of a nailed soil slope is shown in Fig. 10. If the object of the analysis is only to understand the failure mechanism and determine the factor of safety, it is adequate if the entire slip surface is contained within the mesh geometry.

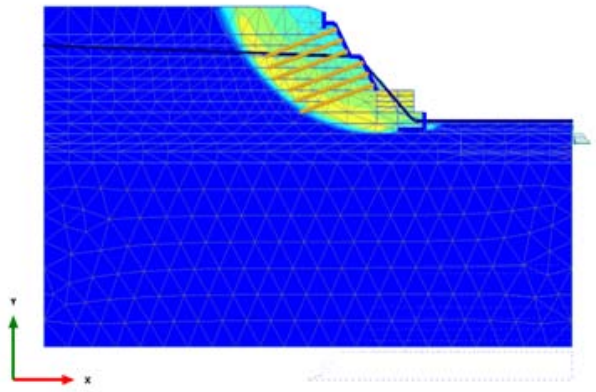

Figure 10: Slip circle failure mechanism of a nailed soil slope

7 SEMI-INFINITE ELEMENTS IN GEOMECHANICS

The numerical analysis of most geotechnical problems needs to deal with semi-infinite nature of the soil medium. Especially, this assumes importance in dynamic problems compared to the static problems. If the boundaries are located too close to the applied loads, the reflected waves from the boundaries interfere with the incident waves leading to spurious deformations and stresses. This is overcome by several different methods like viscous boundaries, etc (this aspect is described in another lecture notes in detail). One recently developed method to overcome this is by using mapped semi-infinite elements which show singularity in one direction. The concept of the mapped infinite element with singularity at natural coordinate ξ=+1 is illustrated in Fig. 11. The singular mapping functions for nodes at ξ= –1 and 0 are shown

$$u(\xi) = \frac{a_o}{1-\xi} + \frac{a_1}{1-\xi}\xi = M_1(\xi)u_1 + M_2(\xi)u_2$$
$$M_1(\xi) = \frac{-2\xi}{1-\xi} \qquad M_2(\xi) = \frac{1+\xi}{1-\xi} \tag{3}$$
$$M_1 + M_2 \equiv 1$$

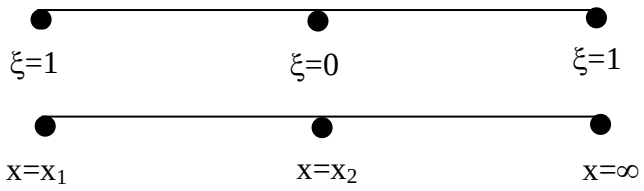

Figure 11: Schematic of a mapped infinite element with singularity at ξ=+1

The singular mapping functions with a singularity at ξ=+1 are developed by using singular polynomial functions as explained in the following. The mapping is performed using the two node points which are located within the finite space (nodes at x_1 and x_2). The sum of these two mapping functions adds to unity thus satisfying the requirements for unique mapping.

The above type of mapped infinite element is quite convenient for applications in different geomechanics problems. The current version of the popular finite element program ABAQUS has these elements in the element library. These elements are recommended for modelling in dynamics problems to take care of the boundary reflection.

These infinite elements are to be necessarily be made of linear-elastic material and should not be assigned any self-weight or surface loading. Any loads applied on these elements means adding an infinite load to the mesh leading to undue deformations.

8 DYNAMIC OR REPEATED LOADING?

Any problem with significant inertial forces requires dynamic analysis. The soil damping properties are very important for realistic predictions under dynamic loading. Repeated load problems are essentially treated as static problems with an appropriate constitutive model that can represent the degradation of the modulus with number of cycles.

9 PRACTICAL APPLICATION

9.1 Modelling of Geosynthetic Reinforcement Layers

The geosynthetic layers are flexible which can support only the tensile forces and cannot support compressive or shear forces. Hence, special bar elements (in 2-d problems) and membrane elements (in 3-d problems) which can support only the axial tensile forces are required to model the response of geosynthetic reinforcement layers. The modulus of these elements is set to a very small value (but not zero) whenever compressive strains are developed to prevent the development of any compressive forces in these elements.

9.2 Simulation of Soil Nails

The soil nails are rigid steel rods either driven into the soil or placed inside a drilled hole and covered with concrete or cement grout (Fig. 12). The elements are linear elements which are capable of supporting axial forces, shear forces and moment. Hence, beam elements are best used to represent the soil nails. The order of the beam elements (number of nodes) should be compatible with the continuum elements, i.e. if 6-node triangular elements are used for soil, then the soil nails can be represented using 3-node beam elements. If 15-node triangular elements are used for soil, the soil nails can be represented using 5-node beam elements.

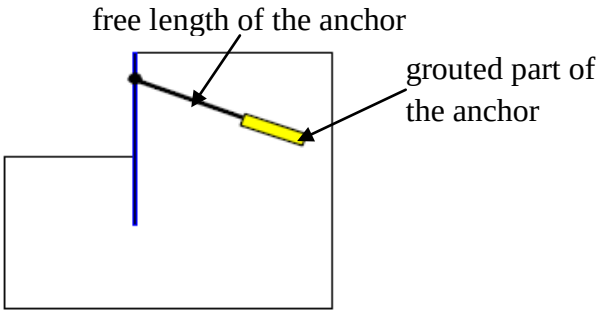

Figure 12: Schematic of a ground anchor

9.3 Node to Node anchors

In the case of grouted nails, there is usually some free length of the nail (in the active zone) which is not in contact with the surrounding soil, Fig. 12. This part of the borehole is not grouted to prevent the contact between the nail and the active soil. This condition can be numerically simulated by directly connecting the node point on the sheet pile wall to the front end of the grouted part of the anchor using a stiff bar element. This is usually a tensile element which cannot carry any shear forces. Hence, this element is simulated using a 2-node bar element. One end of this bar is connected to the sheet pile and the other end to the grouted part of the nail. As the grouted part of the nail is also in tension and in direct contact with the surrounding soil, this part of the nail is simulated using bar elements and connected to the surrounding soil through interface elements.

10 INTERFACE ELEMENTS

The interface elements are provided between structural elements (e.g. geogrid layer, sheet pile, etc.) and the surrounding soil to control the load transfer between the two parts of the domain. These interface elements are also provided between two dissimilar materials to prevent the undue development of artificial shear stresses at the interface. The order of the

interface elements should be compatible with the surrounding continuum elements. The shear strength properties of the interface elements should be a fraction of the shear strength properties of the soil adjacent to the structural element.

11 SIMULATION OF SHEET PILE WALLS

The sheet pile walls are rigid structural elements that can provide shear and flexural support to the soil, Fig. 13. In addition, they can also carry compressive loads. These sheet pile walls are best represented using beam elements in the finite element analysis. The major geometric properties defined for beam elements include their cross-sectional area (A) modulus of inertia (I) in addition to their linear length. These properties per unit length are usually obtained from the standard data given by the manufacturer of the sheet piles.

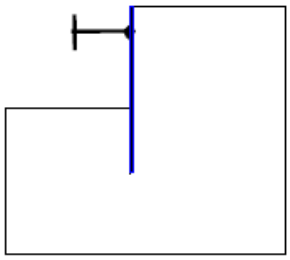

Figure 13: Schematic of a sheet pile wall with strut support

12 PORO-ELASTIC ELEMENTS FOR HYDRO-MECHANICS PROBLEMS

In the hydro-mechanical problems both displacements and pore pressures are the nodal variables. One classic example for these problems is the consolidation analysis of soils. These problems are transient with continuous variation of displacements and pore pressures with time. It is essential that the order of variation of soil stresses and pore pressures within the element is the same to obtain the best results. Eight-node quadrilateral and 6-node triangular elements which are best suited for poro-elastic problems are illustrated in Fig. 14. In both elements, the soil stresses and pore pressures will have linear variation within the element leading to good compatibility.

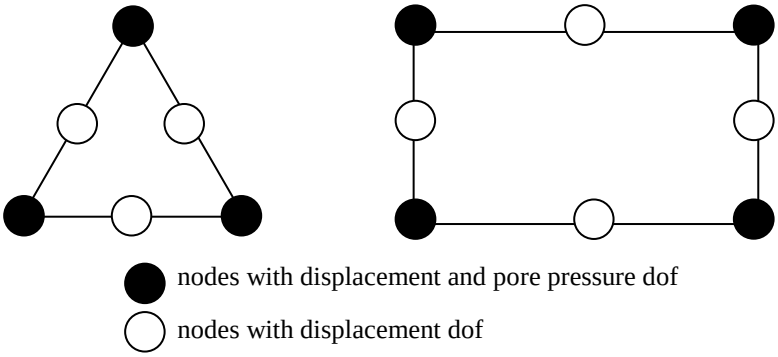

Figure 14: Triangular and quadrilateral poro-elastic finite elements

13 CONSTITUTIVE MODELS IN GEOMECHANICS

There are a number of constitutive models ranging from linear-elastic to nonlinear and advanced plasticity models based on associated and non-associated flow rules.

- Linear Elastic

- Nonlinear elastic
    - Multilinear type
    - Hyperbolic models
- Elastic Plastic (Mohr Coulomb, Drucker-Prager)
- Hierarchical models
- Cam clay and critical state models
- Soft soil models
- Hardening soil models

14 DETERMINATION OF FACTOR OF SAFETY OF GEOTECHNICAL STRUCTURES

Most geotechnical engineers understand the performance through the factor of safety analysis. The finite element programs give a convenient means of determining the factor of safety of geotechnical structures without making any a priori assumptions about the shape or size of the slip surface. Typically, these programs perform repeated analyses by progressively reducing or increasing the Factor of safety (FS) values. The modified shear strength properties are determined as follows:

$$\bar{c} = \frac{c}{FS}$$
$$\bar{\phi} = \tan^{-1}\left(\frac{\tan\phi}{FS}\right) \tag{4}$$

The analyses are performed repeatedly and a plot is made between the factor of safety value on x-axis and a measure of displacement on the y-axis. The critical factor of safety is taken as the value at which the displacements tends to increase rapidly as shown in Fig. 15. At a critical factor of safety of between 1.2 to 1.3, the displacements tend to increase rapidly. Hence, it could be concluded that the factor of safety of this structure will be between 1.2 and 1.3.

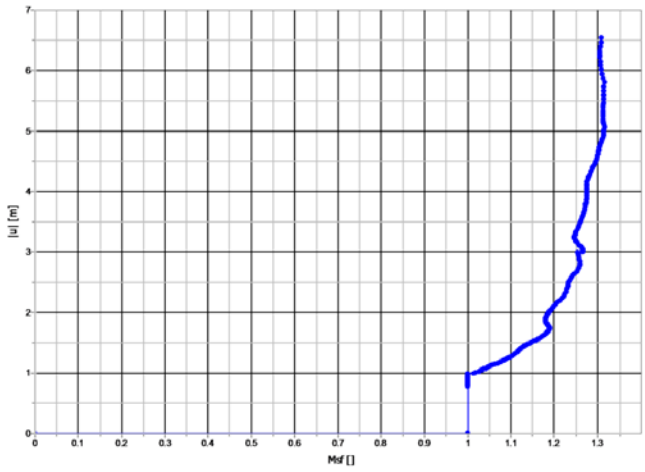

Figure 15: Variation of displacement with the factor of safety

15 AVAILABLE COMMERCIAL PROGRAMS

Several programs are available commercially for numerical modelling of geomechanics problems. These programs can be categorized as finite element, finite difference or discrete element models as follows:

a) Continuum methods:
- Finite element method (FEM)
- Finite Difference method (FDM)
- Boundary element method (BEM)

b) Discontinuum methods:
- Discrete element methods including:
- Distinct element method (DEM)
- Discontinuous deformation analysis (DDA)

Rigorous boundary element methods have not been developed till date to handle inelastic material behaviour and non-homogeneous soil properties. All the methods provide a rigorous solution by reaching equilibrium. The difference lies only in the numerical method and algorithm employed to reach the equilibrium.

Table 5: Numerical Packages used in geomechanics

Methods	Finite Element based packages suitable for geotechnical problems	Finite Difference based packages	Discrete Element Method (DEM)
Continuum methods	Plaxis 2-d & 3-d, Phase, DIANA, EXAMINE, ZSoil, ABAQUS, ANSYS, GEOSTUDIO, CRISP, TOCHNOG, CESAR, GEOFEM 2-d & 3-d	FLAC, FLAC 3D	-
Discontinuum methods	-	-	EDEM UDEC 3DEC

Among the above, only ABAQUS, FLAC, and TOCHNOG programs can handle the drainage under dynamic loading conditions. The present version of PLAXIS program can only perform undrained analyses during dynamic loading.

The speed and stability of the FLAC programs is much superior compared to similar finite element procedures due to the particular solution procedures adopted.

The applicability of some other major finite element programs like ANSYS and NISA for geotechnical problems needs to be assessed for the particular problem on hand as these are not specially developed for solving the geotechnical problems. Especially, these two programs cannot handle the insitu stress state and water pressures.

The Geofem 2-d and 3-d packages can be obtained free of cost from Prof Rajagopal, IIT Madras. These finite element packages include some elementary pre and post-processing capability and user manual to help in preparation of data files.

Physical and Numerical Modeling for Dynamic Soil-Structure Interaction Problems

Dr. B.K. Maheshwari
Professor, Department of Earthquake Engineering,
Indian Institute of Technology Roorkee
bkmahfeq@iitr.ac.in

1 INTRODUCTION

It is utmost important that lifeline infrastructures (such as bridges, hospitals, power plants, dams etc.) are safe and functional during earthquakes as damage or collapse of these structures may have far reaching implications. A lifeline's failure may hamper relief and rescue operations required just after an earthquake and secondly its indirect economical losses may be very severe. Therefore, safety of these structures during earthquakes is vital. Further, damage to nuclear facilities during earthquake may lead to disaster. These structures should be designed adequately taking into account all the important issues.

Soil-Structure Interaction (SSI) is one of the design issues, which cannot be ignored for the structures founded on the weak soils particularly when these are subjected to strong excitation. In last decade, there are many advances in techniques of SSI and those need to be incorporated in practice. Failures of many structures occurred during the 1989 Loma Prieta and 1994 Northridge, California earthquakes, the 1995 Kobe, Japan earthquake and the 2001 Bhuj earthquake due to SSI or a related issue. Many jetties had failed in Andaman and Nicobar islands due to Sumatra earthquake and ensuing tsunamis. It is because of this recent experience that the importance of SSI on dynamic response of structures during earthquakes has been fully realized. General belief that the SSI effects are always beneficial for the structure is not correct. Some cases have been reported where it is shown that SSI effects are detrimental for the stability of the structure.

During strong shaking, the behavior of soil is highly nonlinear; further if it is saturated loose sand, the liquefaction may occur. To deal effectively with such complex scenario, physical and numerical modeling provides the best solution. Normally, two dimensional and three dimensional finite element analyses are performed. However, in such analyses for SSI problems there are many complex issues which need to be addressed adequately for a meaningful analysis and design.

This paper presents the methodology for physical and numerical modeling for SSI problems. Also, advances in SSI studies have been discussed. Most of the issues discussed in this document are identical to that presented by Maheshwari (2014), this is because of same theme. However, these are discussed here again for completeness. The chapter has been divided in following major headings:

1. Importance of SSI
2. Objective and Scope of Study
3. Steps of SSI: Free Field Response, Kinematic Interaction and Inertial Interaction
4. Effects of SSI
5. Direct and Substructure Methods
6. Different Approaches for SSI Analyses
7. Recent Advances in SSI
8. Summary and Conclusions

2 IMPORTANCE OF SSI

There are numerous examples (Seed et al. 1990 and 1992) which clearly demonstrated that structures including buildings, bridges, dams, offshore structures, pile foundations damaged in past earthquakes due to ignorance of soil-structure interaction in design. In the Mexico city earthquake, the time period of 10-12 storey buildings founded on soft clay were increased from 1.0 to 1.5 seconds bringing it closer to resonance conditions.

The role of SSI on the failure of the Hanshin Expressway in 1995 Kobe Earthquake was very destructive, 630 m length of the Hanshin expressway collapsed and overturned (Maheshwari 2014). According to Gazetas and Mylonakis (1998) the effect of SSI in the response of the bridge was to increase the natural period of vibration and thus increase the ductility demand on the pier by twice due to the increased base shear forces. During 2001 Bhuj earthquake cap of pier of a bridge is damaged due to SSI effects.

From above examples as well as many other case histories on damages in past earthquakes, it was realized that there is a need to rationally incorporate soil-structure interaction in the design of structures. Gazetas and Mylonakis (1998) illustrated that ignoring SSI has lead to oversimplification in the design leading to an unsafe design and foundation and superstructure. The current design practice does not recognize effects of SSI fully and need to be revised. This is an important issue and should not be ignored.

3 OBJECTIVE AND SCOPE OF STUDY

For dynamic SSI, there are a number of important issues which need to be dealt rationally for a reasonably accurate analysis. First issue is modeling of unbounded soil media to satisfy the radiation conditions. Second, for dynamic loading, behavior of soil is frequency dependent and it needs to be taken care. This shall be performed in such a way that the effect of interaction between soil-foundation system and structure system is fully realized. Third is modeling material nonlinearity of soil. Fourth is modeling of liquefaction.

First, fundamental concept of SSI is discussed followed by different steps involved i.e. free field response, kinematic interaction and inertial interaction. This is followed by explanation of direct and substructure methods of analysis. For SSI analyses there are a variety of approaches which may be broadly categorized in 2 groups i.e. simplified models and rigorous models. Modeling of unbounded soil domain i.e. modeling of boundary is discussed in detail. Next effect of soil nonlinearity on seismic response is discussed.

The basic principle of dynamic soil-structure interaction is explained as follows (Wolf 1985): Soil is a semi-infinite medium, and a major problem in dynamic soil-structure interaction is the modeling of the unbounded soil domain. For dynamic loading, a structure (it may be foundation or superstructure) always interacts with surrounding soil and it is not adequate to analyze the structure independently. If seismic loading is applied to the soil region around the structure, then one has to model this region along with the structure. In the case of a static loading, a fictitious boundary can be included at a sufficient distance from the structure, where the response is diminished from a practical point of view. However, for dynamic loading this procedure cannot be used. The fictitious boundary would reflect waves originating from the vibrating structure back into the discretized soil region, instead of letting them pass through and propagate through infinity (Fig. 1)

A semi-infinite soil medium should be modeled in such a way as to satisfy the radiation condition i.e. only waves can radiate outside the considered region and they cannot reflect back inside this boundary. Thus this boundary represents an energy sink where only outgoing waves can occur and this boundary should be modeled adequately. In sequel, the fundamental objective of the analysis of soil-structure interaction is that dynamic response of the structure

as well as of soil is to be calculated, taking into account the radiation of energy of the waves propagating into the soil region not included in the model (Fig. 1).

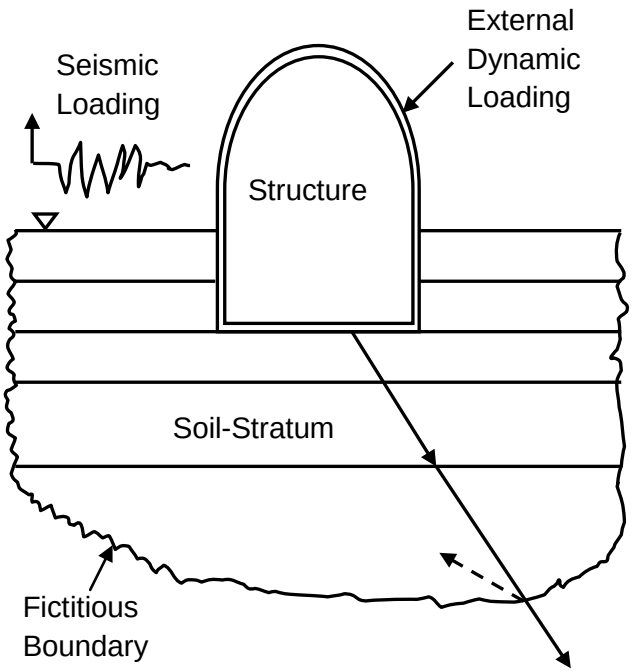

Figure 1: Fundamental objective of soil-structure interaction

4 STEPS OF SSI: Free Field Response, Kinematic Interaction and Inertial Interaction

The salient features of SSI can be best explained by comparing the dynamic response of a structure founded on rock to an identical structure embedded in soil. Fig. 2a shows two identical structures with rigid base, one sitting on rock while other embedded in a soft soil. As the distance between the two structures is small it can be assumed that the incident seismic waves arriving from the source of the earthquake are the same for both structures. For the sake of simplicity, vertically propagating horizontal motion is considered with control point at the free surface. It is explained below that how effect of SSI is very important for structure founded on soft soil while it is not so for those founded on rock.

4.1 For the Structure on the Rock

The horizontal motion can be applied directly to the base of the structure. The input acceleration resulting in the applied horizontal inertial loads will be constant over the height of the structure. During the earthquake, an overturning moment and a transverse shear acting at base will develop. As the rock is very stiff, these two stress resultants will not lead to any (additional) deformation at the base. The resulting horizontal displacement of the base is thus equal to the control motion; no rocking motion arises at the base. For a given control motion, the seismic response of the structure depends only on the properties of the structure.

4.2 For the Structure Founded on Soft Soil

The motion of the base of the structure in point O will be different from control motion in control point A because of the coupling of structure-soil system. The soil affects the dynamic response of the structure in three ways (Wolf 1985).

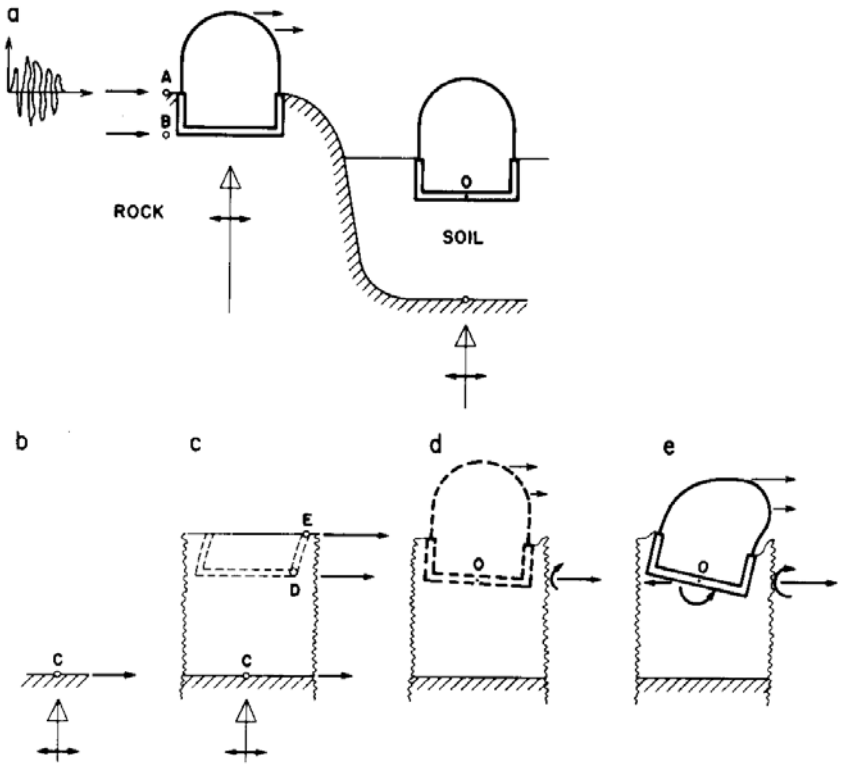

Figure 2: Seismic response of structure founded on rock and on soil. (a) Sites; (b) outcropping rock; (c) free field; (d) kinematic interaction (structure absent or massless); (e) inertial interaction (in the presence of structure) (After Wolf 1985).

It modifies the **free-field motion** (i.e. the motion of the site in the absence of the structure and of any excavation). If there were no soil on top of the rock in point C of Fig. 2c, the motion in this fictitious rock outcrop shown in Fig. 2b would be same as the control motion of the rock in point A. The presence of the soil layer will reduce the motion in point C (Fig. 2c). This wave will propagate vertically through the soil layer, resulting in motions in points D and E which differ from that in C.

Excavating and inserting the rigid base (say foundation) into the site will modify the motion (Fig. 2d). The rigid base will experience some average displacements and a rocking component. This rigid body motion will result in accelerations (leading to inertial loads) which will vary over the height of the structure, in contrast to the applied accelerations in the case of a structure founded on rock. This kind of interaction between soil and base in the absence of superstructure is called **kinematic interaction**.

In the presence of structure, the inertial loads applied to the structure will lead to an overturning moment and a transverse shear acting at point O. This will cause deformation in the soil and thus once again modify the motion at the base. This part of the analysis is referred as **inertial interaction**.

All these three steps can be summarized as shown below:

Effect of soil Effect of Base Effect of Structure

Control Motion → Free Field Motion → Kinematic Interaction → Inertial Interaction

5 EFFECTS OF SSI

Fig. 2 illustrates the main effects of taking soil-structure interaction into consideration (Wolf 1985)

i. First, the seismic-input motion acting on the structure- soil system will change (Fig. 2d). Because of the amplification of the site (free-field response), the translational component will in many cases be larger than the control motion and, in addition, a significant rocking component will arise for an embedded structure. Each frequency component of the motion is affected differently, resulting in, for example, an

acceleration time history, which is quite different from the control motion. This amplification of the seismic motion is held responsible for the fact that structures founded on a deep soft-soil site have been damaged more severely in actual earthquakes than have neighboring structures founded on rock.

ii. Second, the presence of the soil in the final dynamic model (Fig. 2e) will make the system more flexible, decreasing the fundamental frequency to a value which will, in general, be significantly below that applicable for the fixed-base structure. The implication of this reduction will depend on the frequency content of the seismic-input motion. In certain cases, the fundamental frequency will be moved below the range of high seismic excitation, resulting in a significantly smaller seismic input "felt" by the structure. The shape of the vibrational mode will also be changed. The introduced rocking of the base will affect the response, especially at the top of a tall structure.

iii. Third, the radiation of energy of the propagating waves away from the structure will result in an increase of the damping of the final dynamic system (Fig. 2e). For a soil site approaching an elastic half-space, this increase will be significant, leading to a strongly reduced response. For a soil site consisting of a shallow layer, it is possible that no waves propagate away from the structure. In this case, only the material damping of the soil will act, and no beneficial effect on the seismic response is to be expected. In any soil-structure analysis, it is very important to determine for a specific site whether the loss of energy by radiation of waves can actually take place.

It is reasonable to assume that the soil-structure interaction increases the more flexible the soil is and the stiffer the structure is. On the other hand, it will be negligible for a flexible structure founded on firm soil.

It is obvious from the many opposing effects that it is, in general, impossible to determine a priori whether the interaction effects will increase the seismic response. If, however, the first effect discussed above (the change of the seismic-input motion, Fig. 2d) is neglected when the interaction analysis is performed, the response will in many circumstances be smaller than the fixed-base response obtained from an analysis that neglects all interaction effects. For this approximate interaction analysis, the control motion is directly used as input motion in the final dynamic system (Fig. 2e). The fixed-base analysis leads to larger values of the global response, as, for example, the total overturning moment and the total transverse shear, and thus to a conservative design. The displacement at the top of the structure relative to its base may be larger because of the foundation rocking if one takes soil-structure interaction effects into account. Economic considerations normally dictate that, when designing structures, that reduction in seismic forces which results from considering the approximate soil-structure interaction analysis be used. There are also some exceptional cases where the simplified interaction effects will govern the design.

Kinematic Interaction

Kinematic interaction caused foundation level motion to be different from free field motions. The deviation between the motion experienced by the foundation and free field at the same site is usually evaluated in two steps (Kim and Stewart, 2003). In the first step, Foundation Input Motion (FIM), which is the motion that would occur on the base slab if the foundation and the structure had no mass, is evaluated. Difference between the free field motion and FIM result from kinematic interaction and these effects are quantified by Transfer Functions (ratio of FIM to free field motion). In the second step, foundation displacement and rocking associated with base shear, and the shear from the vibrating structure and the foundation inertia are added to the FIM. This approach is called as the substructure approach and applicable for linear analysis.

The reduction of the translational components of foundation and generation of the rocking components as well as filtering of the high frequency component of the excitation are the practical effects of kinematic interaction. Veletsos et al. (1997) evaluated the response of a rigid, massless disk on the surface of an elastic halfspace to incoherent waves propagating vertically or inclined. The result of the analysis is transfer function relating the motion of the foundation to the free field motion. Similar analytical formulations have also been developed by Luco and Wong (1986) for rectangular foundations and Luco and Mita (1987) for circular foundations.

For very stiff sites, it is generally recommended that the surface level ground motion can be used as the foundation level input motion conservatively without deconvoluting the input ground motion. In most cases, the free field surface level ground motion is selected as the control motion used at the foundation level neglecting the kinematic interaction due to wave scattering effects. Michalopoulos and Vardanega (1981) shown that failure to account for the effects of kinematic interaction may affect the response.

Inertial Interaction

There is increase in the fundamental natural period and associated damping due to the effect of inertial acceleration. Meek and Veletsos (1974) observed that the maximum seismically induced deformations could be predicted accurately by an "equivalent fixed base" single degree of freedom oscillator with period T* and damping ξ*. These are referred as "flexible base" parameters. These effects can be approximately quantified by the ratio of flexible to fixed base, first mode period (T*/T) and the structural damping attributable to foundation soil interaction (ξ) first introduced by Bielak (1975). The equivalent damping ratio can be expressed as:

$$\xi^* = \xi_0 + \xi/(T^*/T)^3 \quad (1)$$

Where ξ_0 fixed base damping ratio and ξ is the structural damping (about 2-5%). Thus damping ratio of equivalent system will be more than that of fixed base.

6 BENEFICIAL EFFECTS OF SSI

The beneficial effects of SSI can be explained with the help of Fig. 3 which shows response spectra for 5% material damping (IS: 1893-2002, Part 1) for a single degree of freedom system.

Two identical one-degree-of freedom structures, founded on rock and soft soil, respectively subjected to vertically propagating waves, are considered. It is assumed that the natural frequency of each structure is 2.5 Hz (i.e. natural period of 0.4 seconds). When the structure is founded on rock there will be no change in the natural frequency of the system. However, when the structure is founded on soft soil, the presence of soil makes system flexible decreasing natural frequency to say 0.5 Hz i.e. natural period is increased to 2.0 seconds. If we compare these frequencies on the response spectrum shown in Fig. 3, it can be clearly observed that the acceleration for the structure founded on soft soil is about 2.5 times smaller than the acceleration for the structure founded on rock. Therefore in this case, the presence of the soft soil will reduce the acceleration significantly which can be considered as a beneficial effect of SSI.

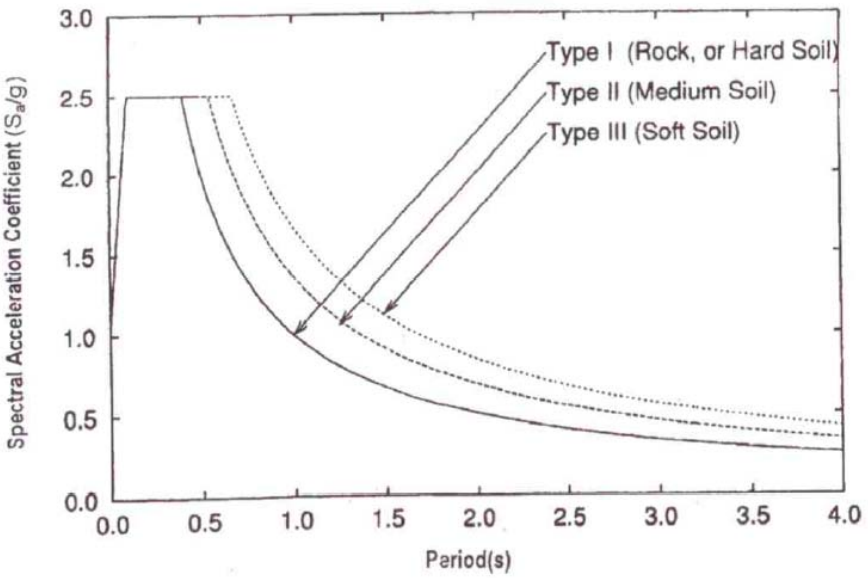

Figure 3: Response Spectra for 5% Damping (IS: 1893-2002, Part 1)

In general, SSI leads to smaller accelerations and stresses in the structure and thereby smaller forces in the structure. However, there are numerous documented case histories where the perceived beneficial effects of SSI have lead to oversimplification in the design leading to unsafe design in foundations and superstructure (Mylonakis and Gazetas, 2000).

The American seismic code for nuclear structures (ASCE 4-1998) indicates that fixed base conditions can be assumed to apply when V_s > 1100 m/s. This condition is generally satisfied in week rocks. Dowrick (1987) indicated that the fixed base conditions can be assumed for structures when $V_s > 20\ fh$. Where, h and f are the height and fundamental fixed based frequency of the structure, respectively.

7 DIRECT AND SUBSTRUCTURE METHODS

Easiest way to analyze soil-structure interaction for seismic excitation is to model a significant part of the soil around the embedded structure and to apply free-field motion at the fictitious boundary. This direct procedure would allow consideration of nonlinearity of the soil medium. However, the number of DOFs in the soil region is high, resulting in a large storage of computer memory and more running time. Since for linear analysis, the law of superposition is assumed to be valid, it is computationally more efficient to use the substructure method (Fig. 4). First, the unbounded soil is analyzed as a dynamic subsystem. The force-displacement relationship of the degrees of freedom of the same nodes is determined and represented as spring-dashpot system. In the second step, the structure supported on this spring-dashpot system is analyzed for a loading case which depends on the free-field motion. The substructure method allows the complicated soil-structure system to be broken down into more manageable parts.

8 DIFFERENT APPROACES FOR SSI ANALYSIS

For soil-structure-interaction analysis, several alternative formulations have been developed and published in the literature, including finite-element formulations, boundary-element, semi-analytical and analytical solutions and a variety of simplified methods. Each approach has its own advantages and limitations. The literature is extensive and reviewed in several specialized reports and research papers (Luco 1980, Wolf 1994). Ghosh and Lubkowski

(2007) presented modeling of dynamic SSI under seismic loads. Maheshwari and Watanabe (2009) reviewed the simplified approaches used for seismic analysis of pile foundations.

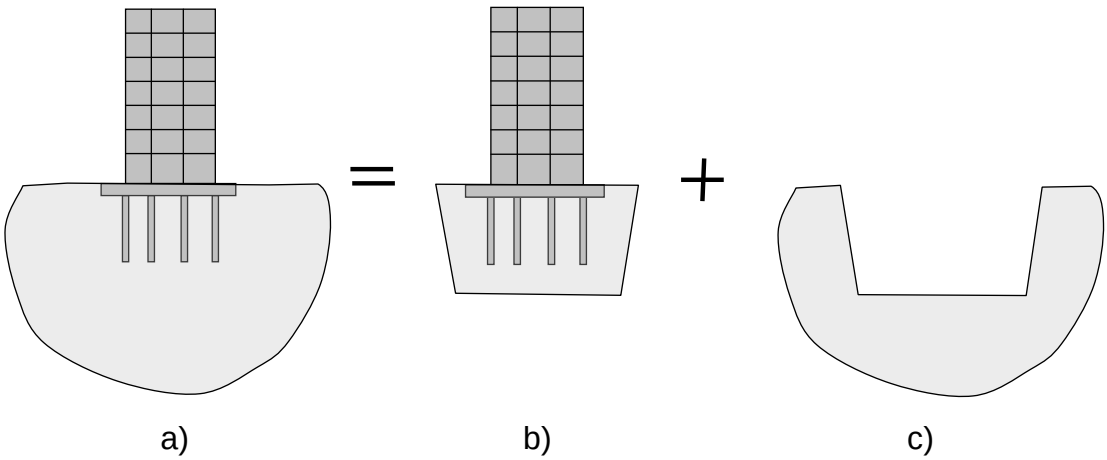

Figure 4: Seismic soil-structure interaction with substructure method (After Emani 2008)

These approaches can be classified as:

1. Continuous model based on the theory of elasticity.
2. Discrete models with lumped masses
3. Finite element techniques.

The continuous models can fully take into account the effect of radiation damping as well as the effect of added mass of soil but it is difficult to effectively model material nonlinearity and loss of bond between soil and pile in such models. On the other hand, the reverse is true in the case of discrete models (such as shown in Fig. 5). Finite element techniques overcome the limitation of both of these but for pile groups it may require enormous computation and prove to be very expensive which may not be justified from the accuracy obtained in the end results. Various steps of second approach are discussed in detail.

In a conventional approach (for linear elastic systems), soil-foundation-structure interaction (SFSI) analysis under seismic excitation can be conveniently performed in three consecutive steps, as schematically illustrated in Fig. 5:

1. Obtain the motion of the foundation in the absence of the superstructure. This so-called foundation input motion includes translational as well as rotational components i.e. basically kinematic interaction.
2. Determine the dynamic stiffness or dynamic impedances (springs and dashpots) associated with swaying (K_x or K_y), rocking (K_{ry} or K_{rx}), and cross-swaying-rocking ($K_{x\text{-}ry}$ or $K_{y\text{-}rx}$) oscillations of the foundation.
3. Compute the seismic response of the superstructure supported on the springs and dashpots of step 2 and subjected at its base to the foundation input motion of step 1.

For step 2, in frequency domain the dynamic impedances (K*) at a particular frequency ω may be defined as follows

(a) For viscous damping: $K^* = K_{st} - M\omega^2 + i\omega C$ (2a)

(b) For hysteretic damping: $K^* = K_{st}(1+2i\zeta)-M\omega^2$ (2b)

Where K_{st} is static stiffness matrix, M mass matrix and C is damping coefficient matrix. In general, dynamic impedances *(K*)* may be represented in a general form

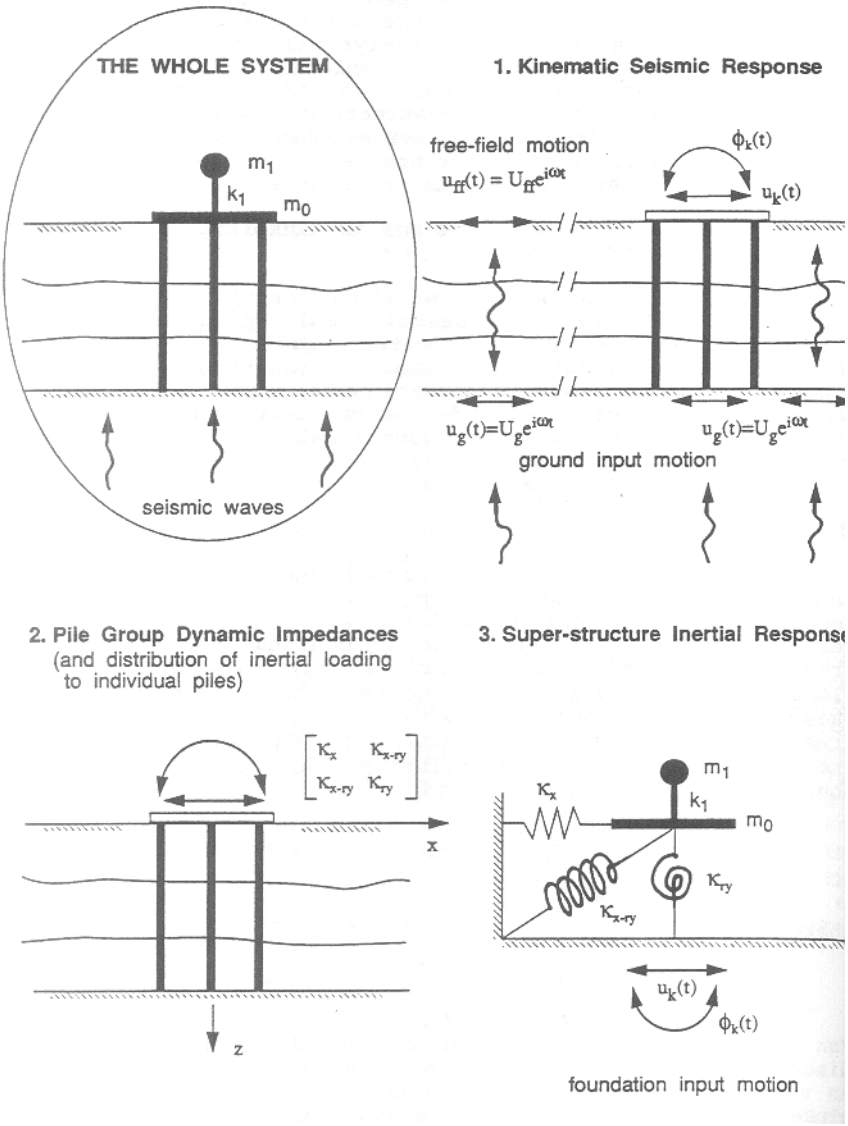

Figure 5: General procedure for seismic soil- (pile)-foundation-structure interaction using discrete models (After Gazetas et al. (1992)

$$K^* = K_{st}(k_1 + ik_2) \quad (3)$$

Where k_1 and k_2 are real and imaginary dimensionless coefficients of impedance respectively. k_1 represents the spring stiffness including the effect of inertia while k_2 represents damping force. The values of K_{st}, k_1 and k_2 can also be found using simple hand

calculations as proposed by few researchers, Gazetas (1991) and Wolf (1988). Whitman (1970) presented these coefficients for seismic design of nuclear power plants.

Simplified Approaches

Some of the simplified approaches where analysis can be performed using hand calculations are presented. These are used only for linear analysis. These are approaches are usually used for interaction between a rigid circular foundation within a homogeneous soil. One of such simple approach as presented by Gazetas (1991) is discussed here. According to this, Eq. 3 can be written as:

$$K^* = K(k + i\omega C) \tag{4}$$

Where K is static stiffness, k spring stiffness and C dashpot coefficient. The values of these can be found from tables and charts presented by Gazetas (1991). Pai (2011) presented a review on SSI analysis using simplified models.

9 RECENT ADVANCES IN SSI

Significant advancement has been made in SSI studies in last two decades. With the advances in computer technology now it is possible to model and analyze SSI problems more rigorously. Most of these advances are on two major and very important issues. First, the soil being an unbounded domain, its precise modeling is a complex issue. Second, the behavior of soil during strong excitation is highly nonlinear and even for saturated loose sands the liquefaction may occur. Considering nonlinearity of soil and liquefaction, further complicate SSI problems. Recent studies performed to deal with these issues are discussed. The author and his Ph.D. students (Emani and Sarkar) worked extensively in the area of SSI.

Maheshwari (2003) used Kelvin Elements to model the boundary and HiSS soil model to deal with nonlinearity. Emani (2008) carried out nonlinear dynamic SSI analysis using CIFECM for boundary and hybrid methods for computation. Sarkar (2009) considered liquefaction for SSI analysis. A number of research publications from these works are listed in references and further discussed in following sections.

10 MODELING OF BOUNDARY

There are many ways of modeling the boundary which can be grouped into following 2 categories

10.1 Approximate Boundaries

The approximate boundaries are local in space and time. Besides modeling the soil's stiffness up to infinity, reflections of the outwardly propagating waves on the interaction horizon are to be avoided. The elementary boundaries are the simplest boundaries, wherein zero displacements or zero surface tractions are implemented on the artificial boundary (Ghosh and Wilson 1969). The viscous boundaries (Lysmer and Kuhlemeyer 1969), can fully transmit only the waves impinging normally, and also lead to permanent deformations in the near-field (Wolf 1988). Maheshwari et al. (2005) used Kelvin elements for boundary.

Liao and Wong (1984) proposed the extrapolation boundaries, based on the premise that the boundary condition at an artificial boundary at a particular instant of time can be extrapolated from the values obtained at other nodes, at previous time stations. For higher transmitting orders, numerical instability occurs at the boundary leading to divergence of the solution (Liao and Liu 1992). Garg (1998) and Al Assady (2005) presented a transient transmitting boundary which extends the scope of extrapolation boundaries to two-

dimensional domains. Also, the problem of divergence at higher-order transmission has been removed.

Infinite element approach (Bettess 1977) incorporates shape functions obtained from a special form of fundamental solution which may not be available for all problems. Many researchers used coupled finite-infinite elements for linear and nonlinear soil-structure interaction problems (Viladkar et al. 1990, Godbole et al. 1990, Noorzaei 1991), under static conditions. The double asymptotic multi-directional transmitting boundaries and damping solvent extraction method require that the artificial boundary be situated quite far-away from the energy sink (Wolf and Song 1996). By selecting the interaction horizon to include a significant soil mass, sufficiently accurate results can be obtained, even with these approximate boundary conditions on the horizon. But, these boundaries are not exact for oblique incidence of stress waves. Wolf (1994) described various formulations for modeling the foundation vibrations using simple physical models.

10.2 Rigorous Boundaries

The rigorous boundaries are global in space and time. These boundaries can simulate the whole far-field, and so the interaction horizon is chosen such that the near-field effects are just-enclosed. In the frequency domain, the rigorous boundaries or consistent boundaries are formulated in the form of dynamic stiffness matrices. This matrix represents the force-displacement relationship at the artificial interface, and is fully coupled in spatial discretization. The evaluation of this matrix requires a separate and independent analysis of the unbounded far-field. The coupling with the near-field analysis is provided through the frequency variation of the dynamic stiffness matrix. This is the sub-structure approach to the dynamic soil-structure interaction analysis (Wolf 1985). For the time domain analysis, total coupling of time discretization also occurs, while evaluating the convolution integrals of the dynamic stiffness coefficients (Wolf 1988). Rigorous boundaries are formulated in four different forms (Wolf and Deeks 2004): 1) the boundary element methods, 2) the consistent boundary method or thin layer method, 3) the scaled-boundary finite element method, and 4) the Dirichlet-to Neuman method.

Boundary Element Methods: Rigorous boundary element methods (Brebbia et al. 1984, Beskos 1987, Dominiguez 1993, Banerjee 1994) are extensively used during the early stages of SSI analysis. This method is exact in satisfying the radiation boundary condition. Further, the spatial dimension is reduced by one, because only the boundary needs to be discretized, and not the domain being enclosed or excluded.

Consistent Boundaries: Use of consistent boundaries, also called Thin Layer method (Lysmer and Wass 1972, Waas 1972, Kausel and Roesset 1975 and Kausel et al. 1975) is a semi-analytical method developed for the analysis of foundations on layered strata. This boundary makes use of exact displacement functions in the horizontal direction that satisfy the radiation condition and an expansion in the vertical direction consistent with that used for finite element method. This consistent boundary formulation is exact in the horizontal direction and converges to the exact solution in a finite element sense in the vertical direction. It is based on finite element methodology and thus does not require a fundamental solution. This method is well suited to process horizontal layers with material properties varying in the vertical direction. The extension of this method in time domain has been made by Kausel (1994). However, the method is too rigorous for linear analysis itself, and becomes impractical to adopt for routine nonlinear analyses.

Consistent Infinitesimal Finite Element Cell Method (CIFECM): As an alternative to the boundary element method which applies analytical solution to include the radiation damping, a cloning algorithm based solely on the finite element formulation has been suggested by Das Gupta (1982). This algorithm is based on the similarity principle. He assumed a constant

average value of dynamic stiffness within the finite element cell formed by similar soil-structure interfaces. Wolf and Weber (1982) have extended the idea of cloning algorithm to take into account the variation of dimensionless frequency from interior to exterior of the cell. Later on, using the same concept as in the generalized cloning method, a new procedure called as Consistent Infinitesimal Finite Element Cell Method (CIFECM) has been developed by Wolf and Song (1996). This procedure has been re-derived recently, to make it more appealing mathematically, and also to make it consistent with finite element methodology in the circumferential direction (Wolf and Song 2000a, b). Emani and Maheshwari (2009) used CIFECM (Fig. 6) to model the boundary for SSI problems.

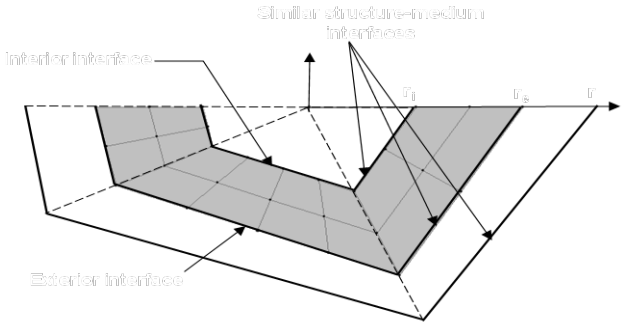

Figure 6: Concept of CIFECM

11 NONLINEARITY OF SOIL

Matlock et al. (1978) developed a unit load transfer curve (*p-y* curves), for the time domain nonlinear analysis for soil-pile interaction. Approximate modeling of soil domain using one dimensional Winkler models, e.g. Nogami and Konagai (1986 & 1988), Nogami et al. (1992), Badoni and Makris (1996), El Naggar and Novak (1995 & 1996), Wang et al. (1998). Other time domain methods, based on finite element formulation, are Wu and Finn (1997), Mylonakis and Gazetas (1999), Bentley and El Naggar (2000), Cai et al. (2000), Maheshwari et al. (2005). But in these methods, the frequency dependence of the unbounded soil can only be modeled in an approximate manner, especially so, when the loading is also transient, as in the case of seismic loading. Further, the local/ transmitting boundaries adopted in these methods cannot simulate the radiation boundary condition for oblique incidence of stress waves. These limitations can be overcome by using coupled Finite Element- Boundary Element (FE-BE) formulations.

Rigorous analytical methods in frequency domain, using the boundary integral methods e.g., Tajimi (1969), Kaynia and Kausel (1982), Mamoon et al. (1988), Fan et al. (1991), Miura et al. (1994), Maheshwari and Watanabe (2005) are restricted to steady-state response analysis of linear or at the most equivalent linear systems. Mamoon and Banerjee (1992) developed a direct time-domain and transformed time domain models for dynamic pile-soil interaction. Cheung et al. (1995) reported transient response of single pile under horizontal excitation, using boundary element method. Feng et al. (2003) reported a time domain BEM for dynamic response of a cylinder embedded in soil with frictional slip at the interface. For

obtaining the true nonlinear (or three-dimensional inelastic) dynamic response, the frequency dependence of the system is to be fully accounted for, while considering the temporal and three-dimensional spatial variation of system's response. These requirements are fulfilled by the coupling of frequency domain and time domain techniques along with FE-BE coupling. The authors demonstrated the ability of FE-BE coupled model to analyze 3D soil-pile systems with elastic behaviors (Emani and Maheshwari 2009) and cyclic nonlinear behaviors (Emani and Maheshwari 2008).

Emani (2008) proposed and demonstrated a hybrid framework of analysis. With respect to spatial discretization, the developed formulation is a mixture of both direct and substructure methods, wherein the near-field soil is modeled, along with the foundation structure, using finite elements, while enforcing a radiation condition at the boundary of the near-field. With respect to temporal variation, the procedure alternates between the frequency and time domains, within each iteration of nonlinear analysis. This method is based on the Hybrid Frequency Time Domain (HFTD) formulation described by Wolf (1988). To satisfy the radiation conditions, the CIFECM (Wolf and Song 1996) is used and to account for material nonlinearity of soil, HiSS model (Desai 2001), Fig. 7, is employed. Two types of SSI studies are done: 1) pile Cap-Soil-Pile Interactions (CSPI) under elasto-dynamic conditions, and 2) Pile-Soil-Pile Interaction (PSPI) under inelastic dynamic conditions. The developed frequency domain FE-CIFECM coupling algorithm is used to study the CSPI in pile groups having embedded pile caps and ground-contacting pile caps, while the 3D HFTD algorithm is used to study the PSPI effects in pile foundations with free-standing pile caps.

12 SSI IN LIQUEFIABLE SOIL

Iida (1998) performed three-dimensional nonlinear soil-building interaction analysis for several types of low to high rise buildings during hypothetical Guerrero earthquake. Input earthquake and the local site effects are reasonably taken into account. The results were consistent with the damage pattern observed during the Michoacan earthquake (1985). Wilson (1998), in his doctoral dissertation, studied the dynamic response of pile foundations in liquefying sand and soft clay during strong shaking. Finn and Fujita (2002) presented the design and analysis of pile foundations in liquefiable soils. Liyanapathirana and Poulos (2004) investigated the effect of nature of the earthquake on the assessment of liquefaction potential of a soil deposit during earthquake loading.

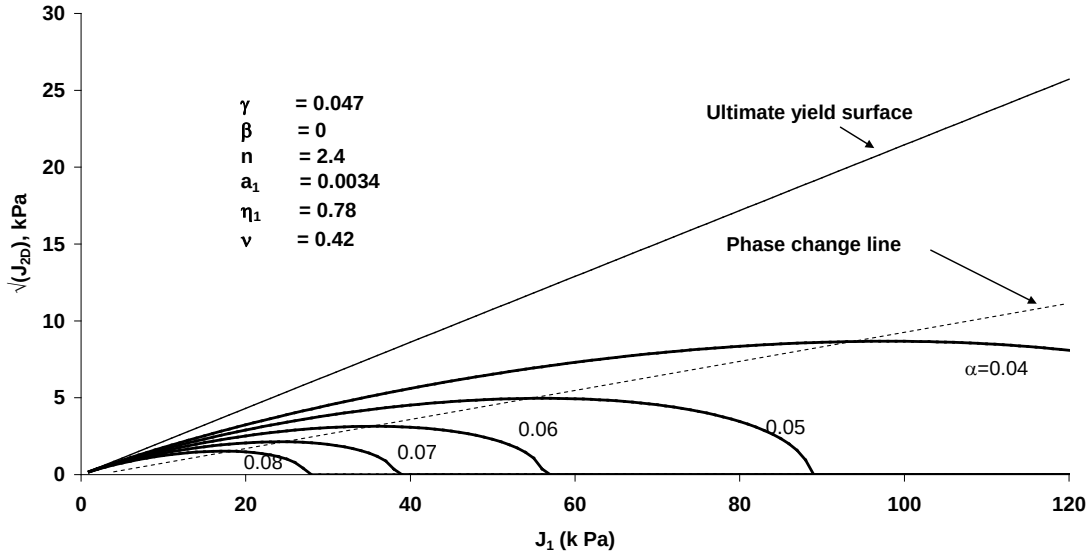

Figure 7: Shape of Yield Surface for HiSS soil model

Liyanapathirana and Poulos (2005) modelled piles in liquefying soil with dynamically loaded beam on Winkler foundation. Using the numerical model proposed by Seed *et al.* (1976), Maheshwari *et al.* (2008) presented the effect of liquefaction on response of pile foundation for vertical vibration. Li *et al.* (2006) conducted shaking table tests and analysis on soil-pile-structure interaction system with liquefaction of soil. The experimental results were compared with the analytical results with equivalent linear soil model.
Uzuoka *et al.* (2007) studied a five-story building that tilted northeastward because of serious pile damage during the Kobe earthquake (1995). Three-dimensional study was performed with elasto-plastic soil medium. Soil-water coupled analysis was performed for soil-pile-building model. Lopez-Cabalerro and Farahmand-Razavi (2008) carried out a 2D coupled finite element modeling using an elastoplastic multi-mechanism model to represent the soil behaviour. A significant parametric study on the influence of soil liquefaction on a Single Degree of Freedom (SDOF) structure was performed. Sarkar (2009) investigated the three-dimensional soil-pile behaviour under dynamic condition for the soil with liquefaction. The readers are referred to Maheshwari & Sarkar (2011, 2012), Sarkar and Maheshwari (2012a and 2012b), Syed (2014), Syed and Maheshwari (2014, 2015), Maheshwari and Emani (2015), Maheshwari & Syed (2015).

13 SUMMARY AND CONCLUSIONS

It can be observed from the discussion presented in this chapter that the soil-structure interaction is a very important issue to be considered in the design of structures. Ignoring this effect may not only lead to an uneconomical design but also it may be unsafe. It is not always the case that considering SSI would lead to conservative design, rather it may provide an economical as well as rational design. Effects of SSI are not always detrimental but may be favorable too. Some of the key conclusions from advanced studies in SSI (Emani 2008 and Sarkar 2009) are as follows

- The results from inelastic dynamic analysis of pile groups showed significant reduction, caused by soil plasticity, in both lateral stiffness and damping of the pile groups.

- The inelastic seismic analysis, in terms of kinematic interaction factors, shows that the effect of soil plasticity is not significant on the kinematic interaction effects in the considered pile group model.
- Both the real and imaginary parts of the dynamic stiffness reduce significantly due to nonlinearity of the soil medium. For the pile groups, the group effect also reduces significantly due to nonlinearity of the soil medium.
- Consideration of pore water pressure further reduces the dynamic stiffnesses significantly. It may also be concluded that in the presence of the pore pressure generation, the type of nonlinearity of the soil medium does not have significant influence on the behaviour of the soil-pile systems.
- The seismic response of the soil-pile systems for work hardening soil nonlinearity is greater than those with the soil nonlinearity without work hardening.
- Due to incorporation of pore water pressure generation in the soil medium, the seismic response increases significantly. Since both translation and rotation increases significantly, for design of piles in liquefying soil medium rotation needs to be taken into account which is not a common practice.
- From the investigation for real earthquake excitations, it is observed that the effect is very much dependent on PGA and frequency characteristics of input motion. The results obtained by real earthquake time history are consistent with the harmonic loading results.
- The translational KIF of the soil-pile system increases significantly for the softer soil with pore pressure.

REFERENCES

1. Al Assady, A. K. M. S. (2005) Modeling of nonlinear dynamic soil-structure interaction problems. Ph.D. Dissertation, Indian Institute of technology Roorkee, Roorkee, India.
2. ASCE (4-1998) Standard for Seismic Analysis of Safety-Related Nuclear Structures. ASCE 4-98, American Society of Civil Engineers.
3. Badoni, D. and Makris, N. (1996) Nonlinear response of single piles under lateral inertial and seismic loads. *Soil Dynamics and Earthquake Engineering*, 15, 29-43.
4. Banerjee, P. K. (1994) The Boundary Element Methods in Engineering, *McGraw-Hill*, London.
5. Bentley, K. J. and El Naggar, M. H. (2000) Numerical analysis of kinematic response of single piles. *Canadian Geotechnical Journal*, 37, 1368-1382.
6. Beskos, D. E. (1987) Boundary Element Methods in Dynamic Analysis. *Applied Mechanics Reviews*, 40, 1-23.
7. Bettess, P. (1977) Infinite elements. *International Journal of Numerical Methods in Engineering*. 11, 233-250.
8. Bielak, J. (1975) Dynamic behaviour of structures with embedded foundations. Journal *Earth. Engr. and Struct. Dynamics*, 3(3), 259-274.
9. Brebbia, C. A, Telles, J. C. F. and Wrobel, L. C. (1984) Boundary Element Techniques, *Springer*, Berlin.
10. Cai, Y.X., Gould, P.L. and Desai, C.S. (2000) Nonlinear analysis of 3D seismic interaction of soil-pile-structure system and application. *Engineering Structures*, 22 (2), 191-199.

11. Cheung, Y. K., Tharn, L. G., Lie, Z. X. (1995) Transient response of single pile under harmonic excitation. *Earthquake Engineering and Structural Dynamics*, 24, 1017-1038.
12. Dasgupta, G. (1982) A finite-element formulation for unbounded homogeneous continua. *Journal of Engineering Mechanics, ASCE*, 49, 136-140.
13. Desai, C. S. (2001). Mechanics of Materials and Interfaces: The Disturbed State Concept, CRC Press LLC.
14. Dominguez, J. (1993) Boundary Elements in Dynamics, *Computational Mechanics Publications*, Southampton.
15. Dowrick, D. (1987) Earthquake Resistance Design, *John Wiley & Sons*.
16. El Naggar, M.H. and Novak M. (1995) Nonlinear lateral interaction in pile dynamics. *Soil Dynamics and Earthquake Engineering*, 14, 141-157.
17. El Naggar, M. H. and Novak, M. (1996) Nonlinear analysis for dynamic lateral pile response. *Soil Dynamics and Earthquake Engineering*, 15, 233-244.
18. Emani, P.K. (2008), Nonlinear dynamic soil-structure interaction analysis using hybrid methods, Ph.D. Thesis, Dept. of Earthquake Eng., Indian Institute of Technology, Roorkee, India.
19. Emani, P.K. and Maheshwari, B.K. (2008) Nonlinear analysis of pile groups using hybrid domain method, *Proc. of 12th International Conference of IACMAG*, Goa, India, Paper No. 1590.
20. Emani, P.K. and Maheshwari, B.K. (2009) Dynamic impedances of pile groups with embedded caps in homogeneous elastic soils using CIFECM. *Soil Dynamics and Earthquake Engineering*, 29(6), pp. 963-973.
21. Fan, K., Gazetas, G., Kaynia, A. M., Kausel, E. and Shahid, A. (1991) Kinematic Seismic response of single piles and pile groups. *J. of Geotechnical Eng. ASCE*, 117 (12), 1860-1879.
22. Finn, W.D.L. and Fujita, N. (2002) Piles in liquefiable soils: seismic analysis and design issues. *Soil Dynamics and Earthquake Engineering*, 22, 731-742.
23. Feng, Y-D., Wang, Y-S. and Zhang, Z-M. (2003). Time domain BEM analysis of dynamic response of a cylinder embedded in soil with frictional slip at the interface., *Soil Dynamics and Earthquake Eng*., 23, 303-311.
24. Garg, S. K. (1998). Nonlinear transient dynamic soil-structure interaction with special reference to blast loading. Ph.D. Dissertation, University of Roorkee, Roorkee, India.
25. Gazetas, G. (1991) Formulas and charts for impedances of surface and embedded foundations. *J. of Geotechnical Engineering ASCE* 117, No.9, 1363-1381.
26. Gazetas G., Fan K., Tazoh T., Shimizu K., Kavvadas M. and Makris N. (1992), Seismic Pile-Group-Structure Interaction, in Piles Under Dynamic Loads, *Edited by Shamsher Prakash, Geotechnical Special Publication*, 34, ASCE, New York.
27. Gazetas, G. and Mylonakis, G. (1998) Seismic soil structure interaction: new evidence and emerging issues. *Geotechnical Special publication*, 75, 1119-1174.
28. Ghosh B. and Lubkowski Z. (2007) Modeling Dynamic Soil-Structure Interaction under Seismic Loads, Chapter 7 in Design of Foundation in Seismic Areas: Principles and Applications, *Editor, Bhattacharya S., NICEE, IIT Kanpur*, pp. 353-386.
29. Ghosh, S. and Wilson, E. L. (1969) Analysis of axi-symmetric structures under arbitrary loading. *EERC report No.69-10, University of California*, Berkeley, USA.
30. Godbole, P. N., Viladkar, M. N. and Noorzaei, J. (1990) Nonlinear soil-structure interaction analysis using coupled finite-infinite element elements. *Computers and Structures*, 36(6), 1089-1096.

31. Iida, M. (1998) Three-dimensional non-linear soil building interaction analysis in the lakebed zone of Mexico city during the hypothetical Guerrero earthquake. *Earthquake Engineering and Structural Dynamics*, 27, 1483-1502.
32. IS: 1893-2002 – Part 1: Criteria for Earthquake Resistant Design of Structures: General Provisions and Buildings, *Bureau of Indian Standards*, New Delhi.
33. Kaynia, A.M. and Kausel, E. (1982) Dynamic behavior of pile groups, *Proceedings of 2nd Int. Conf. on Numerical Methods in Offshore Piling*, Austin, Texas, 509-532.
34. Kausel, E. (1994). Thin-layer method: formulation in the time domain. *International Journal of Numerical Methods in Engineering*, 37, 927-941.
35. Kausel, E. and Roesset, J. M. (1975) Dynamic stiffness of circular foundations. *Journal of Engineering Mechanics Division, ASCE*, 101, 771-785.
36. Kausel, E., Roesset, J. M. and Waas, G. (1975) Dynamic analysis of footings in layered media. *Journal of Engineering Mechanics Division, ASCE*, 101, 679-693.
37. Kim, S. & Stewart, J.P. (2003) Kinematic Soil-Structure Interaction from Strong Motion Recordings. *J. of Geotech. and Geoenv. Eng., ASCE*, Vol. 129(4), 323-335.
38. Li, P., Lu, X. and Chen, Y. (2006) Study and analysis on shaking table tests of dynamic interaction of soil-structure considering soil liquefaction. *In Proc. of the 4th International Conference on Earthquake Engineering*, Taipei, Taiwan.
39. Liao, Z.P. and Liu, J. B. (1992) Numerical instability of a local transmitting boundary. *Earthquake Engineering and Structural Dynamics*, 21, 65-77.
40. Liao, Z. P. and Wong, H. L. (1984) A transmitting boundary for the numerical simulation of elastic wave propagation. *Soil Dynamics and Earthquake Engineering*, 2, 174-183.
41. Liyanapathirana, D.S. and Poulos, H.G. (2004) Assessment of soil liquefaction incorporating earthquake characteristics. *Soil Dynamics and Earthquake Engineering*, 24, 867-875.
42. Liyanapathirana, D.S. and Poulos, H.G. (2005) Seismic lateral response of piles in liquefying soil. *Journal of Geotechnical and Geoenvironmental Engineering, ASCE*, 131(12), 1466-1478.
43. Lopez-Cabalerro, F. and Farahmand-Razavi, A.M. (2008) Numerical simulation of liquefaction effects on seismic SSI. *Soil Dynamics and Earthquake Engineering*, 28, 85-98.
44. Luco, J.E. (1980) Linear soil structure interaction in Seismic Safety Margins Research program. *U.S. Nuclear Regulatory Commission*, Washington D.C.
45. Luco, J.E. and Wong, H.L. (1986) Response of rigid foundation to a spatially ground motion. *Journal; of Earth. Eng. Struct. Dynamics*, 14(6),891-908.
46. Luco, J.E. and Mita, A. (1987). "Response of circular foundation to spatially random ground motion." Journal Eng. Mech. ASCE, 113(1), 1-15.
47. Lysmer, J. and Kuhlemeyer, R. L. (1969) Finite dynamic model for infinite media. *Journal of Engineering Mechanics ASCE*, 95(4), 859-875.
48. Lysmer, J. and Waas, G. (1972) Shear waves in plane infinite structures. *Journal of Engineering Mechanics Division, ASCE*, 98, 85-105.
49. Maheshwari B.K. (1997) Soil-Structure-Interaction on the Structures with Pile Foundations-A Three Dimensional Nonlinear Dynamic Analysis of Pile Foundations, Ph.D. Dissertation, Dept. of Civil Engineering, Saitama University, Japan Sept. 1997.
50. Maheshwari B.K. (2003) Three-dimensional finite element nonlinear dynamic analyses for soil-pile-structure interaction in the time domain, *Research report submitted to Mid America Earthquake Center (NSF), Dept. of Civil Engineering, Washington University*, St. Louis, Missouri, March 2003.

51. Maheshwari B.K., Truman K.Z., El Naggar M.H. and Gould P.L. (2004a) Three-dimensional Finite Element Nonlinear Dynamic Analysis of Pile Groups for Lateral Transient and Seismic Excitations, *Canadian Geotechnical J.*, 41,118-133.
52. Maheshwari B.K., Truman K.Z., El Naggar M.H. and Gould P.L. (2004b) 3-D Nonlinear Analysis for Seismic Soil-Pile-Structure Interaction", *Soil Dynamics and Earthquake Engineering, Elsevier*, 24(4), 345-358.
53. Maheshwari B.K., Truman K.Z., Gould P.L. and El Naggar M.H. (2005) Three-Dimensional Nonlinear Seismic Analysis of Single Piles using FEM: Effects of Plasticity of Soil, *Int. Journal of Geomechanics, ASCE*, 5(1), March 2005.
54. Maheshwari, B.K. and Watanabe H. (2005). Dynamic analysis of pile foundations: effects of material nonlinearity of soil, Electronic *Journal of Geotechnical Engineering*, 10 (E), Paper No. 0585.
55. Maheshwari B.K. and Watanabe H. (2006) Nonlinear Dynamic Behavior of Pile Foundations: Effects of Separation at the Soil-Pile Interface, *Soils and Foundations, Japanese Geotechnical Society*, Paper No. 3234, 46 (4), pp. 437-448.
56. Maheshwari, B.K., Nath, U.K. and Ramasamy, G. (2008) Influence of liquefaction on pile-soil interaction in vertical vibration. *ISET Journal of Earthquake Technology*, 45(1), 1-13.
57. Maheshwari B.K. and Watanabe H. (2009). Seismic Analysis of Pile Foundations using Simplified Approaches, *International Journal of Geotechnical Eng*., 3 (3), 387-404.
58. Maheshwari B.K. (2011) Advances in Soil-Structure Interaction Studies, *Proc. of Post-SMiRT-21 Conference Seminar on Advances in Seismic Design of Structures, Systems and Components of Nuclear Facilities*, NPCI, BARC, Mumbai, India.
59. Maheshwari B.K. and Sarkar R. (2011) Seismic Behavior of Soil-Pile-Structure Interaction in Liquefiable Soils: Parametric Study, *International Journal of Geomechanics, ASCE*, 11 (4), 335-347.
60. Maheshwari B.K. and Sarkar R. (2012) Effect of Soil Nonlinearity and Liquefaction on Seismic Response of Pile Groups, *International J. of Geotechnical Engineering*, 6 (4), 497-506.
61. Maheshwari (2014), Recent Advances in Seismic Soil-Structure Interaction, *Proc. of the Indian Geotechnical Conference held in Kakinada*, Andhra Pradesh, pp. 2463-2477.
62. Maheshwari B.K. and Emani P.K. (2015) Three Dimensional Nonlinear Seismic Analysis of Pile Groups using FE-CIFECM coupling in Hybrid Domain and HiSS Plasticity Model, *International Journal of Geomechanics, ASCE*, 15(3), 04014055-1-12.
63. Maheshwari B.K. and Syed N.M. (2015), Verification of Implementation of HiSS soil model in the coupled FEM-SBFEM SSI Analysis, DOI: 10.1061/(ASCE)GM.1943-5622.0000511.
64. Mamoon, S. M. and Banerjee, P. K. (1992) Time domain analysis of dynamically loaded single piles. *Journal of Engineering Mechanics Division, ASCE*, 118, 14-160.
65. Mamoon, S. M., Banerjee, P. K. and Ahmad, S. (1988) Seismic response of pile foundations. *Technical Rep. No. NCEER-88-003, Dept. of Civil Engineering*, State Univ. of Newyork, Buffalo, N.Y.
66. Meek J. W., Veletsos A. S. (1974), Simple models for foundations in lateral rocking motions. *Proceedings of Fifth World Congress on Earthquake Engineering, Rome*; Vol. 2, pp. 2610–3.
67. Michalopoulos, A.P. and Vardanega, C. (1981) Effects of soil stiffness and embedment on reactor building response, SMiRT-6, K4/5.

68. Miura, K., Kaynia, A. M., Masuda, K., Kitamura, E. and Seto, Y. (1994) Dynamic behavior of pile foundations in homogenous and non-homogenous media. *Earthquake Eng. and Structural Dynamics*, 23, 183-192.
69. Mylanokis, G. and Gazetas, G. (1999) Lateral vibrations and internal forces of grouped piles in layered soil. *J. of Geotechnical and Geoenvironmental Eng. ASCE*, 125 (1), 16-25.
70. Mylonakis, G. and Gazaetas, G. (2000) Seismic soil structure interaction: Detrimental or Beneficial. *Journal of Earthquake Engineering*, 4 (3), 277-301.
71. Nogami, T. and Konagai, K. (1986) Time domain axial response of dynamically loaded single piles, *J. Eng. Mech., ASCE*, 112(11), 1241-1252.
72. Nogami, T. and Konagai, K. (1988) Time domain flexural response of dynamically loaded single piles, *J. Eng. Mech., ASCE*, 114(9), 1512-1525.
73. Nogami, T., Otani, J., Konagai, K. and Chen, H. L. (1992) Nonlinear soil-pile interaction model for dynamic lateral motion. *Journal of Geotech. Engg. ASCE*, 118 (1), 89-106.
74. Noorzaei, J. (1991). Non-linear Soil-Structure Interaction in Framed Structures. Ph. D Thesis, Civil Engineering Department, University of Roorkee, Roorkee, India.
75. Pai Ganesh M. (2011), Soil-Structure Interaction using Simplified Models, M. Tech. Dissertation, Dept. of Earthquake Eng., Indian Institute of Technology, Roorkee, India.
76. Sarkar Rajib (2009), Three Dimensional Seismic Behavior of Soil-Pile Interaction with Liquefaction, Ph.D. Thesis, Dept. of Earthquake Eng., Indian Institute of Technology, Roorkee, India.
77. Sarkar R. and Maheshwari B.K. (2012a) Effects of Separation on the Behavior of Soil-Pile Interaction in Liquefiable Soils, *Int. Journal of Geomechanics, ASCE*, 12(1), 1-13.
78. Sarkar R. and Maheshwari B.K. (2012b) Effect of Soil Nonlinearity and Liquefaction on Dynamic Stiffness of Pile Groups, *Int. J. of Geotechnical Eng.*, 6 (3), 319-329.
79. Seed, H. B., Martin, P. P. and Lysmer, J. (1976) Pore-water pressure changes during soil liquefaction. *Journal of Geotechnical Engineering Division, ASCE*, 102(GT4), 323-346.
80. Seed, R.B., Dickenson, S.E., Riemer, M.F., Bray, J.D., Sitar, N. Mitchell, J. et al. (1990). Permeability report on the principal geotechnical aspects of the October 17, 1989 Loma Prieta Earthquake. *Report No. UCB/EERC-90/05*.
81. Seed, R.B., Dickenson, S.E. and Mok, C.M. (1992) Recent lessons regarding seismic response analyses of soft and deep clay sites. *Proc. Seminar on seismic design and retrofit of bridges*, Univ. of California, 18-39.
82. Syed (2014), Nonlinear Seismic Soil-Structure Interaction using Scaled Boundary Finite Element Method, Ph.D. Thesis, Dept. of Earthquake Eng., IIT Roorkee.
83. Syed N.M. and Maheshwari B.K. (2014), Modeling using Coupled FEM-SBFEM for Three Dimensional Seismic SSI in Time Domain, *International Journal of Geomechanics, ASCE*, Vol. 14, No. 1, pp. 118-129.
84. Syed N.M. and Maheshwari B.K. (2015), Improvement in the Computational Efficiency of the Coupled FEM-SBFEM approach for 3D Seismic SSI Analysis in the Time Domain, *Computers and Geotechnics*, 67, 204-2012.
85. Tajimi, H. (1969). Dynamic analysis of a structure embedded in an elastic stratum. *Proc., 4th World Conference on Earthquake Engineering*, Chile Association on Seismology and Earthquake Engineering, Santiago, Chile, Vol. 3, 53-69.

86. Uzuoka, R., Sento, N., Kazama, M., Zhang, F., Yashima, A. and Oka, F. (2007) Three-dimensional numerical simulation of earthquake damage to group-piles in a liquefied ground. *Soil Dynamics and Earthquake Engineering*, 27, 395–413.
87. Veletsos A. S., Prasad A. M. and Wu W. H. (1997). Transfer functions for rigid rectangular foundations, *J. of Earthquake Engg. and Structural Dyn.*, 26 (5), 5-17.
88. Waas, G. (1972) Linear two-dimensional analysis of soil dynamics problems in semi-infinite layered media. Ph.D. Dissertation, Univ. of California, Berkeley, CA.
89. Whitman R.V. (1970) Soil-Structure Interaction, In Seismic Design for Nuclear Power Plants, *Editor Hansen R.J., The M.I.T. Press, Cambridge, Massachusetts*, USA, pp. 245-269.
90. Wolf, J.P. (1985) Dynamic Soil-Structure-Interaction, *Prentice-Hall, Inc., Englewood* Cliffs, New Jersey.
91. Wolf, J.P. (1988) Soil-Structure-Interaction in the Time Domain, *Prentice-Hall, Inc., Englewood Cliffs*, New Jersey.
92. Wolf J. P. (1994) Foundation vibration analysis using simple physical models. PTR Prentice-Hall, Englewood Cliffs, NJ, USA.
93. Wolf, J. P. and Deeks, A. (2004) Foundation Vibration Analysis: A Strength-of-Materials Approach, *Elsevier*, Oxford.
94. Wolf, J. P., and Song, C. (1996) Finite element modeling of unbounded domain, *John Wiley and Sons Ltd*, Chichester.
95. Wolf, J. P. and Song, C. (2000a) The scaled boundary finite element method- a premier: derivations. *Computers and Structures*, 78, 191-210.
96. Wolf, J. P. and Song, C. (2000b) The scaled boundary finite element method- a premier: solution procedures. *Computers and Structures*, 78, 211-225.
97. Wolf, J. P. and Weber, B. (1982) On a matrix Ricatti equation of stochastic control. *SIAM Journal of Applied Mechanics*, Society for Industrial and Applied Mathematics, 6, 681-697.

Finite Difference Method in Numerical Modelling

Priti Maheshwari
Associate Professor, Department of Civil Engineering,
Indian Institute of Technology Roorkee
pritifce@iitr.ac.in

1 INTRODUCTION

In case, modelling of any system leads to a differential equation which cannot be integrated in closed form, one of the solutions employing the numerical methods is finite difference method (FDM). It has an advantage of solving the differential equation without the knowledge of higher mathematics or of physics. The numerical solution of differential equations consists essentially in obtaining the numerical values of unknown integral, *f* at some pivotal points spaced in the domain of interest with respect to the system. To obtain the pivotal values of the integral *f*, the derivative of *f* appearing in differential equation are approximated either by the derivatives of n^{th} degree parabolas passing through a certain number of pivotal points or by Taylor expansions of the unknown function *f*.

2 DIFFERENTIATION EXPRESSIONS

For obtaining the approximate expressions for the derivatives of a function *y(x)* at pivotal points, first the spacing between the pivotal points is to be decided. This can be equal or unequal depending upon the requirement. Whenever pivotal points are evenly spaced (Fig. 1), the Taylor series technique can be applied symbolically in conjunction with the concept of difference, which plays an important role in all numerical computations. A large variety of practical approximations for the derivatives and the corresponding errors may be economically obtained.

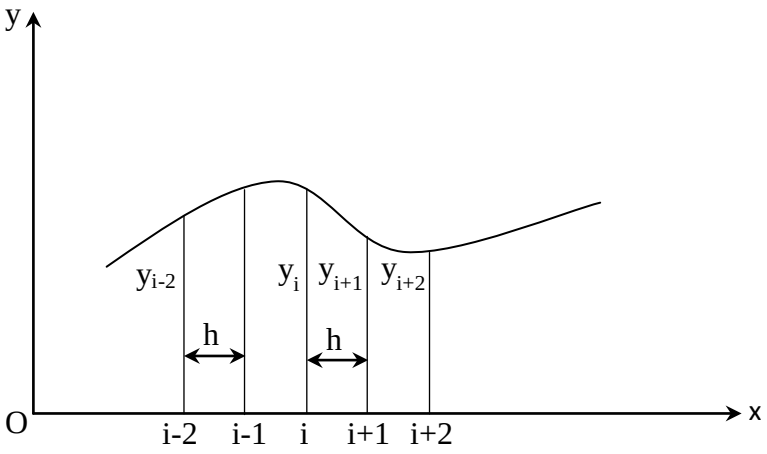

Figure 1: Equal spacing of pivotal points

Backward, forward and central difference schemes are available to obtain the expressions for the derivatives of a function at pivotal points. In case of backward and forward differences, if the first *m* terms of the derivative expansions are taken into account, the corresponding expressions have errors of order h^m. However, for central difference schemes, the order of errors is h^{2m} [1]. Typical derivative expressions (*D*) in terms of central

differences have been given in the mathematical molecules of Fig. 2 with corresponding order of error in the derivatives.

The spacing of the pivotal points should be chosen judiciously. Larger spacing will not yield correct results and associated errors will also be very large. Too small a spacing may reduce the errors but may cause non-convergence of the solution. Further, even for converging situation, the solution process will take much longer time without any benefit towards the accuracy of results.

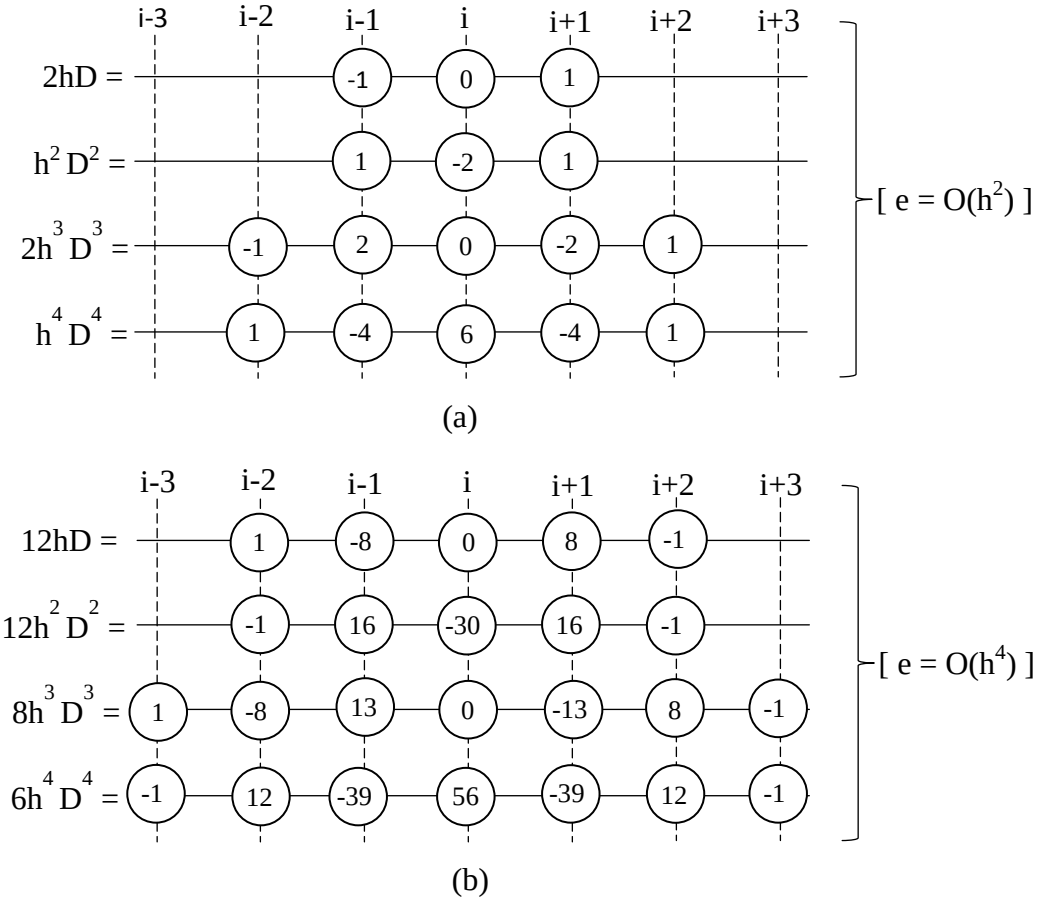

Figure 2: Central difference operators

The differential equation is written at each pivotal point, in finite difference form as mentioned above, resulting into a set of algebraic equations. This set is then solved employing appropriate numerical method along with proper boundary, continuity and initial conditions (as applicable to the relevant system).

3 APPLICATION

The above methodology has been explained with the help of a very simple soil-structure interaction problem. The problem is related to a beam resting on soil mass as shown in Fig. 3. Length and flexural rigidity of the beam is taken as *L* and *EI* respectively. The beam is subjected to a uniformly distributed load of intensity *q*. To analyze the problem, the soil mass is replaced by equivalent elastic springs (Winkler's concept) having stiffness *k*.

The resulting governing differential equation can be obtained by bending of the beam as follows:

$$EI\frac{d^4y}{dx^4}+ky=q \tag{1}$$

Where, y is the deflection of the beam at any point which is a function of x.

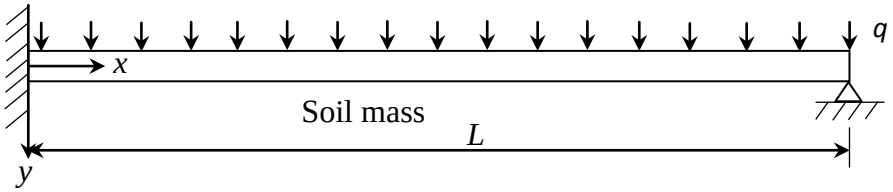

Figure 3: Beam resting on soil mass

The appropriate boundary conditions are as follows:

At $x = 0$, $y = 0$ and $\frac{dy}{dx}=0$, and

At $x = L$, $y = 0$ and $\frac{d^2y}{dx^2}=0$ (2)

For the solution purpose, a non-dimensional parameter is defined as $z = x/L$, and therefore equation (1) results:

$$\frac{d^4y}{dz^4}+\left(\frac{kL^4}{EI}\right)y=\left(\frac{qL^4}{EI}\right) \tag{3}$$

Assuming, $\left(\frac{kL^4}{EI}\right)=6$ and $\left(\frac{qL^4}{EI}\right)=265$

For the process of discretization, say, the beam is divided into 4 nodes resulting into 1, 2, 3 and 4 nodal points (Fig. 4). Nodes -1 and -4 are fictitious nodes.

Figure 4: Discretization

For nodal point 2, equation (3) can be written in finite difference form as –

$$\left(y_4 - 4y_3 + 6y_2 - 4y_1 + y_{-1}\right) + \left(\frac{6}{81}\right) y_2 = \left(\frac{265}{81}\right) \tag{4}$$

From boundary conditions, $y_1 = 0$ and $y_4 = 0$ and therefore, equation (4) becomes:

$$\left(-4y_3 + 6y_2 + y_{-1}\right) + \left(\frac{6}{81}\right) y_2 = \left(\frac{265}{81}\right) \tag{5}$$

Now, from equation (5) y_{-1} is to be eliminated for which second boundary condition at $x = 0$ is to be employed. This will result into $y_{-1} = y_2$ and therefore equation (5) will reduce to the following:

$$\left(-4y_3 + 6\left(\frac{1}{81} + \frac{7}{6}\right) y_2\right) = \left(\frac{265}{81}\right) \tag{6}$$

Similarly, for nodal point 3, the finite difference form of equation (3) will be written as:

$$\left(y_{-4} - 4y_4 + 6y_3 - 4y_2 + y_1\right) + \left(\frac{6}{81}\right) y_3 = \left(\frac{265}{81}\right) \tag{7}$$

From boundary conditions: $y_4 = 0$ and $y_{-4} = 2y_4 - y_3 = -y_3$

Therefore, equation (7) becomes

$$\left(-4y_2 + 6\left(\frac{1}{81} + \frac{5}{6}\right) y_3\right) = \left(\frac{265}{81}\right) \tag{8}$$

Equations (6) and (8) are solved to get the values of y_2 and y_3.

The above example shows the methodology to be adopted for using finite difference method. The choice of number of nodal points is to be decided based on the convergence study. The governing differential equation is then applied to all the nodal points along with appropriate boundary conditions. This results into set of algebraic equations which can be solved by using any available method to obtain the unknowns.

REFERENCES

1. Salvadori, M.G. and Baron, M.L. (1963), *Numerical Methods in Engineering*. Prentice-Hall of India (Pvt.) Ltd.

Inverse Analysis in Geotechnical Engineering

Tadikonda Venkata Bharat
Assistant Professor,Department of Civil Engineering,
Indian Institute of Technology Guwahati
tvb@iitg.ernet.in

Understanding and prediction of natural phenomena such as weather fluctuations, earthquake and rainfall events, occurrences of disasters, etc. are interest to mankind. Similarly, the geotechnical and allied engineering disciplines strive to understand the soil behavior due to changes in nature (slope failures during rainfall and earthquake events) or man-made factors such as application of loads, chemical contamination, etc. Measurement of soil state using instrumentation provides useful insights into the soil behavior under specified conditions.

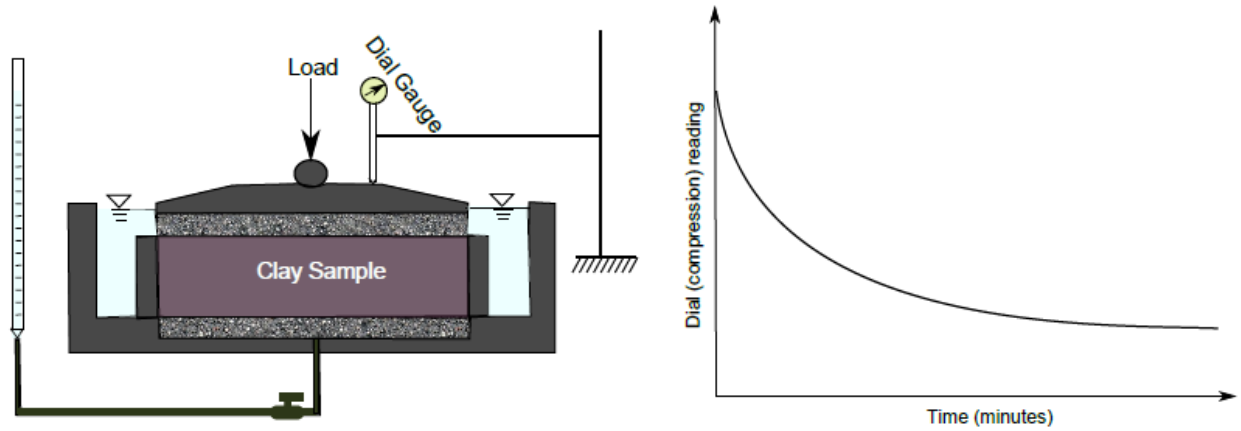

Figure 1: Settlement measurement in consolidation set-up (after Bharat and Sridharan, 2015)

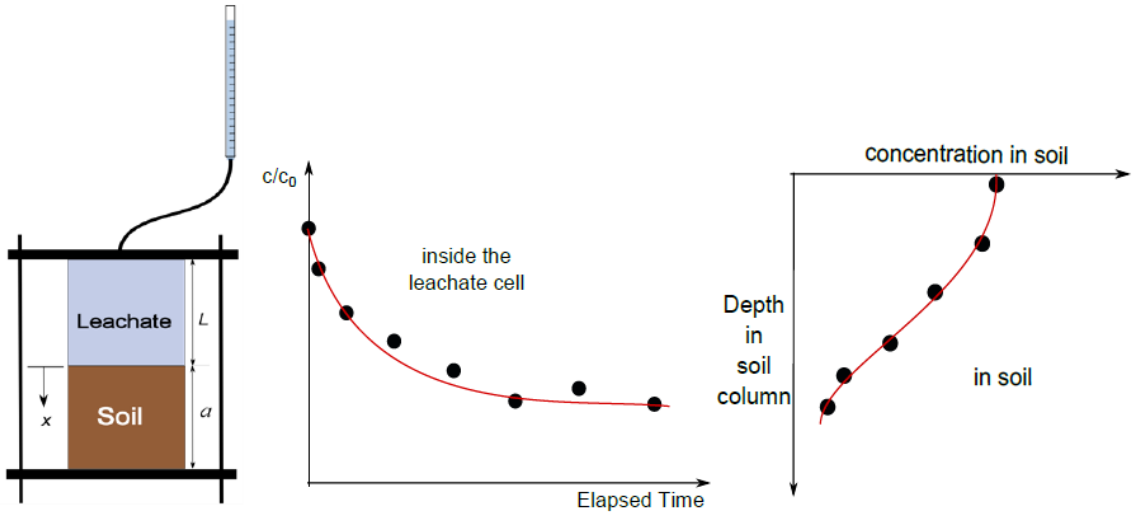

Figure 2: Contaminant diffusion through soil (Shackelford and Daniel, 1991)

For example, consolidation behavior of soils is routinely estimated in the laboratory using consolidation set-up by noting the change in dial gauge readings with time under application of load as illustrated in Fig. 1. Similarly, the diffusion behavior of contaminants through soil column is estimated using in-diffusion cell by maintaining a concentration gradient across the soil sample as shown in Fig. 2. A spatial and temporal variation of concentration is shown in

the same figure. However, the observed data in the laboratory experiments viz. rate of consolidation settlement, spatial distribution of contaminant concentration, or temporal variation are influenced by the sample dimensions and laboratory conditions. Therefore, material dependent quantities such as coefficient of consolidation, C_v (m^2/s), and diffusion coefficient, D_e (m^2/s) are extracted from the data obtained in controlled experiments and mathematical equations as follows:

$$\frac{\partial u}{\partial t} = C_v \frac{\partial^2 u}{\partial x^2} \tag{1}$$

and

$$\frac{\partial c}{\partial t} = D_e \frac{\partial^2 c}{\partial x^2} \tag{2}$$

and c is the contaminant concentration. In-situ settlement behavior of soils and diffusion rates of contaminants through soils under different field conditions can be predicted once the material constants are estimated. The estimation of C_v or D_e from eq. (1) or (2), respectively, using the observed data $u_o(x,t)$ or $c_o(x,t)$ requires inverse analysis. The parameter C_v is routinely estimated from the settlement data using graphical analysis (Taylor, 1948) thus inverse analysis is circumvented for consolidation problems. Nevertheless, other geotechnical problems such as contaminant diffusion through soils, transient flows through soils, etc. require inverse analysis for the prediction of soil behavior under different realistic conditions. The inverse problems are commonly addressed using optimization techniques. In a diffusion problem, for example, the theoretical concentration data, $c_t(x,t)$, is obtained by solving eq. (2) along with appropriate boundary and initial conditions for an assumed D_e. The objective of any optimization problem is to find a minimum error between $c_o(x,t)$ and $c_t(x,t)$ by varying D_e. Any suitable objective function (i.e., error norms), O, can be considered for optimization.

Gradient based optimization strategies such as Levenberg-Marquardt (1963) algorithm are classical techniques used in various science and engineering disciplines. In this technique, the solution is searched in an n-dimensional search space obtained by the objective function, $O(\vec{x})$, where $\vec{x} = D_e$ for diffusion problem (Fig. 2). The objective function is thereby approximated by a terminated Taylor series expansion around i, which is an initial guess. Once the initial guess is chosen and the objective function is computed using the initial guess value, movement phase is performed based on the gradient and step length. In gradient-based methods, the unknown parameter vector, $\vec{x}$, is searched iteratively as illustrated in Fig. 2.Superior methods also use Hessian matrix for better convergence. The readers can refer standard textbook for a detailed explanation of these methods (Rao, 1993).

Gradient-based techniques show several limitations. The major limitation with these techniques is that convergence to the global optimum solution is not guaranteed for non-convex search spaces. The solution convergence also depends on the initial guess solution when multiple local optima are available and/or the search space is non-convex. For example, consider the search space illustrated in Fig. 2. If the initial guess is assumed to be i_1, according to the gradient descent the solution converges to M_1 which happens to be a local optimum. On the other hand, if the chosen initial guess is i_2, the solution convergences to global optimum. However, the presence of local minima or number of minima is not known a priori. Further, for some methods the computation of Hessian matrix and the gradients of the objective function with respect to the design parameters are required. The inverse of the modified Hessian matrix needs to be computed at every iteration. Determination of gradients of the objective function analytically may be difficult in many engineering problems and,

therefore, numerical solutions are required. The size of the Hessian matrix is equal to the number of parameters to be estimated. Therefore, when more number of parameters needs to be estimated the computational cost also increases relatively.

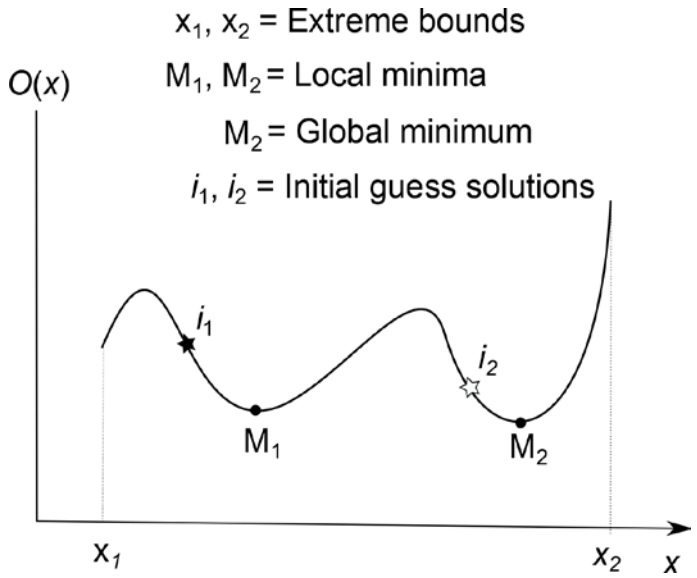

Figure 3: Strategy of classical optimization techniques

Gradient-free algorithms became popular with the advent of high-speed computers and growing requirement for optimization problems in multi-disciplinary areas such as combinatorial problems. Algorithms based on swarm intelligence are the class of derivative-free and population-based stochastic techniques. Ant colony optimization (ACO), Particle swarm optimization (PSO), and Bee colony optimization (BCO) are some of such techniques widely used for many industrial and research applications using the strategies drawn from the nature viz. behavior of ants, birds, and honeybees, respectively. A pre-defined swarm of agents move through the solution space using probabilistic rules and primitive mathematical operators for finding the global optimum solution. The probabilistic rules differ from technique to technique. The agents represent each potential solution of the target function directly. In PSO (PSO-Tutorial), each agent representing a potential solution moves in the search space, adaptively updates its velocity and position according to its own flying experience, and the flying experience of others; aiming at a better position for itself. Moreover, each individual enjoys a memory and remember the best position of the search space ever visited. Therefore, the movement is based on the direction of its best previously visited position and the best individual of whole swarm. For example, consider a swarm of three agents i_1, i_2, and i_3 on the search space as shown in Fig. 3. The velocity of each agent, v_i, is estimated by

$$v_i = v_i + k_1\left(pbest_i - i_1\right) + k_2\left(gbest - i_1\right) \tag{3}$$

where k_1 and k_2 are two random numbers, *pbest* is the individual best position of an agnet (determined using objective function), *gbest* is the global best solution. The position of the individual agent is updated using

$$x_i = v_i + x_i \tag{4}$$

where x_i is the current position of the agent. The agents determine the respective objective functions at the current location and update their positions according to the aforementioned

equations. As the agents i_3 and i_2 find i_1 as the better position (minimum objective function) according to Fig. 4, agents i_3 and i_2 will be pulled towards i_1 in small spatial increments over number of iterations. During this search process, when i_2 reaches M_2 while moving towards i_1 realizes that M_2 is the best location (minimum objective function) and other agents will be drawn towards him. If other agents do not find a better position during the exploration phase, all the agents converge at M_2.

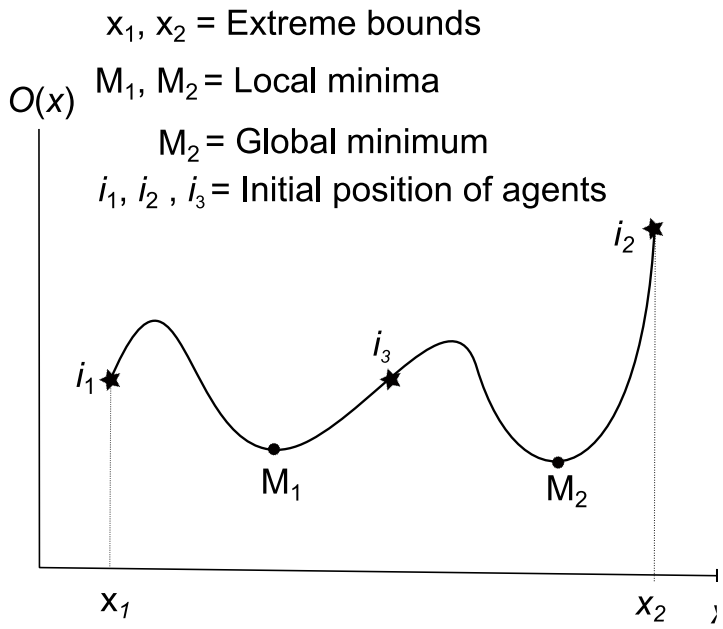

Figure 4: Strategy of agent based techniques

As PSO is a simple and robust technique, it is widely used for finding (non-circular) critical slip surface in slope stability analysis, finding the design parameters of landfill & vertical barriers, consolidation settlements of soft clays, etc. Studies on the application of the stochastic algorithms on some complex benchmark functions indicate that the agents stagnate at suboptimal solutions. Agents may prematurely converge at local optima or even other suboptimal solutions indicating the failure in exploring the search space thoroughly. Of late, hybrid techniques that combine both gradient-based and stochastic algorithms are proved to be superior as the limitations of each algorithm are nullified by other. Combinatorial problems such as design of a multilayer sorptive barrier system for landfill applications for minimizing the transport of common organic contaminants are solved using hybrid techniques.

REFERENCES

1. Bharat, TV and Sridharan, A. (2015) Prediction of Compressibility Data for Highly Plastic Clays Using Diffuse Double-Layer Theory. *Clays and Clay Minerals*, 63(1), 30-42.
2. Marquardt, D. (1963) An algorithm for least-squares estimation of nonlinear parameters. *SIAM Journal of Applied Mathematics*, 11 (1963), 431–441.
3. PSO-Tutorial: http://www.swarmintelligence.org/tutorials.php.
4. Rao, SS. (1993) Engineering Optimization – Theory and Practice, *John Wiley & Sons*, Inc., Canada.
5. Shackelford, CD and Daniel, DE (1991a) Diffusion in saturated soil. 1. Background. *Journal of Geotechnical Engineering*, 117(3), 467–484.
6. Taylor, DW. (1948) Fundamentals of Soil Mechanics. *Asia publishing house*, Japan.

Reliability Based Load Resistance Factor Design (LRFD) for External Seismic Stability of Reinforced Soil Walls

B Munwar Basha
Assistant Professor, Department of Civil Engineering,
Indian Institute of Technology Hyderabad
basha@iith.ac.in

1 INTRODUCTION

Allowable Stress Design (ASD) philosophy has been used for the design of reinforced soil walls for decades. However, this approach does not ensure a consistent reliability for mechanically stabilized earth retaining walls. The design considerations for a reinforced soil structure are the stability assessment of the potential external failure modes of the wall. The design earthquake imposes several types of dynamic loads on the structure. Seismic design of a mechanically stabilized soil structure subjected to earthquake ground motions requires explicit satisfaction of multiple performance criteria such as sliding stability, overturning (or eccentricity) stability and bearing capacity modes. FHWA (2001a) reported that the reinforced soil walls must be designed to avoid external modes of failure, viz. sliding failure on its base, overturning failure (or in terms of eccentricity failure of the resultant force striking the footing base) and bearing capacity failure of the foundation soil. American Association of State Highway and Transportation Officials, AASHTO (1996) recommended that for static loading, the minimum factors of safety in relation to sliding and overturning modes are 1.5 and 2.0 respectively, and eccentricity of the resultant force should be lesser than one sixth of the width of wall. Further, the minimum factor of safety against bearing capacity failure mode should vary between 2.0 to 2.5. In addition, it recommended that during seismic conditions, a minimum factor of safety of 1.0 shall be used for the design of walls for seismic loads. Currently used design manuals for the design of reinforced soil walls rely primarily on the traditional ASD format in which the safety factors are prescribed deterministically. These deterministic safety factors are based on several years of experience and supporting observations from the test data.

Load and Resistance Factor Design (LRFD) is an improved approach to the design of mechanically stabilized earth walls, MSEW (FHWA 2001a). It involves explicit consideration of limit states, multiple load factors, and resistance factors, and implicit probabilistic determination of reliability. The designation LRFD reflects the concept of factoring both loads and resistance. This type of factoring differs from the allowable stress design (ASD) specifications (AASHTO 1996), where only the resistance is divided by a factor of safety (to obtain allowable stress). The LRFD method was devised to offer the designer greater flexibility, more rationality, and possible overall economy. The format of using resistance factors and multiple load factors is not new, as several such design codes are in effect (AASHTO 2004), nor should the new LRFD method give designs radically different from the older methods, since it was calibrated to typical representative designs of the earlier methods. The present paper makes use of a probabilistic mathematical model in the development of the load and resistance factors, which made it possible to give proper weight to the accuracy with which the various loads and resistances can be determined.

The partial safety factors are dependent on the degree of uncertainty and influence of the relevant quantities, and on the desired level of safety. The magnitude of the load and resistance factors is established using probabilistic calculations and code calibration procedures based on test data. A design code developed using LRFD concept provides risk consistency, is likely to result in more economical designs. The reference manual by FHWA

(2001a) reported LRFD approach (in Chapter 14) for the mechanically stabilized earth walls, and presented a first step toward developing load and resistance factors, addressing static loading. For the design of reinforced soil walls, the current FHWA (2001a) recommends the resistance factors in bearing capacity mode range from 0.35 to 0.60 depending on the design method and for base sliding mode it should be 1.0. AASHTO (2004) LRFD bridge design specifications additionally reported partial factors for mechanically stabilized earth walls.

2 RECOMMENDATION OF LOAD AND RESISTANCE FACTORS

The review of the literature clearly indicates that the load and resistance factors have been reported for a target reliability index against one specific failure mode at a time (i.e. sliding). The load factors (η_k) and resistance factors (Ψ_k) computed for different failure modes are presented in Figs. 2 to 9. The partial factors for sliding, eccentricity and bearing capacity failure modes are computed under static and earthquake loading using the expressions, $\Psi_\phi = \phi^* / \mu_\phi$, $\Psi_{\phi_b} = \phi_b^* / \mu_{\phi_b}$, $\Psi_c = c^* / \mu_c$, $\Psi_q = q^* / \mu_q$, $\eta_\gamma = \gamma^* / \mu_\gamma$ and $\eta_{k_h} = k_h^* / \mu_{k_h}$. The terms in these expressions, viz. ϕ^*, ϕ_b^*, c^*, q^*, γ^* and k_h^* are the design values (corresponding to target value of reliability index, β_t) of ϕ, ϕ_b, c, q, γ and k_h respectively and μ_ϕ, μ_{ϕ_b}, μ_c, μ_Q, μ_γ and μ_{k_h} are the mean values of the random variables ϕ, ϕ_b, c, Q, γ and k_h respectively. The load and resistance factors (η_k and Ψ_k) are presented in Figs. 3 to 11 for target values of reliability indices, β_{sli} = 3, β_e = 3 and β_b = 3 against sliding, eccentricity and bearing failure modes respectively.

3 EXTERNAL STABILITY ANALYSIS

FHWA (2001b) guidelines for the external stability of geosynthetic reinforced soil walls have been followed. The mass of retained soil that is reinforced by horizontal layers of geo-synthetics can be imagined to act as a monolithic block of material. The sliding wedge failure mechanism is considered for the external stability analysis as shown in Fig. 1. A free body diagram of the wall showing different forces coming onto it from soil, and due to seismic loading along with their respective points of applications is shown in Fig. 1.

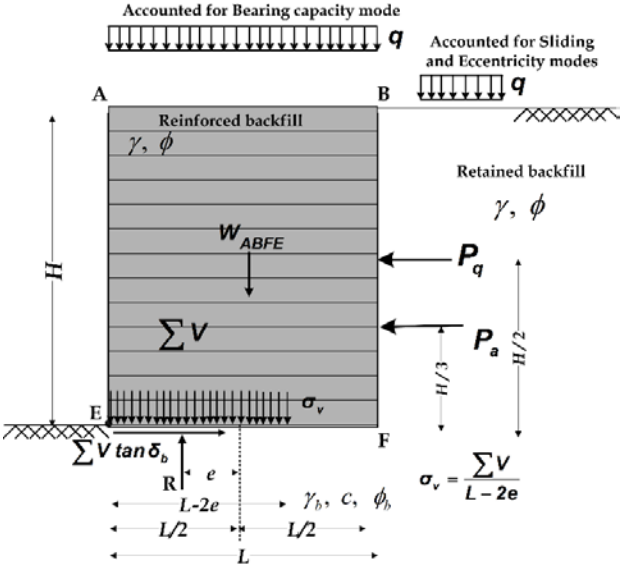

Figure 1: Forces and earth pressures considered for the external stability analysis of GRS wall.

During an earthquake loading, reinforced earth wall is subjected to a dynamic thrust at the back of the reinforced zone and to inertial forces within the reinforced in addition to static forces. The external seismic stability of the wall can be analyzed by the following procedure as reported in FHWA (2001b). The expressions of limit state functions for sliding, eccentricity and bearing modes of failure are presented below. The probabilistic constraints in the form of performance functions are:

$$g_{sli}(x) = FS_{sli} - 1;\ g_{ot}(x) = FS_{ot} - 1;\ g_e(x) = FS_e - 1;\ g_b(x) = FS_b - 1 \quad (1)$$

The load factors (η_k) and resistance factors (Ψ_k) computed for different failure modes are presented in Figs. 2 to 9. The partial factors for sliding, eccentricity and bearing capacity failure modes are computed under static and earthquake loading using the expressions, $\Psi_\phi = \phi^* / \mu_\phi$, $\Psi_{\phi_b} = \phi_b^* / \mu_{\phi_b}$, $\Psi_c = c^* / \mu_c$, $\Psi_q = q^* / \mu_q$, $\eta_\gamma = \gamma^* / \mu_\gamma$ and $\eta_{k_h} = k_h^* / \mu_{k_h}$. The terms in these expressions, viz. ϕ^*, ϕ_b^*, c^*, q^*, γ^* and k_h^* are the design values (corresponding to target value of reliability index, β_t) of ϕ, ϕ_b, c, q, γ and k_h respectively and μ_ϕ, μ_{ϕ_b}, μ_c, μ_Q, μ_γ and μ_{k_h} are the mean values of the random variables ϕ, ϕ_b, c, Q, γ and k_h respectively. The load and resistance factors (η_k and Ψ_k) are presented in Figs. 2 to 9 for target values of reliability indices, β_{sli} = 3, β_e = 3 and β_b = 3 against sliding, eccentricity and bearing failure modes respectively.

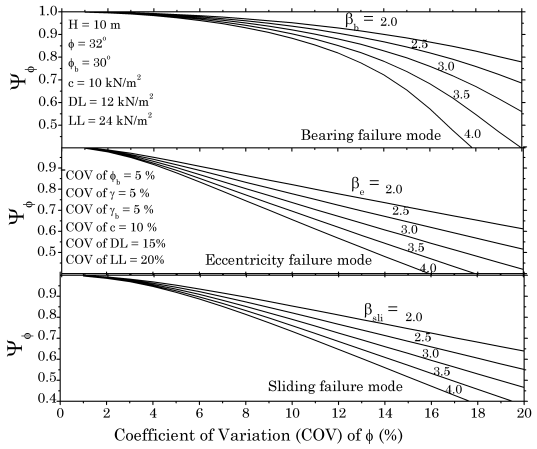

Figure 2: Influence of COV values of ϕ on resistance factors for the friction angle of the backfill (Ψ_ϕ)

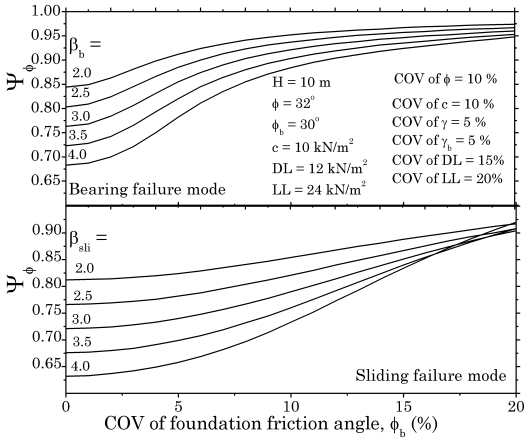

Figure 3: Influence of COV values of ϕ_b on resistance factors for the friction angle of the backfill (Ψ_ϕ)

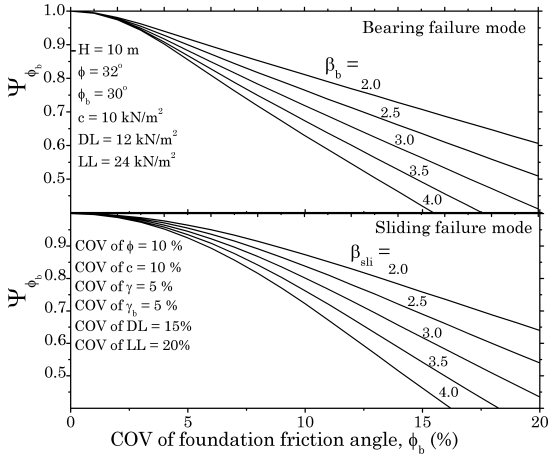

Figure 4: Influence of COV values of ϕ_b on resistance factors for the friction angle of the foundation soil (Ψ_{ϕ_b})

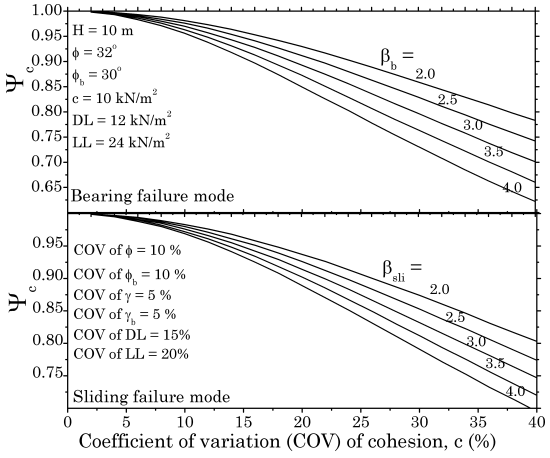

Figure 5: Influence of COV values of cohesion of the foundation soil (c) on resistance factors for the cohesion (Ψ_c)

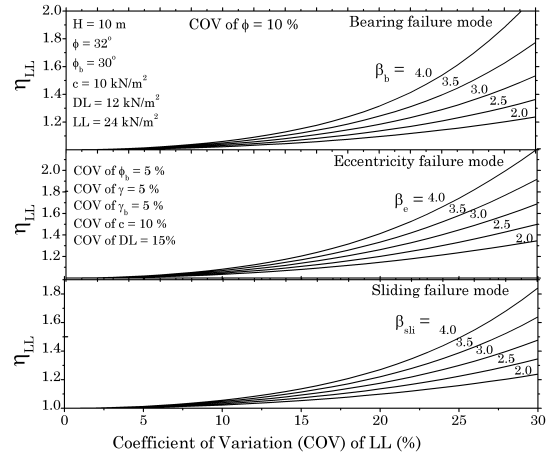

Figure 6: Influence of COV values of live load (LL) on load factors for LL against sliding, eccentricity and bearing failure modes

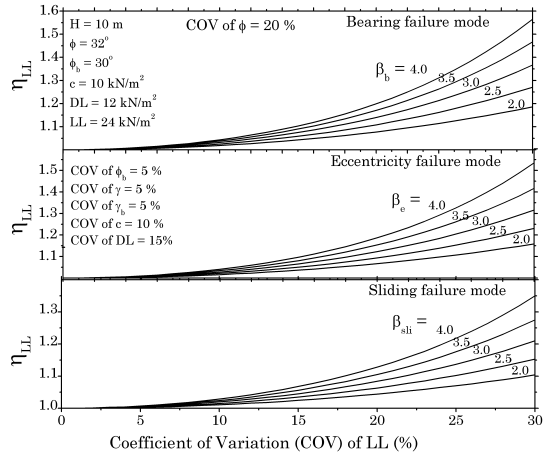

Figure 7: Influence of COV values of live load (LL) on load factors for LL against sliding, eccentricity and bearing failure modes

4 RECOMMENDATIONS

The partial factors presented in the report considering the variability associated with static as well as earthquake loading, may be used to support adaptation of the partial factors to enable inclusion in Indian codal specifications. The following are the guidelines:

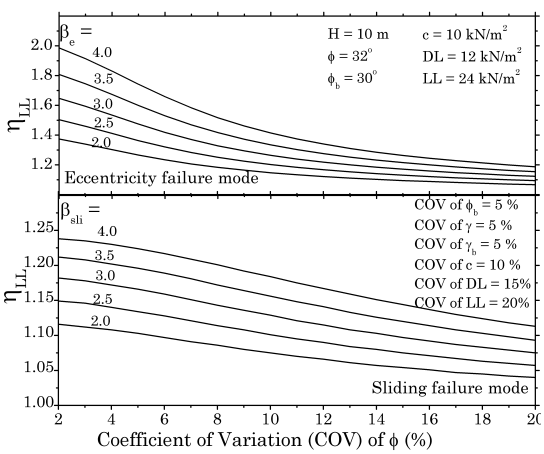

Fig. 8. Influence of COV of ϕ on load factors for LL against sliding, eccentricity and bearing failure modes.

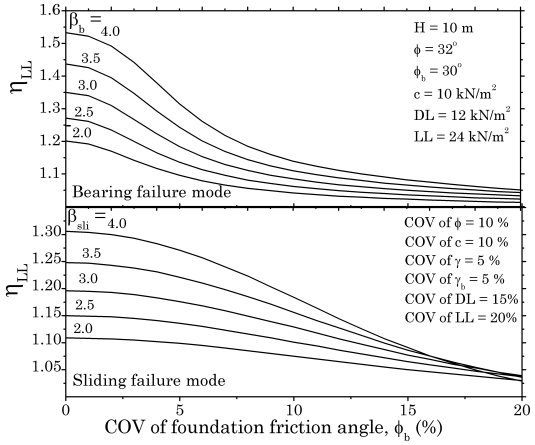

Fig. 9. Influence of COV of ϕ_b on load factors for LL against sliding, eccentricity and bearing failure modes.

1. It is found that for various magnitudes of target reliability index, COVs of ϕ and ϕ_b, the resistance factors, Ψ_ϕ and Ψ_{ϕ_b} range from 0.4 to 1.0 for all the failure modes, and the resistance factor for cohesion of the foundation soil (Ψ_c) varies from 0.70 to 1.0 for sliding mode and 0.6 to 1.0 for bearing capacity mode.
2. Since the dead loads can be estimated more accurately than live loads, the COV for live load is usually higher than that used for dead loads. Therefore due consideration must be paid to determine the *COV of LL* as it influences the MSEW design significantly.
3. It is observed from the study that the load factors (η_{LL}) ranges from 1.0 – 1.8 for sliding stability mode, 1.0 – 2.2 for eccentricity stability mode and 1.0 – 2.0 for bearing stability mode when *COV* of *LL* changes from 0 - 30% and *COV* of ϕ = 10%. Similarly when *COV* of ϕ = 20%, it can be noted that load factor (η_{LL}) ranges from 1.0 – 1.35 for sliding stability mode, 1.0 – 1.5 for eccentricity stability mode and 1.0 – 1.55 for bearing stability mode.

REFERENCES

1. AASHTO (1996) Standard Specifications for highway bridges. *American Association of State Highway and Transportation Officials, 16th ed.*, Washington, D.C.
2. AASHTO (2004) Standard Specifications for highway bridges. *American Association of State Highway and Transportation Officials, 3rd ed.*, Washington, D.C.
3. AASHTO (2007) LRFD bridge design specifications, *American Association of State Highway and Transportation Officials, 4th ed.*, Washington, D.C.
4. FHWA (2001a) Load and resistance factor design (LRFD) for highway bridge substructures: Reference manual and participant workbook. Publication No. FHWA HI-98-032. *Federal Highway Administration and National Highway Institute,* Washington, DC, USA.
5. FHWA (2001b) Mechanically stabilized earth walls and reinforced soil slopes: design and construction guidelines. Publication FHWA NHI-00-43. *Federal Highway Administration and National Highway Institute*, Washington, DC, USA.